Theme V: Application of high-strength steels including weathering steels to high-rise and long-span structures

V

Emploi des aciers à haute résistance et à protection naturelle pour les structures hautes ou à grande portée

Anwendung hochfester Stähle, inklusive wetterfester Stähle, für hohe und weitgespannte Tragwerke

Application of high-strength Steels including weathering Steels to high-rise and long-span Structures

Va

Comportement sous charges en incluant les constructions hybrides

Tragverhalten, einschliesslich hybride Tragwerke

Structural Behaviour including Hybrid Construction

Leere Seite
Blank page
Page vide

Strength and Ductility of A572 (Grade 65) Steel Structures

La résistance et la ductilité des structures en acier A572 (grade 65)

Festigkeit und plastische Verformungsfähigkeit der Stahlkonstruktionen aus Stahl A572 (Grad 65)

S. IYENGAR
Structural Engineer
Gilbert Associates, Inc.
Reading, Pennsylvania, USA

LYNN S. BEEDLE
Director, Fritz Eng. Lab.

LE-WU LU
Professor of Civil Engineering
Lehigh University
Bethlehem, Pennsylvania, USA

1. Introduction

A572 (Grade 65) steel, a low-alloy columbium-vanadium steel, is the highest strength steel for which the use of plastic design method is permitted by the American Institute of Steel Construction Specification. The properties of this steel are specified in ASTM Specification A572-74b which covers all six grades of the A572 steel with minimum yield values of 42, 50, 55, 60, and 65 ksi.

Many of the problems encountered in the design of building frames using high strength steels relate to buckling or to instability phenomena; namely, local buckling of cross sections, instability of beam-columns, lateral-torsional buckling of beams and beam-columns, and overall instability of frames. These problems occur in structures made of low carbon steel also but become more dominant as the yield stress of the material increases.

Consider local buckling as an example. Local buckling can occur either in the flange or in the web of a cross section, depending on the width-to-thickness ratios of the elements. For steels up to 50 ksi yield, limiting ratios have been developed in order to ensure that large strains can take place without buckling. This, in turn, assures adequate deformation capacity which is one of the requirements for plastic design. The formula defining the limiting ratios, derived primarily for lower strength steels, have been extended to include high strength steels. Experimental data are needed to confirm this extension.

A research program has been carried out at Lehigh University to study the mechanical properties of the steel and the behavior of some simple structures in the inelastic range with emphasis on local and lateral buckling.

2. Tensile Properties

The required minimum tensile properties (mill tests) of A572 (Grade 65) steel are: yield point σ_y = 65 ksi, tensile strength σ_u = 80 ksi, and elongation = 15% over an 8" gage. As part of the research program, 52 tension tests were conducted, the details of which have been documented elsewhere (1).

Figure 1 shows the stress-strain curve obtained from plotting average

values of the significant quantities. The static yield stress σ_{ys} is the most important property of steel and plays a significant role in plastic design. It is the yield stress value at zero strain rate. In the tests, the machine was stopped for five minutes at a strain of approximately 0.005 in/in and σ_{ys} was recorded. Its average value was 62.1 ksi. The corresponding dynamic yield stress σ_{yd} at the testing speed of 0.025 ipm was found to be 64.6 ksi. Simulated mill tests at 0.5 ipm gave an average value of 69.3 ksi. The tensile strength σ_u averaged 85.7 ksi. The value of strain ε_{st} at which strain-hardening commenced was 0.0186 in/in which is about 9 times the yield strain ε_y. The average value of percentage elongation in 8" gage length and percentage reduction of cross-sectional area were 21.5 and 51.0 respectively.

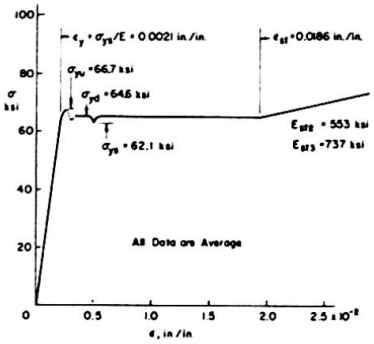

FIG. 1 IDEALIZED STRESS-STRAIN CURVE FROM TENSION TEST

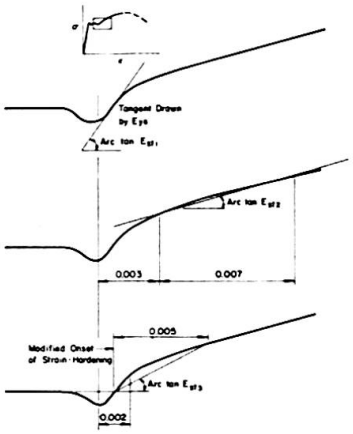

FIG. 2 SKETCH DEFINING E_{st1}, E_{st2} and E_{st3}

3. Strain-Hardening Modulus

The value of strain-hardening modulus E_{st} is important in the study of inelastic buckling of structural members. Three approaches have been used to evaluate E_{st} in this series of tests, as shown in Fig. 2. The modulus E_{st1} is the instantaneous value as measured by a tangent to the curve at the point where strain-hardening commences. This tangent is often difficult to determine consistently. Values of E_{st1} from different tests for the same material are likely to exhibit a wide scatter.

The modulus E_{st2} was measured as the chord slope between strains ε_{st}=0.003 and ε_{st} = 0.010. This specific range was chosen as it confines measurements to a fairly linear and stable range of the stress-strain curve and eliminates the initial erratic portion. Since measurements are made at a greater value of strain than in other methods, E_{st2} provides a conservative value.

In the "Column Research Council approach" (2), the modulus E_{st3} is the average value in the range ε_{st} to ε_{st} + 0.005, where ε_{st} is defined as the strain corresponding to the intersection on the stress-strain curve of the yield stress level in the plastic range with the tangent to the curve in the strain-hardening range. This tangent is drawn as the average value in an increment of 0.002 in/in after the apparent onset of strain-hardening. The attempt is to eliminate the effect of the frequently encountered drop in load immediately prior to the apparent onset of strain-hardening. E_{st3}, however, includes the effect of the steep initial slope and is hence less conservative than E_{st2}.

E_{st1} values varied, in this series, from 393 ksi to 9825 ksi. The straining process in the region of strain-hardening and the inherent difficulties in determining this function have contributed to the wide scatter of values. E_{st2} values averaged 553 ksi (min. 322 ksi, max. 775 ksi). E_{st3} values ranged from 382 ksi to 1160 ksi with an average of 771 ksi.

4. Compressive Properties

Compression tests were performed on ten specimens whose dimensions were generally in accordance with ASTM standards. Minor deviations, however, were necessary in order to be able to test the full thickness of the flange or web element and still use a special strain-recording instrument of fixed gage length 0.5" in the plastic range (3).

A typical stress-strain curve is shown in Fig. 3. The average values for the three most significant quantities are: σ_y = 65.14 ksi, ε_{st} = 0.0086 in/in, E_{st2} = 820 ksi. For comparison, three additional tests were performed on A441 steel specimens. The corresponding average values are: σ_y = 55.8 ksi, ε_{st} = 0.0147 in/in, E_{st2} = 815 ksi.

In general, strain ε_{st} is smaller than in tension tests while modulus E_{st2} is larger. The higher modulus is partly due to Poisson's ratio effect since the cross-sectional area in a compression test increases. However, the increase in E_{st} is not fully accounted for even with the assumption of 0.5 for Poisson's ratio in the inelastic range.

5. Residual Stresses

Residual stresses, determined by the method of sectioning (3), in a W12 x 19 shape are shown in Fig. 4. The stresses are seen to relatively small and there is no evidence of cold-straightening. In A36 steel, it has been found that the maximum residual stress at flange tips is about 0.3 σ_y or approximately 10 ksi (4). The present study shows that the magnitude of the maximum residual stress does not increase with yield stress level. This was also found to be true for other types of high strength steels.

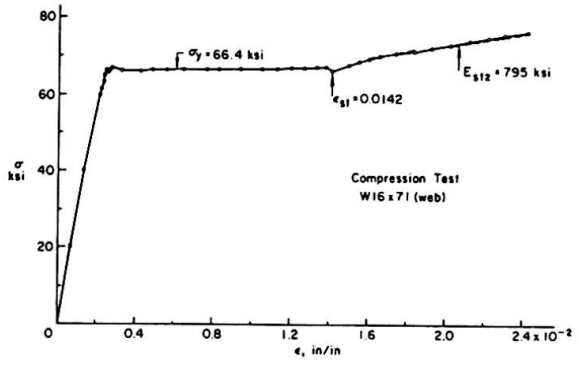

FIG. 3 STRESS-STRAIN CURVE FROM COMPRESSION TEST

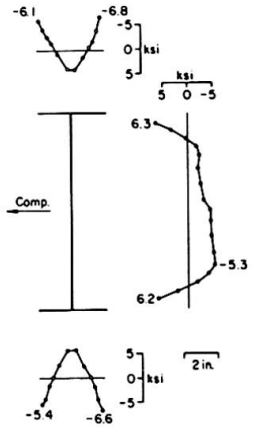

FIG. 4 RESIDUAL STRESS DISTRIBUTION IN W12 x 19 SHAPE

6. Stub Column Tests

Stub column tests were used to examine the local buckling characteristics of the plate elements under uniform compression (2). Previous research on lower strength steels has based the geometry of the plate elements on the criterion that the shape must undergo a strain at least equal to the strain-hardening strain without their buckling locally (5). The relevant formulas have been extended to include A572 (Grade 65) steel. Using these formulas and assuming σ_y = 65 ksi, E_{st} = 600 ksi, Poisson's ratio ν = 0.3 and E = 29,000 ksi, the required flange slenderness ratio b/t is 11.8 and the web slenderness ratio d/w is 30.6. For the first test, a W16 x 71 shape was selected since its listed properties b/t = 10.75, d/w = 33.2 are fairly close to the requirements. The

actual ratios were 10.72 and 32.50 respectively. Web buckling was, therefore, anticipated to precede flange buckling.

The test results are shown in Fig. 5. The web buckled at a strain of 0.0073 in/in, followed almost immediately by flange buckling at a strain of 0.0079 in/in. These strains are much lower than ε_{st} in tension (0.0186 in/in) but close to ε_{st} in compression (0.0086 in/in). However, the load continued to be sustained until the strain reached 0.038 in/in.

Results of two other tests on modified W10 x 54 shapes are shown in Fig. 6. The flanges were machined down to yield b/t ratios of 11.8 and 13.3 for the two tests, while the web ratio d/w was maintained at 27.5. In the test with b/t = 11.8, the flanges buckled at a strain of 0.010 in/in and the webs at 0.015 in/in. Strain-hardening was evident later (E_{st} = 950 ksi) and the load began to drop off past the strain of 0.025 in/in. The third test with b/t = 13.3 showed nearly the same trends. Web buckling began at 0.006 in/in followed by flange buckling at 0.007 in/in with other details identical.

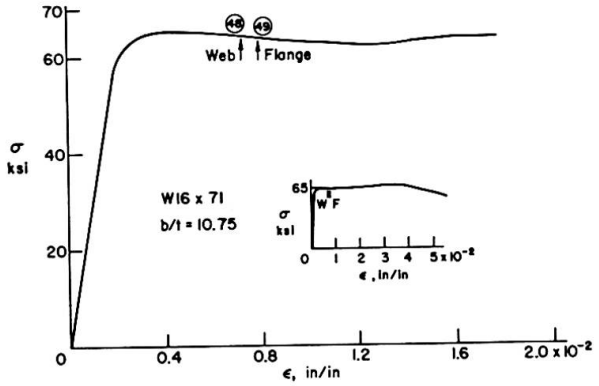

FIG. 5 STRESS-STRAIN CURVE FROM STUB COLUMN TEST - W16 x 71 SHAPE

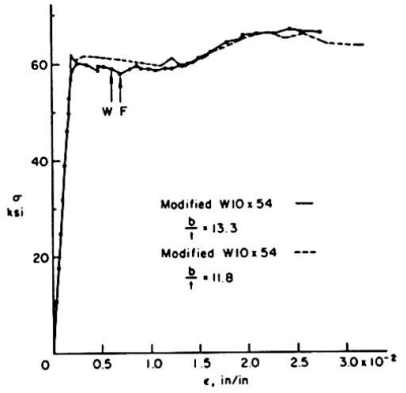

FIG. 6 STRESS-STRAIN CURVE FROM STUB COLUMN TEST - W10 x 54 SHAPE

The results show that local buckling occurred in Grade 65 steels at a strain smaller than that predicted by the theories developed for lower strength steels. Buckling, however, did not precipitate failure and resulting reduction in strength.

7. Beam Tests

Two beams fabricated from a length of W12 x 19 shape were tested, one under moment gradient and the other under uniform moment. Details are given elsewhere (6). Available theories indicate that the slenderness ratios b/t and d/w should be limited to 11.2 and 52.1, respectively, for σ_y = 65 ksi and E_{st} = 600 ksi. The W12 x 19 shape is one of the few having nearly these same ratios.

The beam under moment gradient had a simply supported span of 10'-5" and was loaded at the center. Lateral braces were provided at midspan, supports and at 37.5" on either side of midspan, as against the requirement of 46 r_y or 38.5" according to available theories (7).

The non-dimensionalized moment M/M_p against midspan deflection δ/δ_p is given in Fig. 7. The terms M and δ are the moments and deflections, M_p is the theoretical plastic moment, and δ_p is the deflection at $M = M_p$, assuming ideal elastic behavior. Strain-hardening setting in soon after the plastic moment was reached at the center. Local buckling in the compression flange near midspan was visible at load No. 9. The compression flange also displaced laterally at load No. 13.

The rotation capacity of a beam is usually defined as $R = (\theta/\theta_p)-1$ where θ is the sum of the end rotations at which the moment drops below 0.95 M_p and θ_p is the rotation at $M = M_p$. The R value is 3.1 in this test. A precise comparison of R with those obtained in other tests (for lower strength steels) is difficult, since different shapes and unbraced spans have been used. However, it can be said that the rotation capacity of Grade 65 steel beam is less than that for other beams.

The beam under uniform moment was loaded at quarter points over a simple span 15' long. Lateral braces were spaced, in close accordance with present theories (8), at load points, supports and approximately 13" apart between load points. Outside the uniform moment region, two braces were used, 37.5" from each load.

The results are shown in Fig. 8. The discontinuity of the curve between load Nos. 6 and 11 is due to a slip in a lateral brace and subsequent repair. Local buckling was visible at load No. 15 and the compression flange began to deflect laterally. At load No. 16, the lateral deflection was about 0.6 in. Unloading was caused by severe lateral buckling as a result of local buckling of the compression flange. The computed rotation capacity R in this test was 4.8, a value smaller than in comparable structures of lower strength steels.

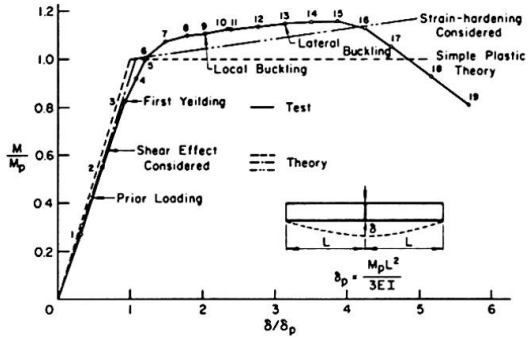

FIG. 7 BEAM UNDER MOMENT GRADIENT

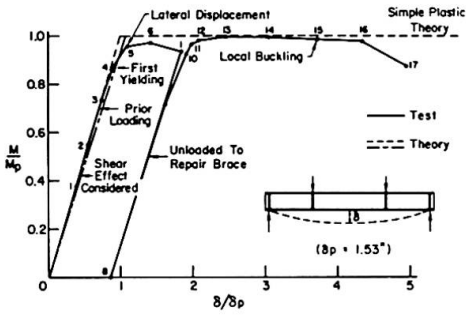

FIG. 8 BEAM UNDER UNIFORM MOMENT

8. Conclusions

A572 (Grade 65) steel exhibits mechanical properties in the inelastic region similar to those of structural carbon steel. The use of E_{st2} for strain-hardening modulus represents a new approach to obtain a more realistic, as well as conservative, value of this property for use in situations where the material is strained into the strain-hardening range. The value of E_{st} in compression is higher than in tension. Since buckling phenomena are associated with compression, a compression test appears to be the appropriate way of obtaining this modulus.

Residual stresses in shapes of higher strength steels are nearly the same in magnitude as in lower strength steels, and are thus independent of yield stress level. Hence, the influence of residual stresses decreases with increase in yield stress.

It was possible to extend the available theories developed for local and lateral buckling to Grade 65 steel although the assumptions of the theory are not fully borne out. This is because the post buckling strength of Grade 65 steel is considerable and reliable to the extent that it offsets any loss of strength as a consequence of premature buckling. Reference 9 contains the design recommendations developed for structures made of this steel.

References

1. Desai, S.
MECHANICAL PROPERTIES OF ASTM A572 GRADE 65 STEEL, Fritz Engineering Laboratory Report No. 343.2, Lehigh University, 1969

2. CRC
STUB COLUMN TEST PROCEDURE, CRC Technical Memorandum No. 3, 1961

3. Huber, A. W.
COMPRESSIVE PROPERTIES OF ROLLED STRUCTURAL STEEL, Fritz Engineering Laboratory Report No. 220A.1, Lehigh University, 1951

4. Huber, A. W. and Beedle, L. S.
RESIDUAL STRESS AND THE COMPRESSIVE STRENGTH OF STEEL, Welding Journal, 33(12) Research Suppl., 589-s, (1954)

5. Haaijer, G. and Thurlimann, B.
ON INELASTIC BUCKLING IN STEEL, Trans. ASCE, 125 (I), p. 308, (1960)

6. Kim. S. W.
EXPERIMENTS ON A512 GRADE 65 STEEL BEAMS, Fritz Engineering Laboratory Report No. 343.4, Lehigh University, 1970

7. Lay, M. G. and Galambos, T. V.
INELASTIC STEEL BEAMS UNDER MOMENT GRADIENT, Proc. ASCE, 93(ST1), (1967)

8. Lay, M. S. and Galambos. T. V.
INELASTIC STEEL BEAMS UNDER UNIFORM MOMENT, Proc. ASCE, 91(ST6), (1965)

9. ASCE-WRC Joint Committee
PLASTIC DESIGN IN STEEL -- A GUIDE AND COMMENTARY, ASCE Manual No. 41, 2nd edition, 1971

SUMMARY

The results of a study of the mechanical properties of ASTM A572 (Grade 65) steel and of the behaviour of simple structures made of this steel are presented. A new approach to define strain-hardening modulus is proposed. This modulus is significantly higher when it is determined from a compression test than from a tension test. Results of experiments on stub columns and beams show substantial post-buckling strength in the inelastic range.

RESUME

Les résultats d'une étude sur les propriétés mécaniques de l'acier désigné par ASTM A572 (grade 65) et sur le comportement de structures simples construites avec cet acier sont présentés. Une nouvelle méthode pour définir le module d'écrouissage est proposée. Ce module déterminé par des essais de compression est nettement plus grand que celui obtenu par des essais de traction. Les résultats des essais sur des colonnes courtes et sur des poutres indiquent que la résistance au flambage est importante dans la région inélastique.

ZUSAMMENFASSUNG

Die Ergebnisse eines Studiums über mechanische Eigenschaften des ASTM A572 (Grad 65) Stahles und das Verhalten der einfachen Konstruktionen aus diesem Stahl beschrieben. Es wurde ein neuer Versuch zur Definition des Verformungsmoduls dieses Stahles im Verfestigungsbereich vorgeschlagen. Dieser Modul ist wesentlich höher, wenn er aus Druckproben, jedoch nicht aus Zugproben bestimmt wird. Die Ergebnisse der Untersuchungen an kurzen Säulen und Balken haben gezeigt, dass der Stahl wesentliche überkritische Reserven im nichtelastischen Bereich aufweist.

Deformation Capacity of High-Strength Steel Members

Capacité de déformation d'éléments en acier à haute résistance

Verformungsfähigkeit von Gliedern aus hochfestem Stahl

TOSHIRO SUZUKI
Associate Professor, Dr. of Eng.

TETSURO ONO
Assistant, Dr. of Eng.

Tokyo Institute of Technology
Tokyo, Japan

§1. INTRODUCTION

As large sized steel structures have been developed, high-strength steels having high yield stress level have attracted special interest recently. In this situation, it is becoming to be common to apply high-strength steel on the simple plastic design of structures. On the simple plastic design method, the steel structures must be able to maintain through a sufficient inelastic rotation without a decrease of moment capacity at each plastic hinge to allow the formation of a failure mecnanism. Then, the deformation capacity of members comes up as an important problems. Therefore, there are many difficult problems in using high-strength steel which is less ductile than that of low-alloy steels. There are, however, few reports on high-strength steels concerning the simple plastic design of structures, and not enough of the necessary basic data.

The objectives of this paper are to explain the plastic behavior of high-strength steel members, and to determine quantitatively the relationship between the rotation capacity and the material properties of steels.

§2. OUTLINE OF EXPERIMENTS

2.1 EXPERIMENTS

Experiments are made to explain plastic behavior and deformation capacity of beams and beem-column. Test speciments of beams are built-up H-250×125×12×12 and test speciments of beam-columns are built-up H-150×150×9×9. The kinds of steel used in this experiments are low-alloy steels (SM-41, SM-50) and high-strength steels (HT-60, HT-80). The loading conditions of beams are a uniform moment and a moment gradient, and that of beam-columns are axial load and one end bending moment. In addition to using four kinds of steels, bracing spaces and axial forces are varied, in order to investigate their influences on the rotation capacity of these steel members.

2.2 MATERIAL PROPERTIES

The material properties of each steels are determined by tension tests and stub column tests with wide-flange shape. Yield stress level of high-strength steel has higher level, comparing low-alloy steel. Yield stress level of SM-41

is evaluated 3.24t/cm^2, and that of HT-80 is evaluated 8.80t/cm^2. The yield plateau length is short and the stress strain curve of HT-80 shows the stiff bilinear material. The strain hardening modulus Est is smaller than that of SM-41. Additionally, the yield ratio and elongation of the material are small. These results of each materials are showed in Table-1. The ductilities of material of high-strength steel are small as is obvious from Table-1. There are many difficult problems in applying high-strength steel on the plastic design fo steel frames.

§3. EXPERIMENTAL RESULTS

3.1 LOAD-DEFLECTION CURVES

Fig. 1 ∿ 3 show the experimental load-deflection curves. Moments and rotation angles have been nondimensionalized with full-plastic moment Mp and rotation angle Θpc are used. Fig. 1 shows the load-deflection curves of beams under uniform moment. Moment reaches at full-plastic moment. Except HT-80, moment remains at near-constant value Mp and the in-plane deformations increase. This plastic behaviors are not influenced with the kinds of steel. Fig. 3 shows the load deflection curves of beams under moment gradient. These plastic behaviors are different from the beams under uniform moment. The plastic behaviors are effected with the strain hardening modulus and the plastic plateau length of material. Moments increase exceeding full plastic moment. In general, the strain hardening modulus has effects upon the rigidity of members after yielding. If the plastic plateau length is small, the effects of strain hardening modulus on plastic behaviors are remarkable. As the plastic plateau length decreases, the deformations of members at the same moment level are small. Fig. 4 shows the load deflection curves of beam-columns. In this case, the plastic behaviors are similar to that of beams under moment gradient.

3.2 LATERAL BUCKLING AND LOCAL BUCKLING

Fig. 4 ∿ 6 show the strain distributions as the moments decrease due to local or lateral buckling. Fig. 4 shows the strain distributions along the axis of members at two points of Mp and the decrease of moment. When moments reach at Mp, the strain distributions are not uniform along the axix of members. The strain distribution of HT-80 are uniform and the level of strain is about the strain hardening level εst. Because the strain hardening modulus is small, the moment decreases rapidly. In the case of beams under uniform moment, the main cause of decrease of moment is the increase of torsional deformation. Fig. 5 shows the strain distributions of beams under moment gradient. The distributions are different from that of beams under uniform moment. On high-strength steel, the yield length is shorter than that of low-alloy steel and the gradient of strain distributions is large. On the beams under moment gradient, the local buckling causes the dropping of the applied load. Fig. 6 shows the curvature distributions along the axis of beam-columns and the strain distribution at the decrease of moment. Maximum curvature point moves to center from the end of span as the axial force increases. The behaviors at the decrease of moment are different each other due to the point of maximum moment. When the maximum moment occurs at the end of the beam-columns, strain distributions are uniform and diformations of out of plane are not recognized and the beam-columns have enough deformation capacity. These results show that the plastic behaviors of the beam-columns are same as the beam under moment gradient.

3.3 RELATION OF DEFORMATION CAPACITY AND MATERIAL PROPERTY

The deformation capacity of steel member is influenced with the material properties. Fig. 7 and 8 show the rotation capacity and slenderness ratio relationships of beam. It is clearly that each rotation capacities are different due to the material properties. In Fig. 7 and 8, the curves show the following equations.[9] These equation are obtained from the analysis assuming two models.

Two models are based on the following ideas that are obtained from the experimental behavior. The lateral buckling and local buckling determine the limit of the deformation capacity.

Under uniform moment

$$R = K_1 \frac{1}{\lambda_y^2} (\sigma yo/\sigma y)^2 \sqrt{\frac{B}{H}} \qquad (1)$$

Under moment gradient

$$R = K_2 \frac{1}{\lambda_y^2} \rho (\sigma yo/\sigma y) \left(\frac{t_f}{B}\right) \qquad (2)$$

Fig. 9 shows the load-deflection curves of beam-columns which have same slenderness ratio (λ_x=30) and various axial force. Fig. 10 shows the relations of the rotations capacity and axial force with the slenderness ratio as a parameter. The curves in this figure are obtained from the numerical analysis according to the finit element method. Fig. 1 shows the critical slenderness ratio of beam-columns and experimental results. The rotation capacity of beam-columns is influenced with the axial force, the slenderness ratio and material properties. Especially, the deformation capacity of beam-columns is influenced more significantly with material. High-strength steel beam-columns (HT-60, HT-80) have few the rotation capacity. The curves in this figure show the critical slenderness ratio of beam-columns having enough rotation capacity. The thick solid line shows the critical value which can ensure the rotation capacity above R=3 due to the numerical analytical results. This result is agreement with the experimental results. Specification of AIJ is loose in order to have enough rotation capacity. From these results, the following critical slenderness ratio that is proposed by Lay, M.G[6]. is equivalent to the experimental results.

$$P/Py = \frac{1 - \bar{\lambda}}{1 + \bar{\lambda}} \qquad (3)$$

§4. CONCLUSION

In this paper, the deformation capacity of steel members is explained by the experiment and numerical and theoretical analysis. In general, high-strength steel is seemed to be disadvantageous applying on the simple plastic design of steel structures which requires the enough rotation capacity. Especially, it is worth noting that HT-80 having the stiff bi-linear material curve used in this experiments has few deformation capacity. The rotation capacity is directly influenced by the value of yield stress, the plastic plateau length and the strain hardening modulus. Therefore, we conclued that the effective factors can be represented only by the ratio of yield stress. The rotation capacity is proportional to the square of the reciprocal ratio of yield stress in the case of uniform moment, and to the reciprocal ratio of that in the case of moment gradient. On the beam-columns, the redundant of rotation capacity is remarkable due to the material properties.

ACKNOWLEDGEMENT

In writing this paper the authors are grateful to Sumitomo Metal Industries, Ltd. for providing the test speciments of high-strength steel. Especially, the authors wish to thank Mr. Y. Nishida and Mr. M. Kato of Sumitomo Metal Industries, Ltd..

Table 1 Material Property

STEEL*	THICK-NEESS (mm)	σ_y (t/cm²)	σ_u (t/cm²)	ε_y ($\times 10^{-6}$)	S ($\varepsilon/\varepsilon_y$)	$E\times 10^3$ (t/cm²)	E_{st} (t/cm²)	σ_u/σ_y	h (E/E_{st})	Elong. (%)
SM-41	12	3.24	4.76	1521.	13.8	2.13	47.0	1.47	45.3	28.5
SM-50	12	3.95	5.53	1855.	10.6	2.13	36.1	1.40	59.0	23.4
HT-60-1	12	5.78	6.78	2706.	6.78	2.14	31.0	1.17	69.0	26.6
(HT-60-2)	(12)	(5.45)	(6.66)	(2547.)	(5.89)	(2.14)	(36.4)	(1.20)	(58.0)	(30.7)
HT-80	12	8.80	9.39	4112.	1.00	2.14	15.0	1.07	142.7	24.4

*TEST COUPON DIMENSION (JIS Z 2201) SM-41, SM-50……No. 1 TEST COUPON
HT 60, HT 80……No. 5 TEST COUPON

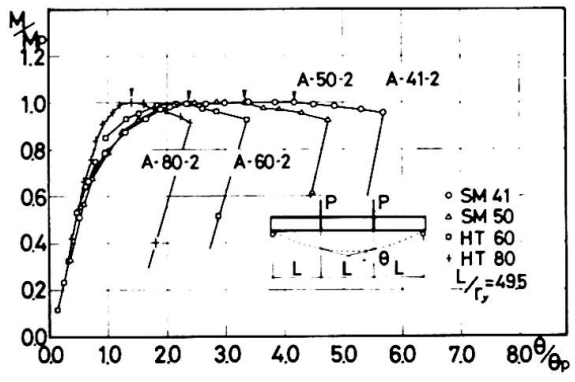

Fig.1 M-Θ Relationships

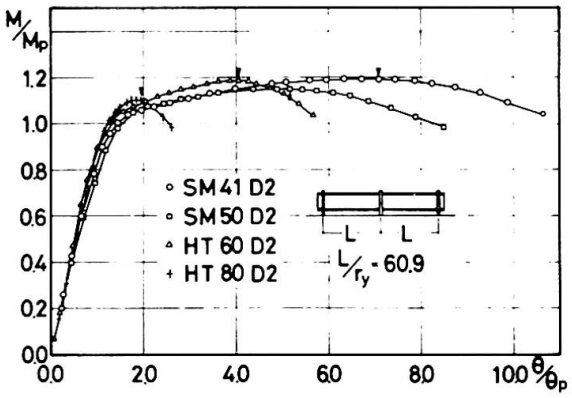

Fig.2 M-Θ Relationships

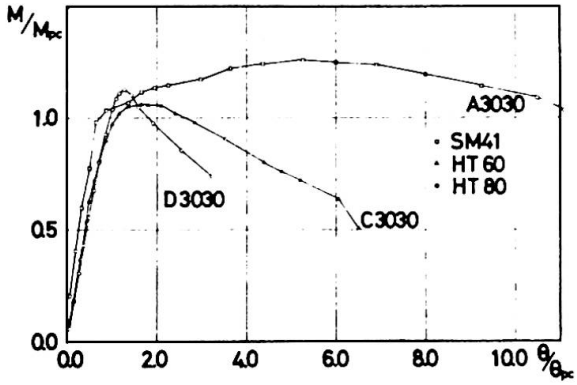

Fig.3 M-Θ Relationships

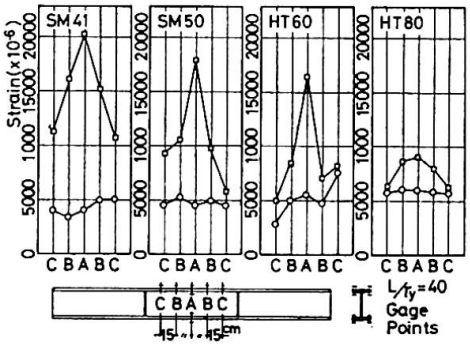

Fig.4 Strain Distribution

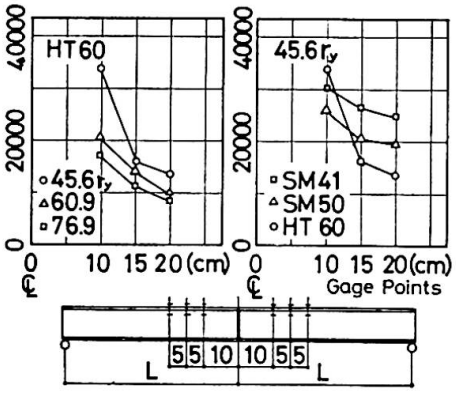

Fig.5 Strain Distributio

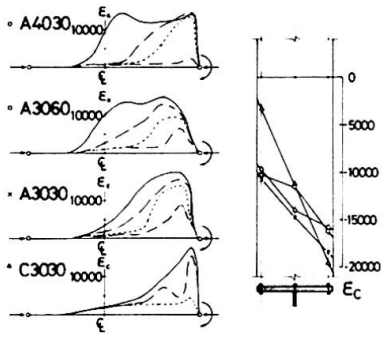

Fig.6 Strain Distributio

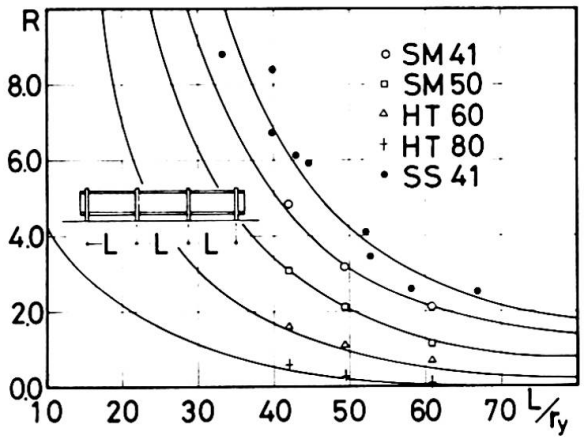

Fig.7 Rotation Capacity

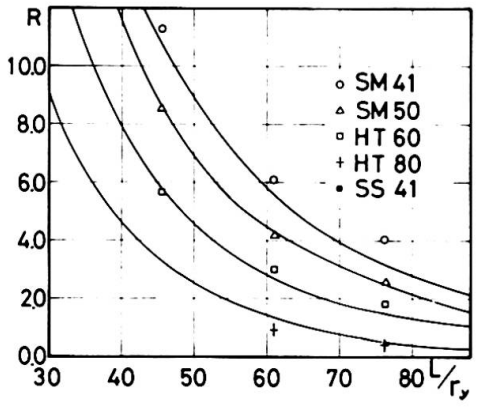

Fig.8 Rotation Capacity

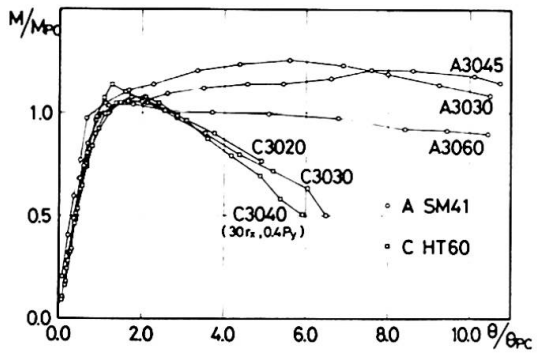

Fig.9 M-Θ Relationships

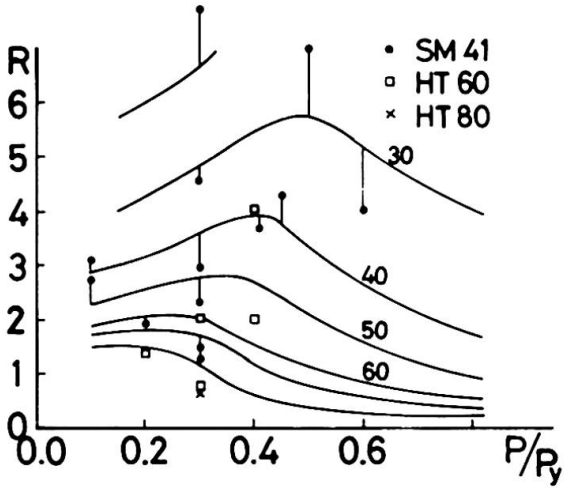

Fig.10 Rotation Capacity

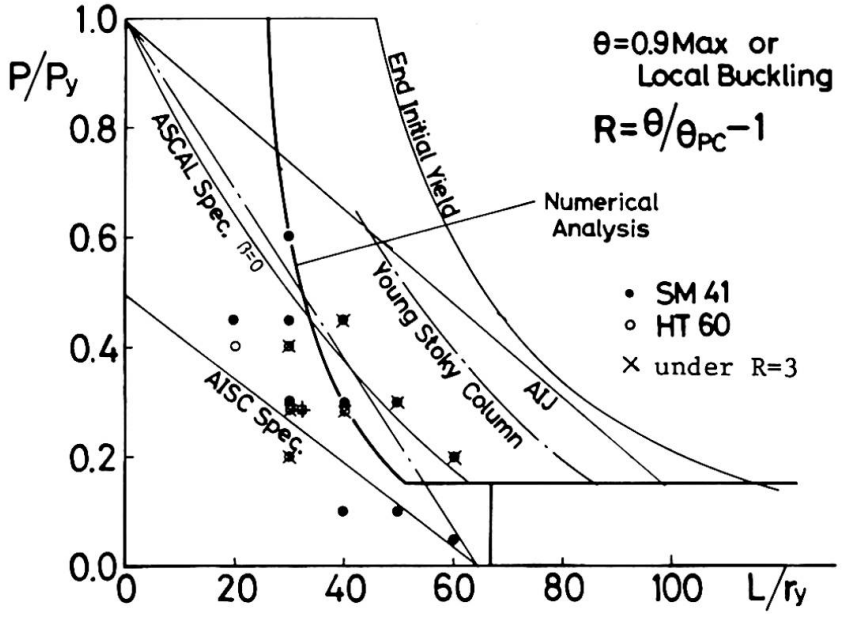

Fig.11 Critical Slenderness Ratio

REFERENCES

1) McDermott, J.F.; Plastic Bending of A514 Steel Beams, Journal of the Structural Div., Proc. ASCE, ST9, Sept. 1969
2) Plastic Design in Steel, A Guide and Commentary, 2nd Edition, ASCE, 1971
3) Adams, P. F., Lay, M. G. and Galambos, T. V.; Experimentary on High-Strength Steel Members, WRC Bulletin No. 110, Nov. 1965
4) Augusti, G.; Experimental Rotation Capacity of Steel Beam-Columns, Journal of the Structural Div., Proc. ASCE, ST6, Dec. 1964
5) Adams, P. F.; Plastic Design in High Strength Steel, Fritz Engineering Laboratory Report, No. 297, 19, May, 1966
6) Lay, M. G.; The Static Load-Deformation Behavior of Planner Steel Structures, Ph. D. Dissertation, Lehigh Univ., 1964
7) Suzuki, T. and Ono, T.; Experimental Study of the Inelastic Steel Beams (1), Trans. AIJ, No. 168, Feb. 1970
8) Suzuki, T. and Ono, T.; Experimental Study of the Inelastic Steel Beams (2), Trans. AIJ, No. 170, May, 1970
9) Suzuki, T. and Ono, T.; Experimental Study of the Plastic Design of High-Strength Steel Beams, Trans. AIJ, No. 219, May, 1974

SUMMARY

The plastic behaviour and the deformation capacity of high-strength steel members are discussed on the relation to the low-alloy steel members. High-strength steels seem to be disadvantageous applying on the simple plastic design of steel structures. Especially, it is worth noting that HT-80 used in this experiment has few deformation capacity. While the rotation capacity is directly influenced by the value of yield stress, plastic flow and strain hardening rigidity, we conclude that the effective factors can be represented only by the ratio of yield stress.

RESUME

Le comportement plastique et la capacité de déformation d'éléments en acier à haute résistance sont comparés avec ceux de l'acier doux. Il semble que les aciers à haute résistance sont désavantageux lors du calcul plastique simple de structures en acier. Il faut remarquer que l'acier HT-80 employé dans cette expérience a une faible capacité de déformation. La capacité de rotation d'éléments en acier est directement influencée par la valeur de l'effort à la limite d'écoulement, l'écoulement plastique, et le durcissement par déformation. D'autre part nous concluons que ces facteurs efficaces peuvent être représentés seulement par le rapport d'efforts à la limite d'écoulement.

ZUSAMMENFASSUNG

Plastische Verhalten und Verformungsfähigkeit von Gliedern aus hochfestem Stahl werden in Beziehung zu denselben von Gliedern aus Stahl St 37 diskutiert. Es scheint, dass hochfeste Stähle bei Anwendung der einfachen plastischen Berechnung von Stahlbauten nachteilig sind. Bemerkenswert ist, dass in diesem Experiment HT-80 eine geringe Verformungsfähigkeit zeigt. Die Rotationsfähigkeit von Gliedern aus Stahl werden unmittelbar durch die Höhe der Fliessgrenze, die Fliessverformung und die Steifigkeit im Verfestigungsbereich beeinflusst. Anderseits kommen wir zur Ueberzeugung, dass diese wirksamen Faktoren nur durch das Verhältnis der Fliessgrenzen dargestellt werden können.

Lateral Buckling of Welded Beams and Girders in HT 80 Steel

Déversement de poutres soudées en acier HT 80

Kippen von geschweissten Balken aus HT 80 Stahl

YUHSHI FUKUMOTO
Professor of Civil Engineering
Nagoya University
Nagoya, Japan

1. INTRODUCTION

Lateral instability of compression flange has been one of the important limit state criteria for the determination of the ultimate bending strength of flexural members when the compression flange is not restrained enough against lateral deflection. The author has shown the results of the investigation on the ultimate strength of beams with lateral bracing at the intermediate points[1)2)] and without any lateral supports in between[3),4),5)] from theory and test.

This paper briefly describes the lateral buckling test[3)] on welded beams and girders with steels of SM 50 and quenched and tempered HT 80 (nominal yield stresses σ_y = 3200kg/cm^2 and 7000kg/cm^2, respectively), and the initial imperfections such as welding residual stresses and initial deformations are discussed with the test results. The comparisons are also made between theory and test.

2. THE TEST SPECIMEN

No lateral bracings are provided except at the both ends of the specimen where the loading beams with heavy box cross section are connected using high strength bolts. The end condition of the specimen is thus clamped laterally and torsionally at the both ends. The test setup is shown in Fig. 1.

The detailed nominal dimension of the beam-type specimens are given in Table 1(a). The beam types are of 25cm or 30cm in beam height with the span length ranging from 2.5m to 4.5m. Total number of beam specimens is thrity-six of which

SM 50 : twenty-one including nine annealed beams, and
HT 80 : fifteen including three annealed beams.

Table 1(b) shows for the plate girders of 80cm or 100cm in height with the span length ranging from 2.8m to 4.0m. Number of sub-panels in web is two for G-D and the others have three sub-panels.

The specimens are tested under uniform bending and under moment gradient with the end moment ratio of 0.5.

3. INITIAL IMPERFECTIONS

After the test specimen is set in the position for testing and just prior to loading, the initial imperfections are measured in flanges and web plates. Table 2 summarizes the maximum lateral deflections of the compression flange δ_u and tension flange δ_ℓ at the span center. Effective length of the specimens against lateral buckling becomes $L_e = L/2$ (L=length of the specimen) under uniform bending since the clamped end condition is met at the connections of the specimens and the loading beams.

4. WELDING AND ANNEALING DATA

Welding data for HT 80 steel specimens are as follows ;

For beams : Manual welding with 5mmϕ electrode (YAWATA L80). 180 - 230 amp. current and preheating at 120^0c.

For girders : Manual welding with 4mmϕ electrode (KAWASAKI KS116, B-1). 165 - 175 amp. current and preheating at 120^0c.

Annealing conditions are set for relieving the welding residual stress as shown in Fig. 2.

5. THE TEST RESULTS

a) Tension Coupon Test

Test coupons with 20cm gage length for SM 50 and with 5cm gage length for HT 80 are cut out from the flange and web plates. The averaged values of static yield stress are listed below.

Beams { SM 50 : 3428 kg/cm^2
HT 80 : 7841 "

Girders { SM 50 : 3810 kg/cm^2 (8mm) and 3236 kg/cm^2 (10mm)
HT 80 : 7850 " (10mm) and 6610 " (6mm)

b) Lateral Buckling Test

Figs 3a and 3b show the load-deflection curves of a beam and a girder in HT 80, respectively, in which β = angle of rotation of the compression flange, u_1 and u_2 = lateral deflection of lower and upper flanges and v = vertical deflection at the span center. At the early stage of loading, the lateral and torsional deformations of the girder flanges are observed together with the buckled patterns in each web panel. Lateral deflection of the compression flange at failure is influenced considerably by the direction of the buckled deformation of the web in bending.

A summary of test results with the reference loads is listed in Table 3.

Fig. 4 shows a presentation of the test points plotted on the σ_{cr} - $(r_x/r_y)(L_e/d)$ axes[3], in which r_x and r_y are the radii of gyration of cross section about x and y axes, respectively and d = the beam height. The test points for HT 80 indicate less scatter and the reduction of lateral buckling strength becomes less for HT 80 specimens compared with SM 50 specimens in the inelastic range.

Fig. 5 shows another presentation of the test points plotted for beam-type specimens on the $\sigma_{cr}/\sigma_y - (L_e/r_y)/(L_e/r_y)_{elastic}$ axes. Non-dimensionalized slenderness ratio λ is taken in the abscissa whereas $(L_e/r_y)_{elastic}$ is the slenderness ratio at which the elastic lateral buckling stress reaches to the yield point, that is, $\sigma_u = \sigma_y$.
The maximum experimental moments M_u are non-dimensionalized by the yield moment M_y. In order to clarify the effect of residual stress distributions on the lateral buckling strength of steel beams, the comparisons are made between the annealed beams and the as-weld beams having the same sizes. Twelve pairs of specimens are tested and by taking the strength ratios $M_{annealed}/M_{as\text{-}weld}$ for each pair, it is obtained that the average strength gains are of 11% for annealed beams compared to the as-weld beams for SM 50 and 6% for HT 80 steel. It may be concluded that the welding residual stress distributions may reduce the lateral buckling strength for about 11% average for SM 50 and 6% average for HT 80 against the beams without residual stresses. Experimental findings may prove that the residual stress effect upon the lateral buckling strength becomes less with the higher yield strength steel.

6. COMPARISONS OF THEORY AND TEST

a) Inelastic Lateral Buckling Strength

Inelastic lateral buckling strength under uniform moment is determined for the arbitrary residual stress patterns using the numerical iteration technique for computing the cross sectional properties.[5) 7)] In Table 4 the calculated ideal critical elastic moment M_E and inelastic moment M_{cr} for the two different residual stress patterns (A) and (B) are given for girder-type specimens.
Fig. 6 shows the theoretical results using the residual stress patterns 1 and 2 ($\sigma_{rc} = 0.3\sigma_y$ inset in Fig. 6) are compared with the test points for the as-weld and annealed A-type beams.[3)]

b) Ultimate Bending Strength

Since the inelastic lateral buckling resistance is furnished mostly by the compression flange, the lateral buckling strength becomes very close to that of a column whose effective cross section is composed of the compression flange and one-sixth of the web[6)]. In this analysis the ultimate bending strength of members with initial imperfections such as residual stresses and lateral deflection of the compression flange is determined by the beam-column concept using the numerical integration technique[5)]. The residual stress patterns used for this analysis is shown in Table 4 as patterns (C) and (D).

In Fig. 5 the ultimate bending strength curves obtained by the beam-column concept are given for the D-type and C-type beams with the initial lateral deflection $u_o = L_e/1000$ and with and without residual stress pattern (C). Ultimate bending strength curves for the residual stress patterns (C) with, $\sigma_{rc} = 0.3\sigma_y$ and initial lateral deflection $u_o = L_e/1000$ may explain the lower bound estimate against the plotted test results. In table 4 the numerical results by the beam-column approach are also given for the plate girders G-A$\sim$G-G.

Table 1 (a) Dimensions of test beams

Test Beams	Steel	d (mm)	b (mm)	t_w (mm)	t (mm)	L (mm)	End Moment Ratios	Remarks
A-1-0	SM50A	250	100	6	8	3000	1.0	annealed
A-1-1		250	100	6	8	3000	1.0	as-weld
A-1-2		250	100	6	8	3000	0.5	as-weld
A-2-0		250	100	6	8	4000	1.0	annealed
A-2-1		250	100	6	8	4000	1.0	as-weld
A-2-2		250	100	6	8	4000	0.5	as-weld
A-3-0		250	100	6	8	4500	1.0	annealed
A-3-1		250	100	6	8	4500	1.0	as-weld
A-3-2		250	100	6	8	4500	0.5	as-weld
B-1-0	SM50A	250	120	6	8	3000	1.0	annealed
B-1-1		250	120	6	8	3000	1.0	as-weld
B-2-0		250	120	6	8	4000	1.0	annealed
B-2-1		250	120	6	8	4000	1.0	as-weld
B-3-0		250	120	6	8	4500	1.0	annealed
B-3-1		250	120	6	8	4500	1.0	as-weld
C-1-0	SM50A	300	100	6	8	3000	1.0	annealed
C-1-1		300	100	6	8	3000	1.0	as-weld
C-2-0		300	100	6	8	4000	1.0	annealed
C-2-1		300	100	6	8	4000	1.0	as-weld
C-3-0		300	100	6	8	4500	1.0	annealed
C-3-1		300	100	6	8	4500	1.0	as-weld
D-1-0	HT80	250	100	7	10	2500	1.0	annealed
D-1-1		250	100	7	10	2500	1.0	as-weld
D-1-2		250	100	7	10	2500	0.5	as-weld
D-2-0		250	100	7	10	3000	1.0	annealed
D-2-1		250	100	7	10	3000	1.0	as-weld
D-2-2		250	100	7	10	3000	0.5	as-weld
D-3-0		250	100	7	10	3500	1.0	annealed
D-3-1		250	100	7	10	3500	1.0	as-weld
D-3-2		250	100	7	10	3500	0.5	as-weld
E-1-0	HT80	250	120	7	10	2500	1.0	as-weld
E-2-0		250	120	7	10	3000	1.0	as-weld
E-3-0		250	120	7	10	3500	1.0	as-weld
F-1-0	HT80	300	100	7	10	2500	1.0	as-weld
F-2-0		300	100	7	10	3000	1.0	as-weld
F-3-0		300	100	7	10	3500	1.0	as-weld

d = beam height, b = flange width, t = flange thickness, t_w = web thickness, L = beam length

Table 1 (b) Dimensions of test girders

Test Girders	Steel	d (mm)	b (mm)	t_w (mm)	t (mm)	L (mm)	End Moment Ratios
G-A	SM50A	1000	130	6	10	4100	1.0
G-B	SM50A	1000	120	6	8	4100	1.0
G-C	HT80	800	110	6	10	3300	1.0
G-D	HT80	800	110	6	10	2800	1.0
G-E	HT80	800	130	6	10	3300	1.0
G-F	HT80	800	130	6	10	2800	1.0
G-G	Flange HT80 Web SM50A	800	110	6	10	3300	1.0

Table 2 Initial imperfections of flanges

Test Beams and Girders	Upper flange δ_u (mm)	Lower flange δ_l (mm)	δ_u/L	δ_l/L
A-1-0	0	0	0	0
A-1-1	1.5	0	1/1960	0
A-3-1	4.5	0	1/1000	0
B-1-0	3	8	1/ 990	1/ 370
B-2-0	0	2	0	1/1985
B-3-1	0	6	0	1/ 745
C-1-0	1.5	1.5	1/1970	1/1970
C-1-1	4.8	6.8	1/ 620	1/ 435
D-2-0	0	0	0	0
D-2-2	0	0	0	0
D-3-1	2.5	0	1/1400	0
D-3-2	1	0	1/3470	0
E-2-0	1	0	1/2960	0
E-3-0	2.5	0	1/1390	0
G-A	1	1.5	1/4100	1/2720
G-B	1	5	1/4100	1/ 820
G-C	1	2	1/3300	1/1650
G-D	3	3	1/ 940	1/ 940
G-E	0	0	0	0
G-F	2	0	1/1400	0
G-G	0	1	0	1/3300

Table 3 Summary of reference and experimental loads

Specimens	M_y (t-m)	M_p (t-m)	M_{max} (t-m)	σ_{max} (kg/cm²)	M_{max}/M_y
A-1-0	8.18	9.45	7.69	3218	0.94
A-1-1			7.00	2929	0.86
A-1-2			9.70	4059	1.19
A-2-0	8.18	9.45	7.94	3322	0.97
A-2-1			6.61	2766	0.81
A-2-2			8.42	3523	1.03
A-3-0	8.18	9.45	6.33	2649	0.77
A-3-1			5.75	2406	0.70
A-3-2			8.54	3573	1.04
B-1-0	9.47	10.78	9.40	3406	0.99
B-1-1			8.00	2899	0.84
B-2-0	8.47	10.78	8.60	3116	0.91
B-2-1			8.76	3174	0.93
B-3-0	9.47	10.78	9.28	3362	0.98
B-3-1			7.10	2572	0.75
C-1-0	10.41	12.16	7.58	2493	0.73
C-1-1			9.20	3026	0.88
C-2-0	10.41	12.16	8.04	2645	0.77
C-2-1			6.88	2263	0.66
C-3-0	10.41	12.16	7.48	2461	0.72
C-3-1			6.89	2266	0.66
D-1-0	22.53	26.08	21.16	7373	0.94
D-1-1			20.89	7279	0.93
D-1-2			27.90	9721	1.24
D-2-0	22.53	26.08	20.68	7206	0.92
D-2-1			18.54	6460	0.82
D-2-2			23.10	8049	1.03
D-3-0	22.53	26.08	19.21	6693	0.85
D-3-1			16.24	5659	0.72
D-3-2			21.84	7610	0.97
E-1-0	26.14	29.84	26.46	7946	1.01
E-2-0	26.14	29.84	24.42	7333	0.93
E-3-0	26.14	29.84	22.79	6844	0.87
F-1-0	28.68	33.50	26.32	7191	0.92
F-2-0	28.68	33.50	22.42	6126	0.78
F-3-0	28.68	33.50	20.78	5678	0.73
G-A	71.68	106.32	43.6	1968	0.61
G-B	72.31	93.74	41.0	2160	0.57
G-C	113.90	128.81	64.4	4436	0.57
G-D	113.90	128.81	83.4	5748	0.73
G-E	126.15	140.23	94.8	5899	0.75
G-F	126.15	140.23	105.1	6540	0.83
G-G	113.90	128.81	65.5	4514	0.58

M_y = Calculated Yield Moment
M_p = Calculated Plastic Moment

Table 4 Comparison of theory and test for girders

Test Girders	Experimental	Theoretical							
		Lateral Buckling Strength					Ultimate Bending Strength		
			Residual Stress Patterns (A)		Residual Stress Patterns (B)		Residual Stress Patterns (C)		Residual Stress Patterns (D)	
	M_{exp} (t-m)	M_y (t-m)	$M_{cr}^{(t-m)}$	M_{cr}/M_{max}	$M_{cr}^{(t-m)}$	M_{cr}/M_{max}	$M_{u_1}^{(t-m)}$	M_{u_1}/M_{max}	$M_{u_2}^{(t-m)}$	M_{u_2}/M_{max}
G-A	43.6	87.55	56.63	1.30	49.82	1.14	48.75* 55.27**	1.12 1.27	44.38 52.79	1.02 1.20
G-B	41.0	55.52	51.32	1.25	46.99	1.15	41.09 47.30	1.00 1.15	38.17 44.46	0.93 1.08
G-C	64.4	69.53	68.75	1.07	68.75	1.06	53.27 58.39	0.83 0.91	51.20 57.37	0.80 0.89
G-D	83.4	96.06	83.60	1.00	75.87	0.91	54.29 78.96	0.65 0.95	52.45 76.99	0.63 0.90
G-E	94.8	114.16	93.83	0.990	81.39	0.86	— 90.54	— 0.96	— 85.43	— 0.90
G-F	105.1	137.99	99.31	0.95	82.40	0.78	76.79 99.24	0.73 0.94	74.93 93.66	0.71 0.91
G-G	65.5	67.60	67.10	1.02	66.62	1.02	— 48.65	— 0.74	— 47.72	— 0.73

* Upper line is for δ_u indicated in Table 2
** Lower line is for infinitesimal small u_o as $u_o = L_e/10{,}000$

Assummed Residual Stress Patterns

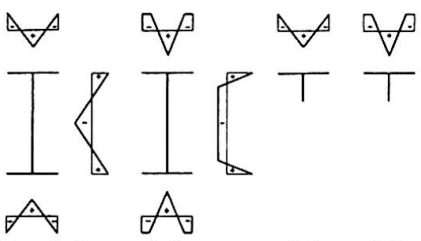

	(A)	(B)	(C)	(D)
σ_{rc}/σ_y	0.3	0.3	0.3	0.3
σ_{rt}/σ_y	0.3	1.0	0.3	1.0

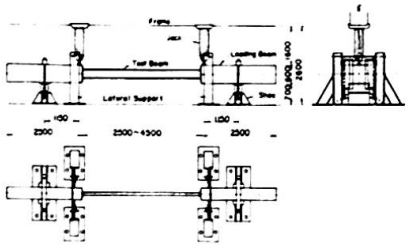

Test setup for beams

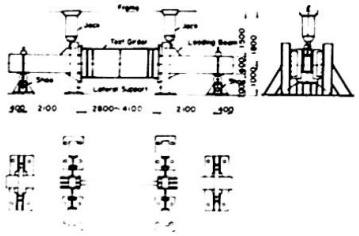

Test setup for girders

Fig. 1

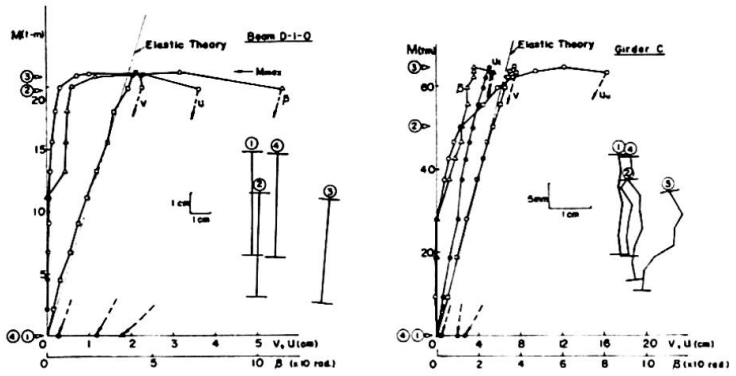

(a) (b)

Load-deflection curves

Fig. 3

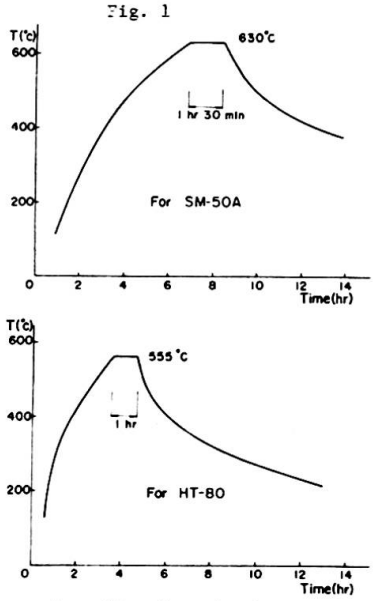

Annealing data for beams

Fig. 2

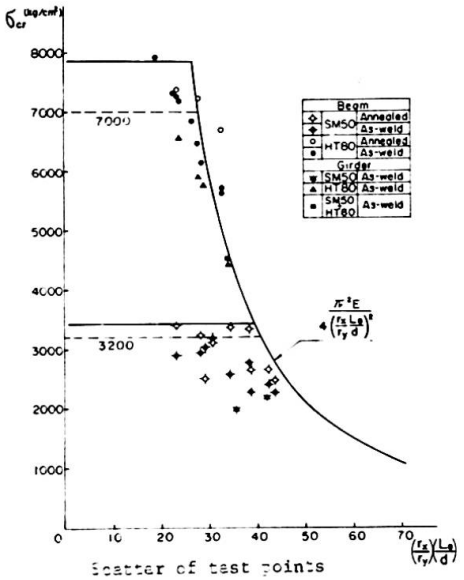

Scatter of test points

Fig. 4

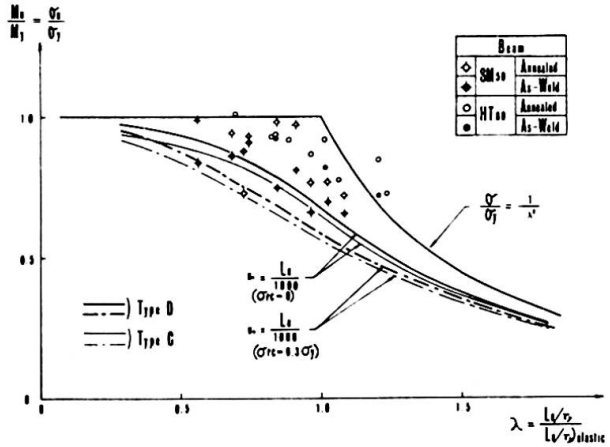

Comparison of the results by beam-column approach and test for beams

Fig. 5

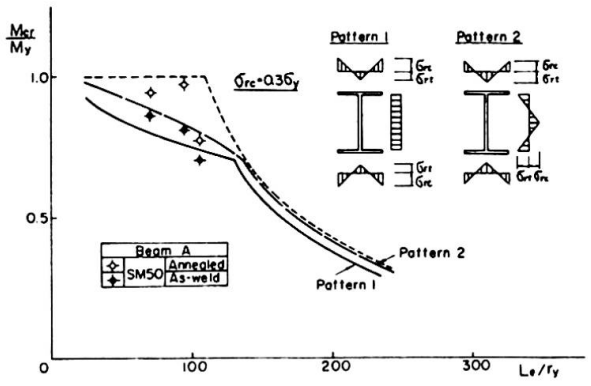

Comparison of the results by lateral buckling theory and test for beam A

Fig. 6

REFERENCES

1) Fukumoto, Y.and Kubo, M., "Lateral Buckling Strength of Girders with Bracing Systems", Preliminary Report, 9th Congress IABSE, Amsterdam, 1972.

2) Fukumoto, Y. and Kubo, M., "Lateral Buckling of Braced Beams", Trans. of Architectural Institute of Japan, No. 206, April, 1973.

3) Fukumoto, Y., Fujiwara, M. and Watanabe, N., "Inelastic Lateral Buckling Tests on Welded Beams and Girders", Proc. of Japan Society of Civil Engineers, No. 189, May, 1971.

4) Fukumoto, Y., et al, "Research Works on Ultimate Strength of Plate Girders, and Japanese Provisions on Plate Girder Design, "Design of Plate and Box Girders for Ultimate Strength", IABSE Colloquium, Proc. Volume II, London, 1971.

5) Fukumoto, Y. and Kubo, M., "Ultimate Bending Strength of Plate Girders with Longitudinal Stiffeners failed by Lateral Instability", to be published from Der Stahlbau.

6) Basler, K. and Thürlimann, B., "Strength of Plate Girders in Bending", Journal of Structural Division, ASCE Vol. 87, No. ST 6, August, 1961.

7) Yoshida, H.,"Lateral Buckling Strength of Plate Girders", Publications, IABSE Vol. 35-II, 1975.

SUMMARY

This report presents the results of an extensive experimental investigation into the behaviour and strength of flexural members with high strength steels which are failed by lateral buckling. A total thirty-six beam-type and seven girder-type members is tested under uniform moment and moment gradient. Test results of as-weld and annealed specimes are compared with the inelastic lateral buckling theory with the specified residual stress patterns and also with the beam-column approach to ultimate bending strength using the effective compressive section with initial imperfections.

RESUME

Ce rapport présente les résultats d'essais détaillés sur le comportement de la résistance d'éléments en acier à haute résistance soumis à la flexion, et qui ont été détruits par déversement. Les essais de spécimens soudés et recuits ont été comparés selon la théorie du déversement, en fonction des contraintes résiduelles, ainsi que selon l'approche "poutres-colonnes" pour le moment fléchissant de rupture, considérant la section effectivement comprimée avec des imperfections initiales.

ZUSAMMENFASSUNG

Dieser Bericht enthält die Resultate einer ausführlichen experimentellen Untersuchung über das Verhalten und die Tragfähigkeit von Biegeträgern aus hochfesten Stählen, die durch Kippen zerstört wurden. Eine Gesamtheit von 36 Trägertypen und 7 Balkenträgern wurden unter konstanten, linear verlaufenden Biegemomenten getestet. Testresultate von geschweissten und spannungsarm geglühten Proben wurden mit der unelastischen Kipptheorie und den bezeichnenden Eigenspannungsverteilungen und ebenso mit einer Näherungsuntersuchung als exzentrischem Knicken verglichen, indem die effektiv zusammendrückenden Abschnitte mit anfänglichen Imperfektionen verwendet werden.

Study on Hybrid Girders

Etude de poutres hybrides

Studien über hybride Tragbalken

TETSUO KUNIHIRO SHOICHI SAEKI KEIICHI INOUE
Public Works Research Institute
Ministry of Construction
Tokyo, Japan

Introduction

Different from the universally used homogeneous girders (girders made homogeneously with the same grades of steel), the hydrid girder is made of different grades of steel in its upper and lower flanges and web. Cost of materials for a hybrid girder can be reduced by using high-strength steel for upper and lower flanges which are effective for the flexural rigidity and using mild steel for the web. It has been made known that the hybrid girder is by no means inferior in bending strength to the homogeneous girder in which high-strength steel is used for both flanges and web of the same section, and that by using mild steel for the web the hybrid girder can be made economical.

Provisions on the design for hybrid girders have already been enforced in the U.S.A. In Japan provisions on this kind of girders will be provided for in the specifications for highway bridges in the near future.

Introduced hereunder are the results of researches continuously conducted on this kind of girders by the Public Works Research Institute, Ministry of Construction.

1. Economical Efficiency of Hybrid Girders

Haaijer has published his thesis on the economical efficiency of the hybrid girders. Reffering to this thesis, the ratio of cost of a hybrid girder to that of homogeneous girder (Chy/Cho) is expressed by the following formula in case where the hybrid girder is fitted with symetrically arranged upper and lower flanges having same bending strength (Mp).

$$\frac{C_{hy}}{C_{ho}} = \eta \left(\frac{h_{hy}}{h_{ho}}\right)^2 \cdot \frac{2\beta - \gamma}{\beta} \qquad (1)$$

where, $\frac{h_{hy}}{h_{ho}} = \left(\frac{\psi\gamma}{2\beta-\gamma}\right)^{1/3}$

$\psi = \dfrac{\text{Wed yield stress of homogeneous girder}}{\text{Web yield stress of hybrid girder}}$

$\eta = \dfrac{\text{Unit price of steel grade for the web of hybrid girder}}{\text{Unit price of steel grade for the web of homogeneous girder}}$

$\beta = \dfrac{\text{Flange yield stress of hybrid girder}}{\text{Web yield stress of hybrid girder}}$

$\gamma = \dfrac{\text{Unit price of steel grade for the flange of hybrid girder}}{\text{Unit price of steel grade for the Web of hybrid girder}}$

Using the above formulae and unit prices in 1971 and in 1975, cost was compared between the hybrid girders in which steel grades of SM41, SM50 were used for the webs and SM50Y, SM58, HT70, HT80 (Table 1) for flanges and the homogeneous girders. The results are shown in Fig. 1. The results show that a maximum of 13% cost down can be obtained with the steel up to SM58 as provided for in the specifications for highway bridges by 1971's prices, but that the hybrid girders don't make

Table 1. Mechanical Property of Steel

Grades of Steel	Yielding point (kg/mm)	Tensil strength (kg/mm)
SS 41	24	41
SM 50	32	50
SM 50 Y	36	50
SM 58	46	58
HT 70	56	70
HT 80	70	80

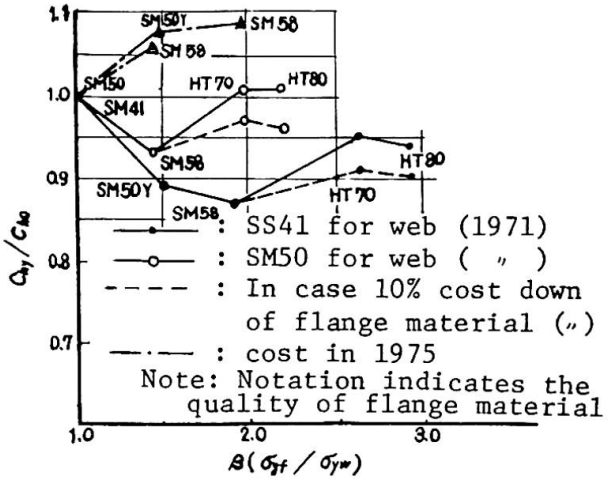

Fig. 1 Relations between β and C_{hy}/C_{ho}

economical efficiency due to the relative reduction of prices of SM50Y and SM58 in 1975.

As steel products under the grade of SM58 is so popular that the unit prices of these steels have been reduced in Japan, the hybrid girder is not superior economically, but when unit price of ultra high strength steel as HT80 is reduced in future, this type of girder will be superior economically.

Apart from the foregoing, economical efficiency is under study as to the girders made under the standards (draft) drawn up by our research institute for the hybrid plate girders.

2. Design Problems in Hybrid Girders

As mentioned already, different grades of steel are used respectively for the flanges and webs of hybrid girders. Therefore, in the case of the hybrid girders, the webs start yielding before the flanges do it, while in the case of the homogeneous girders yielding stresses both in webs and flanges are equal. This means that when the flange of the hybrid girder starts yielding, not a small part of the web has already yielded. Thus, under a load for which the flanges are still in elastic region, part of the web has already yielded and thereby gives rise to problems on the following 4 points as viewed comparatively with the homogeneous girder.

(i) Bending characteristics (ii) Buckling
(iii) Fatigue strength (iv) Design on field joint

With reference to the bending characteristics, buckling of compression flanges and fatigue strength, results of experiments carried out by the Public Works Research Institute will be explained in paragraphs 3, 4 and 5.

As regards another problem of web buckling, the minimum thickness of the web plate, that is subject to bending and shearing, is determined from the following formula in the existing highway bridge specifications.

$$\left(\frac{b}{t}\right)^2 \geq \frac{\nu_B \sigma_c}{(1378\,K)^2}\left\{\frac{1+\psi}{4k_\sigma}+\sqrt{\left(\frac{3-\psi}{4k_\sigma}\right)^2+\left(\frac{\eta}{k_\tau}\right)^2}\right\}$$

ν_B : Buckling safety factor $1.25+(0.30+0.15\psi)e^{-4.3\eta} < 1.25$

$K = 0.09 - 0.10\psi$

k_σ : Buckling coefficient for fiber stress intensity

k_τ : Buckling coefficient for shearing stress intensity

μ : Poisson's ratio

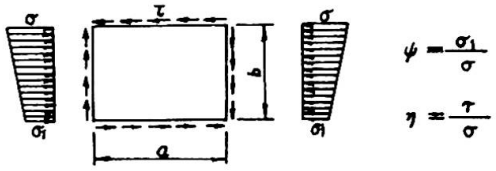

If this concept can be extended, the normal value of the minimum plate thickness becomes $1/\sqrt{R}$ times thicker. In this respect, experimental proving may be necessary. Here, R is the reduction factor of the allowable stress adopted in the AASHTO's specifications for highway bridges or the ratio between the stress obtained from the section modulus calculated for the homogeneous girder and the actual stress of the hybrid girder. This ratio can be expressed by the following formula if the flange thickness is disregarded.

$$R = 1 - \frac{\beta\psi(1-\alpha^2)(3-\psi+\psi\alpha)}{6+\beta\psi(3-\psi)},\quad \alpha = \frac{\sigma_{yw}}{\sigma_{yf}},\quad \beta = \frac{2A_w}{A_f},\quad \psi = \frac{\bar{x}}{h}$$

In designing the field joints we are confronted with a problem of how to deal with the reduction of the axial force in the high strength bolts at the yielding part of the web. Our research institute has been doing the experiments thereof.

3. Experiments on Bending Characteristics of Hybrid Girders

Referring to the results of studies both at home and abroad on the plate girders, especially those for hybrid girders static load tests were conducted using a total of 8 specimens which were composed of 2 girders each of the following types 1 and 2 (shown in Fig. 3) and 2 girders each of the following modified girders of types 1 and 2 (shown in Fig. 4).

Type 1: A girder whose flanges were made of SM58 and web SS41 and the depth/thickness ratio (D/T) of the web was 160.

Type 2: A girder made of same construction but the depth/thickness ratio of the web was 200.

Modified girder: Above types 1 and 2 fitted with a slab to prevent local buckling of the compression flanges and transverse buckling of the girder.

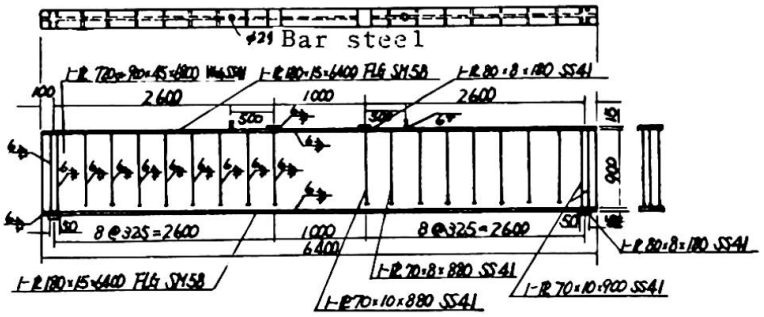

Fig. 3 Bending Test Specimen (Type G)

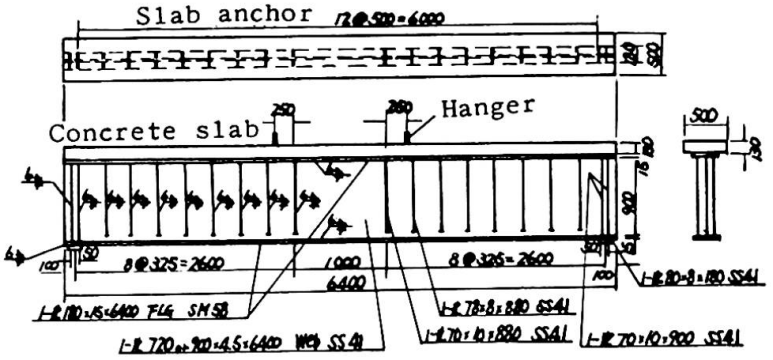

Fig. 4 Bending Test Specimen with Slab (Type GS)

Table 2 shows the moment inertia, section modulus and various load values for all girders. Fig. 5 shows the loading methods. The results of test on materials used are shown in Table 3. The load-deformation curves for all test specimens are shown in Fig. 6.1 - Fig. 6.2. In the case of the test specimens made of steel alone, experimental values retains linear relations until the load (Fa in the Fig. 6) comes up to the allowable stress of the flange. Thereafter, the linear relations come to be broken gradually. This suggests that yielding of the web occurs earlier than expected at a point lower than the yielding load of the web due to the effects of the residual stress, etc. Then, deformation becomes serious rapidly and collapse occurs (shown in Fig. 6.1). Collapse was

Table 2. Section Performance and Value of Load

Type	Moment inertia (cm^4)	Section modulus (cm^3)	Standardized values of loads: Web yielding load (Wy) (ton)	Flange allowable load (Fa) (ton)	Flange yielding load (Fy) (ton)	Perfect plastic moment load (Mp) (ton)	Measured values of loads: Web yielding load	Flange yielding load	Perfect plastic moment load
G1 GS1	86.937	2,318.32	42.72	46.37	78.21	80.53	62.4	110.2	113.4
G2 GS2	140.373	3,018.77	55.19	60.38	100.69	103.53	81.2	142.0	146.2

Table 3. Results of Tension Test on Materials

Grades of steel	Thickness (mm)	Allowable stress intensity in the highway bridge specifications (kg/mm²)	Yield strength (kg/mm²)	Tensile strength (kg/mm²)	Elongation (%)
SM 58	8	26.00	61.4	67.6	13.1
	6	26.00	63.1	68.6	13.9
SS 41	8	14.00	26.8	44.7	29.6
	6	14.00	29.2	43.8	26.5
	4.5	14.00	27.9	46.7	25.3

supposed to be a result of transverse buckling in type G1 and vertical buckling on the web near the loading point in type G2. In the case of type GS1 (non-composite girder) with the slab, composition of the slab and the steel girder came to be broken gradually beginning near the supports and corrugations appeared in the tension field, indicating shear buckling in the web between the loading point and the support. The concrete near the loading point collapsed when load went beyond the perfect plastic moment. Then, the steel girder beneath that part turned to be a plastic hinge and the whole body collapsed (photo 1). Type GS2 showed the same behaviors as those of type GS1 until the occurrence of shear buckling in the web. Thereafter, cracks occurred running parallel to the girder on the slab concrete and the concrete on one side came off. Under a load a little lower than the perfect plastic moment, transverse buckling occurred on the whole body of the girder.

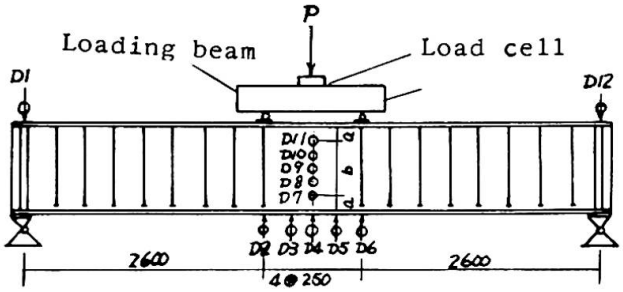

Fig. 5 Loading method for Bending Test

Above behaviors can be summarized as follows:

i) Either of type G1 or G2 girder shows elastic behavior unitl the load reaches the allowable stress intensity of flanges.

ii) In the case of test specimens, types GS1 and GS2, in which transverse buckling is prevented by the attached slab, the slab concrete works well to prevent the local buckling and transverse buckling in flanges, suggesting that the hydrid girder has a bending strength up to the load for the perfect plastic moment.

iii) From the above 2-point views, it is considered that hydrid girders may well be designed on the basis of the yield stress intensity of flanges.

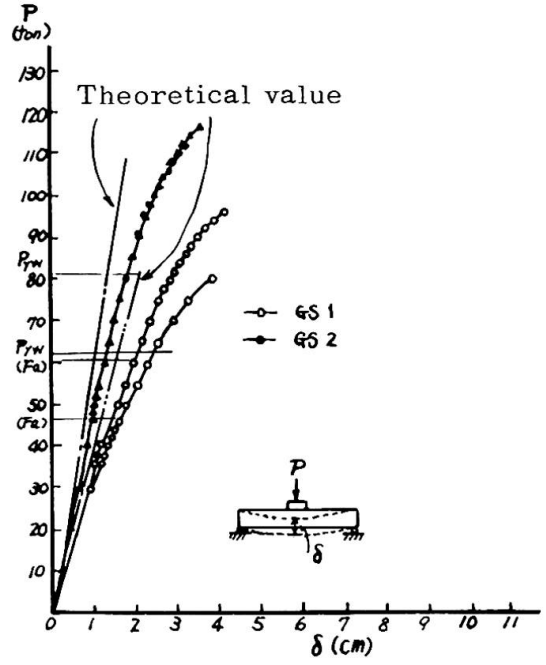

Fig. 6.1

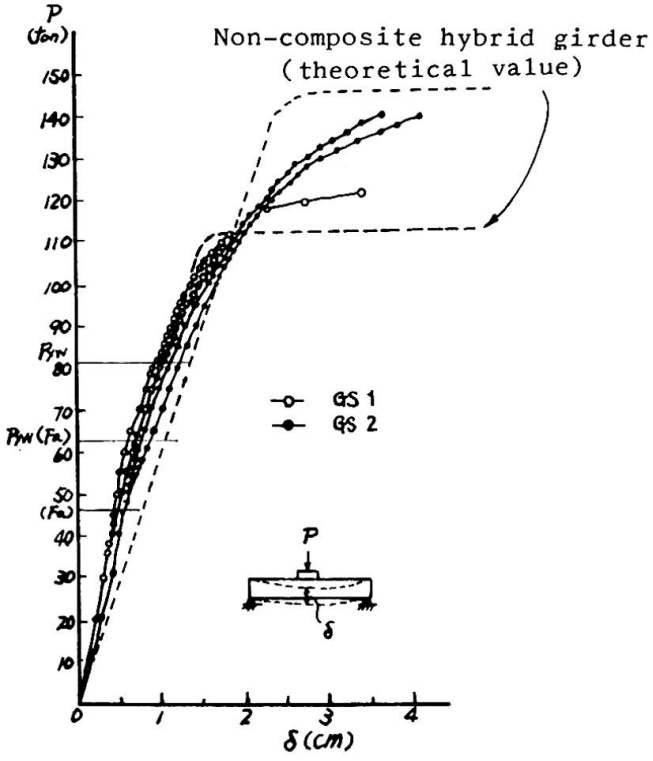

Fig.6.2

4. Buckling

Among three patterns of buckling, (1) transverse buckling, (2) local buckling in compression flanges and (3) web buckling, local buckling in compression flanges was studied.

The web of a homogeneous girder, which is within the elastic region, works as a supporting member against the local buckling in a compression flanges, but in the case of hydrid girder whether or not the web works as a supporting member was left unknown. Thereupon, compression test was conducted using a cross column

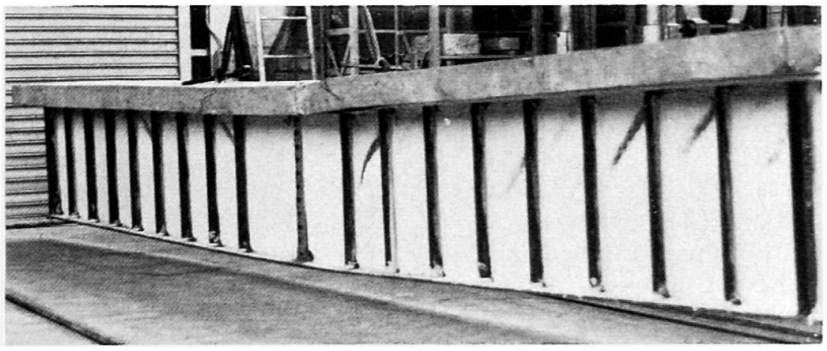

Photo.1

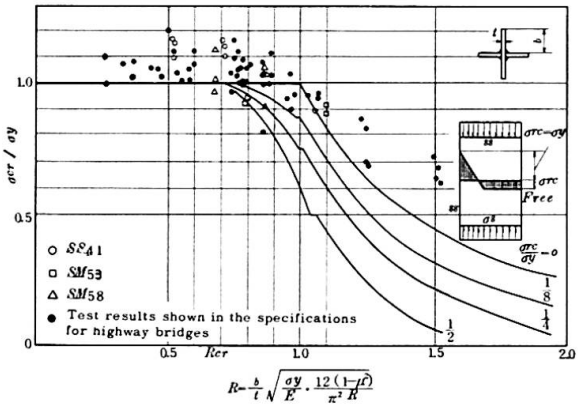

Fig. 8 Buckling Curve for Compression Hybrid Column

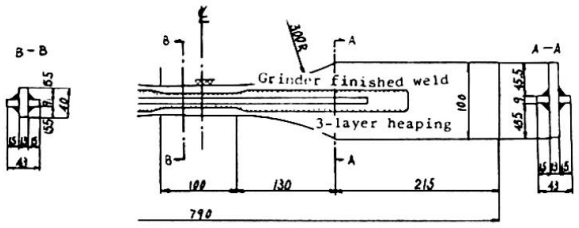

Fig. 9 Tension and Fatigue Test Piece of Hybrid Material

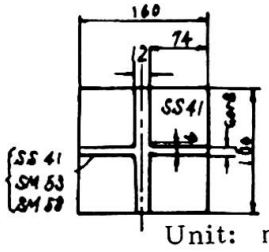

Fig. 7 Hybrid Column Compression Test Piece

made of 3 grades of steel, SS41, SM53 and SM58 combined. The shape and dimensions of the testpieces are shown in Fig. 7.

The results of compression test on the homogeneous cross columns collected for the specifications of the highway bridges and the results of compression test on the hybrid cross columns thus made are shown in Fig. 8.

From Fig. 8 it may well be considered that the local buckling strength of a free-projecting part of the hybrid girder is the same exactly with that of the homogeneous girders.

5. Fatigue

An important problem in comparing a hybrid girder with homogeneous girder was concerned with the fillet weld (longitudinal fillet weld) to connect the web to the flange in the neighborhood of which the web is in a condition of high stress. Accordingly, fatigue test was made on the tension test piece of the hybrid girder made of SS41 combined with HT80 as shown in Fig.9.

A HT80 plate, 13mm in thickness, was assumed to be a flange and a SS41 rib to be a web. In order to avoid lopsided loading, ribs were fitted on both sides of the plate, and the test piece was made applying manual flat welding after pre-hearing of the part at 100°C or over.

The welding rod used was low-hydrogen electrodes in use for 60 kg/mm^2 strength high tension steel. Perfect pulsating tension fatigue tests were made pay ing special attention to the fillet weld parts of HT80 flange and SS41 web. The test results are shown in Fig. 10.

The relation between the total amplitude of the stress

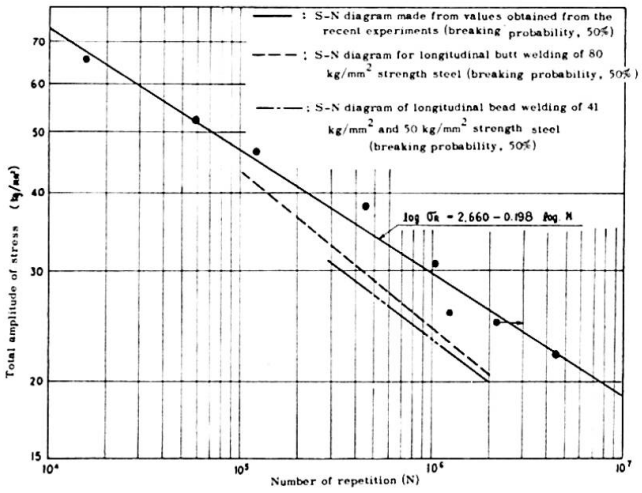

Fig.10 S-N Diagram of Hybrid Material

σ_R (kg/mm^2, in calculation of the stress, the section of the base metal was considered in disregard of that of the weld metal) and its number of repetition (N) was obtained as follows by the method of least square

$$\log \sigma_R = 2.660 - 0.198 \log N$$

The value of fatigue strength is a little higher than that in the data on fatigue strength obtained in the past in the longitudinal fillet weld applied to mild steel of 40 kg or 50 kg/mm^2 strength steel and 80 kg/mm^2 strength steel.
From the foregoing, the fillet weld fatigue strength of flanges and webs of hybrid girders can be regarded same as that of homogeneous girders.

6. Conclusion

1) According to the combination of several grades of steel, hybrid girders become economical occasionally more than 10 percent as compared with homogeneous girders.
2) Hybrid girders can be designed on the basis of the yield stress intensity of flanges.
3) As the local buckling on the compression flange is considered same as in the case of homogeneous girders, the existing provisions can be applicable to the thickness of outstanding parts of the compression flanges.
4) The fatigue strength of the fillet weld portion connecting the web to the flange can be regarded same as that of homogeneous girders.

Postscript

Mentioned above are the results of our experiments on the bending characteristics, buckling and fatigue that occurred in hybrid girders.

Under judgement that from the foregoing it is possible to make out the design standards for the hybrid highway bridges based on the provisions of the existing specifications for highway bridges, we have been proceeding with the work therefor. At the same time we will continue studies on the aforementioned problematical points left unsolved.

Furthermore, we plan to compare from economical viewpoint the bridges made under said standards with those built under the existing standards, and then enter into further details of the economical efficiency of the hygrid girders.

SUMMARY

Economic efficiency and design problems of hybrid girders are studied. It is economical when mild steel and strength steel exceeding 58 kg/mm2 are combined. Bending behaviour, buckling strength of compression flanges and fatigue strength of fillet welds between flanges and webs for hybrid girders are studied. As a result, hybrid girders can be designed by extending the present design methods on homogeneous girders.

RESUME

Une étude a été faite au sujet des problèmes d'économie et de conception des poutres hybrides. Lorsque l'acier doux et l'acier ayant une résistance de plus de 58 kg/mm2 sont associés, une économie peut être réalisée. Le comportement à la flexion, la résistance au flambage des ailes comprimées et la résistance à la fatigue des soudures entre les ailes et les âmes ont été étudiées pour les poutres hybrides. Le résultat montre qu'il est possible de calculer des poutres hybrides en appliquant la conception actuelle pour les poutres homogènes.

ZUSAMMENFASSUNG

Wirtschaftlichkeit und Entwurfsprobleme von hybriden Tragbalken werden untersucht. Wenn Baustahl St 37 und Stahl mit einer Festigkeit über 58 kp/mm2 kombiniert werden, ist dies wirtschaftlich. Das Biegeverhalten, die Kippsicherheit und die Dauerfestigkeit der Kehlnähte zwischen den Flanschen und Stegen der hybriden Tragbalken werden untersucht. Daraus folgt, dass hybride Tragbalken durch Erweiterung der vorliegenden Entwurfsmethoden auf homogene Tragbalken angewendet werden können.

Structural Behaviour of Hybrid Plate Girders in Bending. Application to Actual Bridges

Comportement à la flexion de poutres à âme pleine hybrides. Application aux ponts actuels

Biegeverhalten von hybriden Vollwandträgern. Anwendung im Brückenbau

Y. MAEDA
Professor of Civil Engineering
Osaka University
Suita, Osaka, Japan

M. ISHIWATA
Senior Engineer
Kawasaki Steel Co., Ltd.
Tokyo, Japan

Y. KAWAI
Research Engineer
Kawasaki Steel Co., Ltd.
Chiba, Japan

I Introduction

At the IABSE London Colloquium in 1971, the ultimate strength of hybrid girders was discussed, and especially the fatigue study on thin-walled hybrid girders was encouraged.

The present study is intended to discuss the static and fatigue behavior of thin-walled, stiffened hybrid girders based on the results of tests carried out at Osaka University. Furthrmore, to apply the hybrid girder to long-span bridges, its design and economy are discussed with actual and design illustrations.

II Structural Behavior and Strength

II-1 Static Behavior and Strength

The overall flexural behavior of thin-walled hybrid girders consisting of WES-HW70, JIS-SM58 and JIS-SS41 in tension flange, compression flange and web, respectively, (1) is summarized in Fig. 1 in terms of the relation between applied bending moments and measured curvatures, to study on the influence of web slenderness ratios on the static flexural behavior. In Fig. 1, the calculated moment-curvature curves taking into account measured residual stresses and those neglecting the residual stresses are also given to show the effect of residual stresses. It can be seen in Fig. 1 that the girders with web slenderness ratios less than about 200 will behave like stocky beams owing to single horizontal stiffener located at one-fifth of the web depth, and that the test curves agree fairly well with the calculation curves with residual stresses. In the case of more slender girders of which web slenderness ratio exceeds about 250, however, the additional decrease of rigidity caused by web buckling diverts the test curves from the calculation curves.

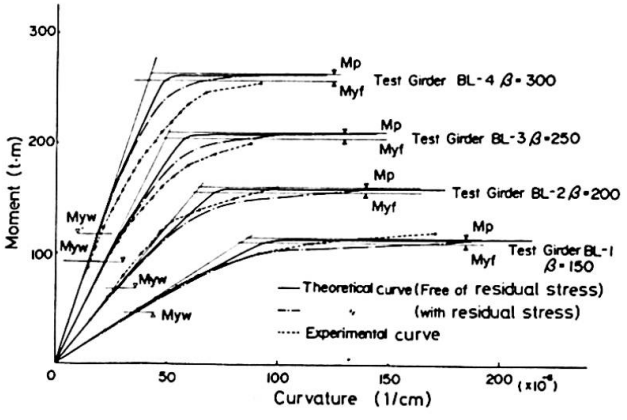

Fig. 1. Moment v.s. curvature curve

Table 1. Ultimate strength and reference loads

Girder	α	β	M_u/M_u^*	M_u/M_{yw}^{th}	M_u/M_{yf}^{th}	M_u/M_p^{th}
AL 1	0.5	141	1.18	3.42	1.18	1.16
BL 1	1.0		1.23	3.29	1.23	1.11
AL 2	0.5	188	1.10	3.09	1.10	1.08
BL 2	1.0		1.09	3.09	1.09	1.06
AL 3	0.5	232	1.15	3.14	1.15	1.12
BL 3	1.0		1.07	2.97	1.07	1.05
AL 4	0.5	281	1.05	2.72	1.01	0.99
BL 4	1.0		1.04	2.70	0.99	0.97

α : Aspect ratio of test panel, β: Web slenderness ratio

M_u^{th}: Experimental ultimate moment, M_u^*: Predicted ultimate moment

M_{yw}^{th}: Theoretical web yield moment,

M_{yf}^{th}: Theoretical flange yield moment

M_p^{th} : Theoretical fully plastic moment

The experimental ultimate loads and the several reference loads calculated by the ordinary beam theory are shown in Table 1, which indicates that the limiting web slenderness ratio β with which a girder carries its theoretical flange yield moment is 323 and 289 for the aspect ratio α of 0.5 and 1.0 respectively. In Table 1, there are also the ultimate bending moment M_u^* predicted by a formula (1) which can estimate the decrease of resisting moment due to web buckling, and such prediction seems to be conservative.

According to the AASHTO Specifications (3), an allowable stress in a tension flange should be reduced depending upon the spreading of web yielding so that the slight decrease of rigidity of a girder due to web yielding can be estimated in design. Since such reduction, however, is derived from stress distribution on a cross section when its tension flange yields, yielded region in the web can be controlled relatively small to a primarily assumed extent in design. In Table 2, comparisons among the experimental ultimate moment (1), the design allowable moment and also the design ultimate moment to be examined at the assumed ultimate state in Load Factor Design (3) are shown. It is revealed that the experimental ultimate moment agrees well with the design ultimate moment and amounts to more than twice as much as the design allowable moment.

II-2 Fatigue Behavior and Strength

Concerning static behavior and strength, it proved that a thin-walled hybrid girder with a web slenderness ratio less than about 290 could be dealt with as a homogeneous girder, only considering the slight decrease of rigidity due to web yielding. On structural behavior under repeated bending, however, the fatigue peculiar to a thin-walled plate girder that is caused by out-of-plane movement of a slender web, has been studied by Yen, Stallmeyer, Toprac and Maeda, etc.

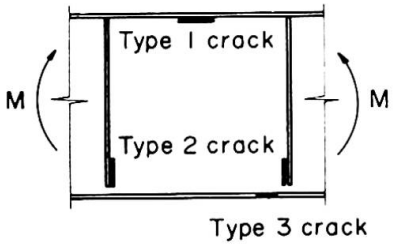

Fig. 2. Types of fatigue cracks under pure bending

Fig. 2 shows typical patterns of fatigue crack initiated in a hybrid girders subjected to pure bending. Among these types of crack, Type 1 cracks are the cracks above mentioned and were actually observed in the extensive fatigue tests of hybrid girders made by Toprac (8), who suggested that it is effective to use horizontal stiffeners and/or to limit the web slenderness ratio to be less than 200 for prevention of the initiation of Type 1 cracks.

In Table 3, the results of fatigue tests of six large-sized hybrid girders conducted by authors (13) are summarized together with parameters to evalulated the test results. All of the test girders failed due to Type 2 cracks initiated at the toe of vertical stiffener-to-web fillet welds. Type 1 crack and Type 3 crack were also observed in Girders B4-L1 and B3-L1, they were not a governing crack to cause the failure of the girders.

The regression analysis based on the method of least squares for the test results obtained by authors (10) and Toprac (8) with regard to the initiation of Type 2 cracks, gives the fatigue strength

Table 2. Comparisons of ultimate moment with design moment

Girder	M_u^{ex}	AASHTO R	AASHTO F_{all}	AASHTO M_{all}	AASHTO M_u	M_{yw}	M_u^{ex}/M_{all}	M_u^{ex}/M_u
AL 1	130	0.86	30.9	47.7	104	38	2.73	1.25
BL 1	125						2.62	1.20
AL 2	170	0.83	29.9	66.9	146	55	2.54	1.16
BL 2	170						2.54	1.16
AL 3	232	0.81	29.0	87.1	191	74	2.66	1.22
BL 3	220						2.52	1.15
AL 4	258	0.79	28.4	109.5	240	95	2.36	1.08
BL 4	257						2.35	1.07

M_u^{ex}: Experimental ultimate moment (t·m)
M_{all}: Allowable bending moment (service load design) (t·m)
M_u: Design ultimate moment (load factor design) (t·m)
R : Reduction factor
M_{yw}: Experimental web yield moment (t·m)
F_{all}: Allowable stress in tension flange (kg/mm^2)

Table 3. Test parameters and test results

Test Girder	β	γ/β^*	S_r	R	Type of crack, N_c Type 1	Type 2	Type 3	Mode of failure
B4L1	413	1	21.1	0.221	46.5	34.1	—	Type 2
B4L7		7	23.1	0.209	—	24.3	—	Type 2
B3L1	310	1	a) 11.7	0.543	—	218.0	218.0	Type 2
B3L6		6	21.1	0.402	—	28.0	—	Type 2
B2L0	206	—	17.6	0.439	—	104.0	—	Type 2
B2L5		5	16.1	0.456	—	116.6	—	Type 2

β : Web slenderness ratio
γ/β^* : Relative rigidity ratio of horizontal stiffener
S_r : Stress range in tension flange (kg/mm^2)
R : Stress ratio, N_c : Number of cycles to crack ($\times 10^4$)
a) Maxmum stress was increased up to 35.1 kg/mm after 2,10cycles

at 2×10^6 cycles in terms of stress range with 12.9 kg/mm^2 (mean value) and 10.7 kg/mm^2 (95% confidence limit) which is more than 25% above the allowable stress range of 8.4 kg/mm^2 (Stress Category: C) at the AASHTO Specifications. It is recognized that the fatigue strengths due to Type 2 crack and Type 3 crack can be respectively compared to those of a transverse non-load carrying fillet welded joint and a longitudinal fillet welded joint (4,7). Since the fatigue strength at 2×10^6 cycles of the latter joint is 30 to 50% higher than that of the former joint. According to a great number of fatigue tests (11) , it may be concluded that Type 1 crack and Type 2 crack characterized the fatigue behavior of thin-walled hybrid girders with vertical stiffeners. As shown in Fig. 3, the test results of transverse non-load carrying fillet welded joints for several steel grades (12) agree well with those of Type 2 cracks at the girder tests (10), and the both fatigue strengths do not significantly differ from each other depending on the steel grades, covering 9 to 13 kg/mm^2. Consequently, it proves that a web in ordinary carbon steel is the most economical for a thin-walled hybrid girders as far as the fatigue strength is limited to the fatigue life of Type 2 crack.

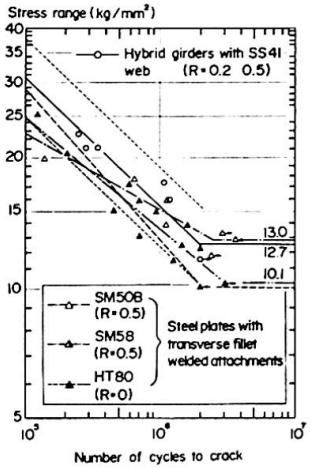

Fig. 3. S-N curves for Type 2 crack

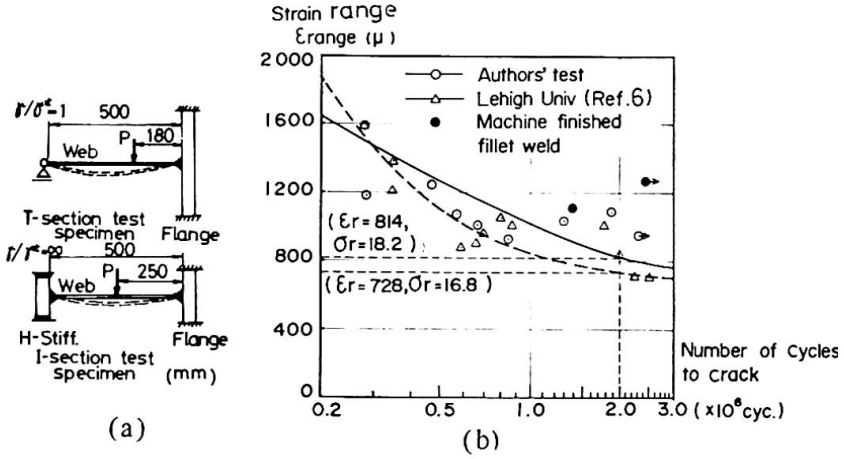

Fig. 4. Fatigue test results for Type 1 crack

On the other hand, few comparable tests for Type 1 crack have been carried out on model specimens of Type 1 crack, because of complicated cracking conditions. In Fig. 4, the relevent results obtained at fatigue tests made by Maeda (14) on model specimens of a web panel enclosed by a compression flange and a horizontal stiffener as shown in Fig. 4(a), are shown in terms of the number of cycles to crack initiation and the local strain range at the toe of fillet weld estimated by F.E.M. plate analysis combined with strain measurements. Available data of fatigue tests of large-sized plate girders conducted by Ostapenko (13) are also given, but they seem considerably dispersed, attributed to inevitable inherent indentations at the toe of fillet weld.

The fatigue strength at 2×10^6 cycles of the fillet weld under bending is estimated to be 814×10^{-6} in strain range or 18.2 kg/mm^2 in stress range with the regression analysis by the method of least squares. To examine the relation between the magnitude of out-of-plane deflection of a web and the fatigue lives of Type 1 crack, a non-dimensional parameter δ_r/h which represents the ratio of web deflection range to panel depth, is introduced. With this parameter the fatigue strength of Type 1 crack is rearranged graphically as shown in Fig. 5. The figure suggests that the magnitude of out-of-plane deflection of a web under a repeated live load should be limited to 1/350 of a web panel depth. To find out the governing

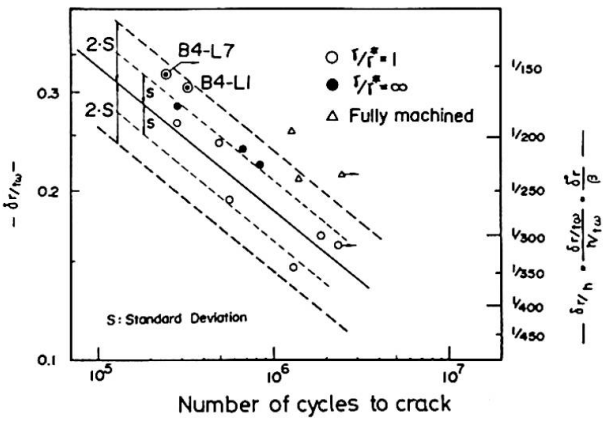

Fig. 5. Relation between magnitude of out-of-plane deflection of a web and fatigue lives of Type 1 crack

design criterion of Type 1 crack, it is desirable to develop the relevant fatigue data to induce the relation between the maximum initial web deflections, δ_0, and the out-of-plane movements, δ_r, under applied live loads in terms of $\delta_r/h = f(\sigma, \delta_0, \gamma/\gamma^*)$, where σ is the calculated bending stress at the extrem fiber of the web and γ/γ^* is the ratio of the relative rigidity ratio of the horizontal stiffener.

III Application of Hybrid Girders to Highway Bridges

Two composite hybrid girder bridges constructed in Japan are introduced in Table 4 as examples of actual highway bridges. Furthermore, including these bridges, the strength and economy of composite and non-composite hybrid girder bridges are discussed.

III-1 Design Problems

In design of hybrid girders, a reduction factor, R, specified at the AASHTO Specifications (3), was used to take into consideration the slight decrease of flexural rigidity due to web yielding; to prevent overstressing at erection, calculated dead load bending stresses at the extreme fiber of web, were limited to 80% of its specified yield stress; and web slenderness ratio were modified with a coefficient $\sqrt{R}$. It is found out that the reduction factor, R, is the most fundamental governing parameter to estimate a flange allowable stress, a web slenderness ratio and even economy of the hybrid girder, and that a further study on the reduction factor R is required.

Regarding fatigue design, it is proved that the initiation of Type 1 crack can be prevented as far as the web slenderness ratio discussed at the previous chapter, are used (1, 10), and Type 2 crack can be prevented if a calculated bending stress at the end of vertical stiffener does not exceed at an allowable fatigue stress at transverse non-load carrying fillet welds. In addition to these cracks, Type 3 crack will be kept away by well controlled welding operations.

III-2 Economy

In Japan, a number of structural steels in various grades can be put to practical use, and a choice of grade of steel, from JIS-SS41 to WES-HW80, is within a designer's choice.

Economy of hybrid girders was examined for hybrid composite girders and non-composite continuous girders in terms of overall costs for combination of different steel grades. The overall costs of the girders including material, fabrication and erection costs were calculated with the costs recommended at the Japan Bridge Construction Association (1972).

Table 4. Composite hybrid girder bridge in Japan

		ARAI Bridge	SORO Bridge
Span (m)		19.2	33.0
Steel sets	U.Flange	Center SM50	Center SM50Y
	Web	SS41	SS41
	L.Flange	HW70	SM58
Reduction factor		R=0.721 (SS41 - HW70)	R = 0.877 (SS41- SM58)
Completed time		June 1974	April 1976

Table 5. Design requirements

Loading	TL-20
Road width (m)	7.5 + 2X1.5 (footway)
Span (m)	26, 32, 36, 44
Web depth	$0.9h_w$, $1.0h_w$, $1.1h_w$
Steel sets	A, B, C, D, (Table 6)

h_w: Web depth of standard design

(1) Hybrid composite girders

Economical comparisons of hybrid composite girders with homogeneous ones were conducted under such design conditions as shown in Table 5. Structural proportions of homogeneous composite girders were designed based on the "Standard Design of Composite Girder Bridges (1972)", published at the Ministry of Construction in Japan.

The relationship between bridge spans and steel weights per unit area in various sets of steel with a girder depth of $1.0\,h_w$, are indicated in Fig. 6. A study of Fig. 6 reveals that the weight for all of the steel sets of the hybrid girders except 'A' are lighter than those of the homogeneous girders by the

standard design. Especially, the weight of the 'D' set is the lightest among the steel sets for spans longer than 38 meters.

A comparison of overall costs of the hybrid girders with those of the homogeneous girders for various steel combination in Table 6, is shown in Fig. 7 with regard to bridge spans.

It can be said that the economy of hybrid girders is noticeable for the steel combination of 'D', 'C', 'B' and 'A' in this order, and 'D' of which cost ratio (=hybrid/homogeneous) is 0.93, will be the most economical.

Table 6. Steel sets for comparative design

	Standard design	A	B	C	D
Upper flange	SM50Y	SM50	SM50	SM50	SM58
Web	SM50Y	SS41	SS41	SM41	SM41
Lower flange	SM50Y	SM50	SM58	HW70	HW70
Web hight	h_w	$0.9h_w$, h_w, $1.1h_w$			h_w

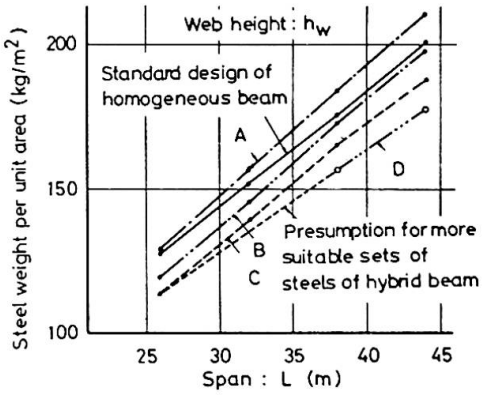

Fig. 6. Weight comparison of hybrid composite girders with homogeneous ones

(2) Three-span continuous non-composite girders

A cost comparison was carried out on three-span continuous non-composite girders with two kinds of equal span, namely 60 meters and 70 meters, under the same design requirements as the former examples. Girder depth in this comparison are fixed to one-twenty first of each span. Consequently, it is proved that hybrid girders can save 3% to 7% in overall cost more than homogeneous girders as shown in Table 7.

Table 7. Cost ratio (Hybrid/Homogeneous) for steel sets

		Homogeneous	Hybrid I	Hybrid II [a]
Steel set	U. Flange Web L. Flange	SM50Y SM50Y SM50Y	SM58 SM41 SM58	HW70(SM58) SM41(SS41) HW70(SM58)
3×60 m 180 m	Total weight (t)	495	465	428
	Cost ratio	1.00	0.94	0.97
3×70 m 210 m	Total weight(t)	671	627	586
	Cost ratio	1.00	0.93	0.97

a) ( ) is for section at center span

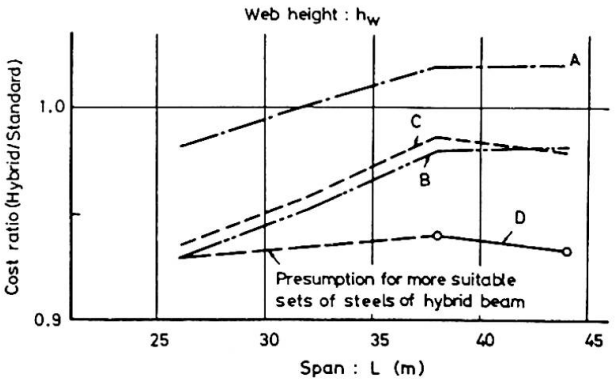

Fig. 7. Cost comparison of hybrid composite girders with homogeneous ones

IV Conclusion

It is concluded for the static behavior that the ultimate flexural strength of hybrid girders can be evaluated well by the reduction factor formula specified at the AASHTO Specifications and their flange yield moment can be carried with single horizontal stiffener up to their web slenderness ratio of about 320 and 290 for the aspect ratio of 0.5 and 1.0, respectively.

There is a possibility of initiation of Type 1 or Type 2 fatigue crack, but the former crack can be prevented for 2×10^6 cycles of loading by limiting out-of-plane movement of web, and the latter

crack by controlling a tensile web stress below the fatigue strength of transverse non-load carrying fillet welded joints.

It has been found out that hybrid girder bridges are generally more economic than homogeneous girder bridges in terms of overall cost, particularly at composite girder bridges, but in long-span continuous plate girders it is required to do more detailed comparison between hybrid and homogeneous girder bridges.

References

1) Y. Maeda and Y. Kawai, 18th Conf. of Bridge and Structual Eng. in Japan, 1971, p137
2) F. Nishino *et al.*, JSSC, Vol. 7, No. 71, 1971, p1-10, (*in Japanese*)
3) Standard Specifications for Highway Bridges, AASHTO, 11th Edit., 1973
4) W. H. Munse and J. E. Stallmeyer, Br. Weld J., 5, 188, 1960
5) T. R. Gurney and C. C. Woodley, Br. Weld J., Vol. 7, 1960 and Vol. 9, 1962
6) B. T. Yen, Fritz Eng. Lab. Rpt., No. 303.1, Lehigh Univ., Nov., 1963
7) L. R. Tall and J. E. Stallmeyer, Univ. of Illinois, C. E. Studies SRS, No. 279, 1964
8) A. A. Toprac and M. Natarajan, Proc. of ASCE, Vol. 97, ST4, 1971
9) Y. Maeda, IABSE Colloquium, London, 1971
10) Y. Maeda, M. Ishiwata and Y. Kawai, IIW. Doc. XIII-734-74, April, 1974
11) T. R. Gurney and S. J. Maddox, The Welding Institute Research Rpt., E/44/72, 1972
12) JSSC, Vol. No. 72, 1971 (*in Japanese*)
13) S. Parsanejad and A. Ostapenko, Lehigh Univ., Fritz Eng. Lab. Rpt. No. 156, Nov., 1970
14) Y. Maeda *et al*, Preprits Papers 30th Annual Conf. of JSCE, 1975 (*in Japanese*)

SUMMARY

For the purpose of optimum use of high-strength steels, static and fatigue behaviour of thin-walled, stiffened plate girders are studied. Design and economy of hybrid girders bridges are discussed with illustrations.

RESUME

Le comportement statique et de fatigue des poutres à âme pleine, mince et raidie est étudié en vue de l'utilisation optimum des aciers à haute résistance. Le calcul et l'économie de ponts à poutres hybrides sont discutés et illustrés.

ZUSAMMENFASSUNG

Zur optimalen Verwendung der Hochfestigkeitsstähle werden das statische Verhalten sowie Ermüdungsverhalten dünnwandiger und verfestigter Vollwandträger untersucht. Wirtschaftlichkeit der Vollwandträgerbrücken werden zusammen mit Bildern erörtert.

Fatigue Strength of Longitudinal Fillet Welded Joints in Hybrid Girders

Résistance à la fatigue des soudures d'angle, dans les poutres hybrides

Dauerfestigkeit der Längskehlnähte bei hybriden Vollwandträgern

T. YAMASAKI, General Manager
M. HARA, Senior Research Engineer
Y. KAWAI, Research Engineer
Steel Structure Research Laboratories, Kawasaki Steel Co., Ltd.
Chiba, Japan

I. Introduction

In this decade several investigations were conducted to study static and fatigue strength of hybrid girders in U. S. A. (1～6) and Japan(7～9), and some of these data were adopted into design specifications for U. S. highway bridges(10) and buildings(11).

On fatigue strength of hybrid girders, Toprac et al. pointed out based on their significant experimental study that there are three distinctive types of fatigue cracks, initiated at different locations and by different causes in hybrid girders under pure bending, as shown in Fig. 1. (5). Regarding Type 3 crack, Specifications for Highway Bridges in U. S. A. (10) specifies that stiffener to web and flange-web fillet weld connection shall be designed for fatigue based on the flange steel.

The purpose of the present work is to explore the data of fatigue strength of Type 3 crack in hybrid girders and to study the crack propagation behavior at tension flanges and webs. Test results obtained by model specimens are discussed on fatigue strength with reference to structural behavior of hybrid plate girders subjected to repeated bending by usual analytical procedures (S-N relations) and fracture mechanics.

II. Test Specimens and Procedures

Test specimens and test procedures were simulated to those proposed by Reemsnyder (13) by using tee-shaped hybrid specimens consisting of WES-HW70 (heat treated constructional alloy steel with minimum specified tensile strength of 80 kg/mm^2) at simulating flange plates and JIS-SS41(structural carbon steel with minimum specified tensile strength of 41 kg/mm^2) at simulating wed plates, under axial pulsating tension.

Ten axially loaded fillet welded tee-shaped specimens were tested at a stress ratio of $R=0.1(\fallingdotseq 0)$ (one of these was a large-sized specimen), and four were at a stress ratio of $R=0.5$. These specimens were submerged-arc welded with an intermediate strength filler metal-flux combination. The lower strength filler metal-flux combination than flange steel is preferred the fillet welding between constructional alloy steel and mild steel because of its economy and its

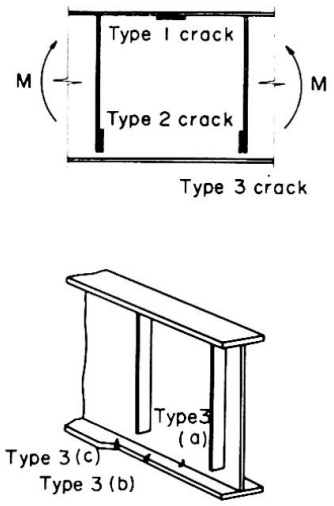

Fig. 1 Types of fatigue cracks under pure bending

ductility (7, 13). No non-destructive inspections, radiography or urtra-sonic inspection were performed before fatigue testing, assuming that the most unfavourable conditions exited. Details of the tee-specimens are shown in Fig. 2, and the mechanical properties and chemical compositions are summarized in Table 1.

All specimens were tested in 150-ton electro-hydraulic alternating testing machine at about 300 c.p.m. and applied stresses during fatigue test were monitored by dynamic strain measurements and a load cell and fatigue crack propagations were measured by using crack gauges when fatigue crack initiations were observed.

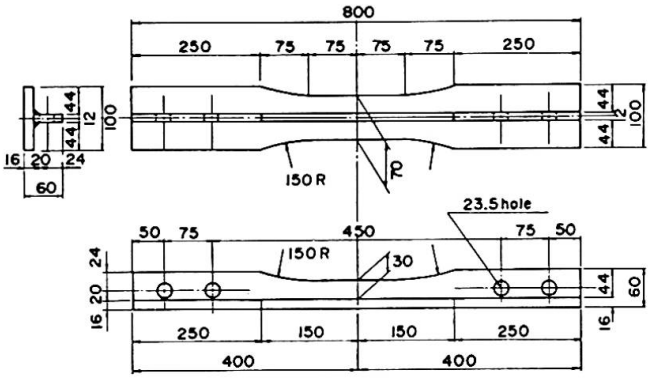

Fig. 2 Details of test specimen

Table 1. Mechanical properties and chemical compositions

	Thickness (mm)	Chemical Compositions (Wt %) C	Si	Mn	P	S	Cu	Ni	Cr	Mo	V	B	Ceq	Mechanical Properties Y.P. (kg/mm²)	U.T.S. (kg/mm²)	Elong. (%)	vE-0 (kg-m)
WES-HW70 (Base Plate)	16	0.100	0.30	0.85	0.007	0.010	0.19	0.78	0.46	0.33	0.035	0.004	0.45	80	84	32	15.6
JIS-SS41 (Rib Plate)	12	0.14	0033	1.17	0.009	0.021	—	—	—	—	—	—	—	29	47	35	—
Weld Metal (KW-101B)	φ4	0.06	0.24	1.45	0.013	0.009	—	0.77	—	0.41	—	—	—	57	66	26	—

III. Test Results and Discussion

III—1 Test Results

The fatigue test results are summarized in Table 2 and are shown graphically in Fig. 3. All the test results are discussed in relation to applied stress range at welds S_r and number of cycles to failure N_f.

Although the test results at different stress ratios of R=0 and R=0.5 are plotted irrespectively, the data fall in a certain scatter band. Judging from this fact, the effect of mean stress may be neglected in these stress ratios of 0 to 0.5. The regression analysis of all the present test results obtained by the method of least squares with reference to the number of cycles to failure and the stress range gives eq. (1).

$$\text{Log } N_f = 11.790 - 4.218 \text{ Log } S_r \quad \cdots\cdots\cdots\cdots\cdots\cdots \quad (1)$$

Table 2. Summary of Test Results

No	TEST PIECE	APPLYIED STRESS (kg/mm²) MAX (Smax)	MIN (Smin)	PANGE (Sr)	STRESS RATIO (R.)	FIRST OBSERVATION (×10⁴)	CYCLES TO FAIFURE (×10⁴)	CRACK INITIATION MODE[b]
1	T.P-No.1	25.9	2.7	23.2	0.1	—	124.50	N
2	T.P-No.2	28.8	2.8	26.0		88.11	91.65	W
3	T.P-No.3	33.8	3.2	30.6		24.85	26.17	N
4	T.P-No.4	20.8	2.2	18.6		—	267.2[a]	—
5	T.P-No.5	21.4	2.1	19.3		—	228.20	C
6	T.P-No.7	32.4	3.1	29.3		—	43.00	W
7	T.P-No.8	24.1	2.3	21.8		205.62	212.60	W
8	T.P-No.9	34.3	1.6	32.7		26.23	27.04	W
9	T.P-No.12	23.2	2.3	20.9		91.00	93.92	W
10	T.P-No.6	47.4	24.2	23.2	0.5	154.13	158.02	W
11	T.P-No.10	40.4	19.7	20.7		162.50	166.88	C
12	T.P-No.11	52.2	26.6	25.6		—	41.91	C
13	T.P-No.13	36.7	18.0	18.7		—	263.52[a]	—
14	T.P-No.14	19.5	1.7	17.8	0.1	—	257.00[a]	—

a) No failure

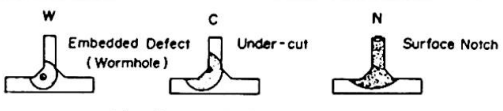

b) Crack Initiation Mode

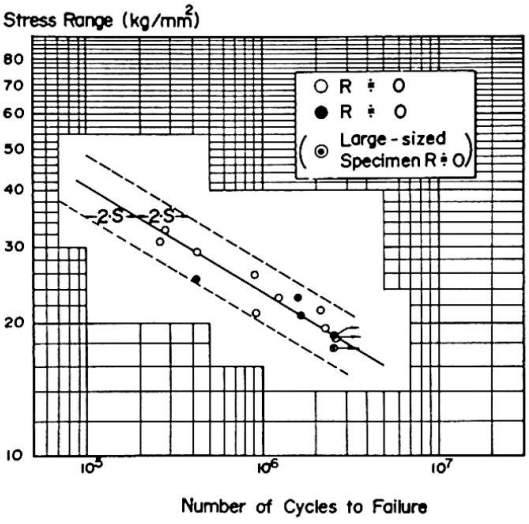

Fig. 3 Fatigue test results

The mean regression line is shown in Fig. 3 together with its confidence limits. The fatigue strength at 2×10^6 cycles in stress range are estimated at 20.0 kg/mm^2 (mean) and 16.9 kg/mm^2 (95% confidence limit). The behavior of cyclic specimens was very consistent in spite of the fact that yielding was occurred at web plates in the several specimens subjected to higher maximum stresses.

The observed crack initiation modes were divided into three types and the mode applying to any specimen is recorded in Table 2 and typical fracture surface of three types of crack initiations are shown in Figs. 4 to 6. Among these initiation modes, the most frequent initiatition was type W, and this fact agreed with the fatigue test results of homogeneous beams by Fisher et al. (14).

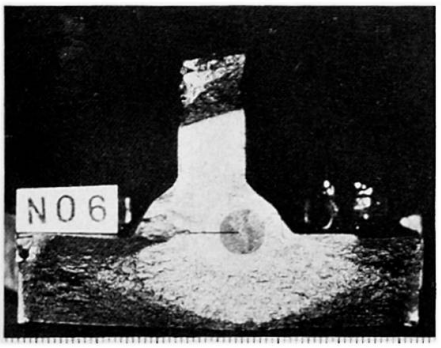

Fig. 4 Fracture surface (from worm-hole)

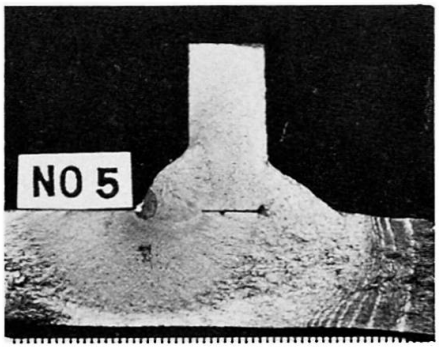

Fig. 5 Fracture surface (from under-cut)

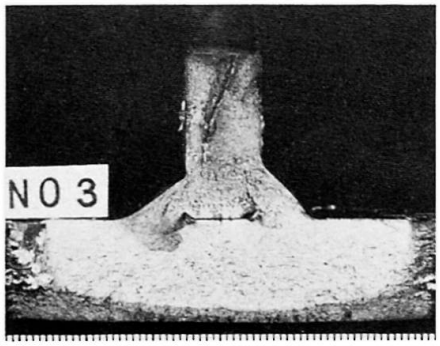

Fig. 6 Fracture surface (from surface notch)

III–2 Comparisons with Previous Fatigue Data

The fatigue data of hybrid girders can be conventionally compared with those of homogeneous ones (5.6). There are several investigations into the fatigue strength of high strength steel girders and longitudinal fillet welded joints comparable with the present test results. The comparisons between these fatigue strength were extensively discussed in Ref. (15). Fig. 7 shows the additional comparisons with these available fatigue data for analysis of Type 3 crack. In paticular, the work by Reemsnyder (13) on the fatigue strength of longitudinal fillet weld in constructional alloy steel is most comparable, because the present test pieces and test procedure are simulated to those of that work. The two test results shown in Fig. 7, that is, solid circles and the hollow circles represent the test results obtained by using hybrid specimens and homogeneous ones respectively, and they seem to agree well with each other in spite of disregarding the effect of the mean stress. Again, a study of Fig. 7 reveals that the fatigue strength of tee-shaped model specimens and those of beams consisting of 80 kg/mm^2 class high strength steel are not significantly different.

Furthermore, there are two other comparable previous works that are essential. Fig. 8(a) and Fig. 8(b) are quoted from these works dy Frost (4) and Toprac (5), respectively. Both figures represent the comparisons between the test results

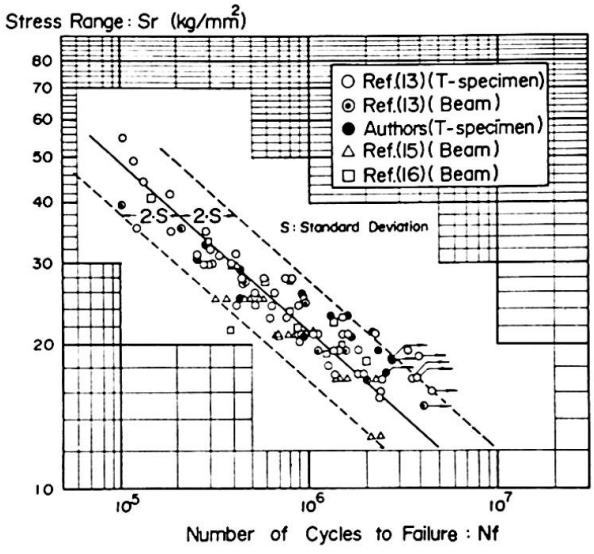

Fig. 7 Comparison of previous work on Type 3 crack with this study

of hybrid girders consisting of 80kg/mm² class high strength steel in flanges (4,5) and these of tee-shaped homogeneous specimens(13). It seems that the former ones are slight higher than the latter, especially in the case of Fig. 8(b). The disagreement in Fig. 8(b) was concluded by Toprac that such a difference could be attributed to the fact that the tee-shaped specimens were fabricated under a controlled condition, whereas the girder specimens were fabricated with an average commercial shop practice. This conclusion implies that the fatigue strength, especially regarding to Type 3 crack, is largely influenced by welding conditions and fabrication methods.

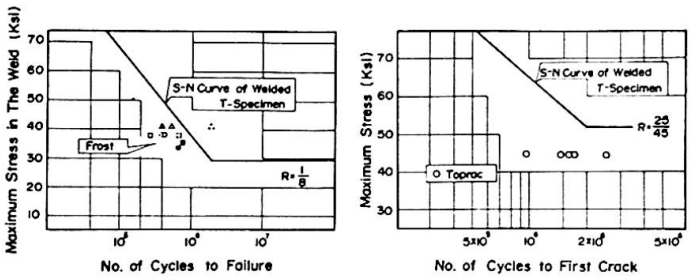

(a) (b)

Fig. 8 Comparison of fatigue date on hybrid beams with homogeneous tee-shaped specimens

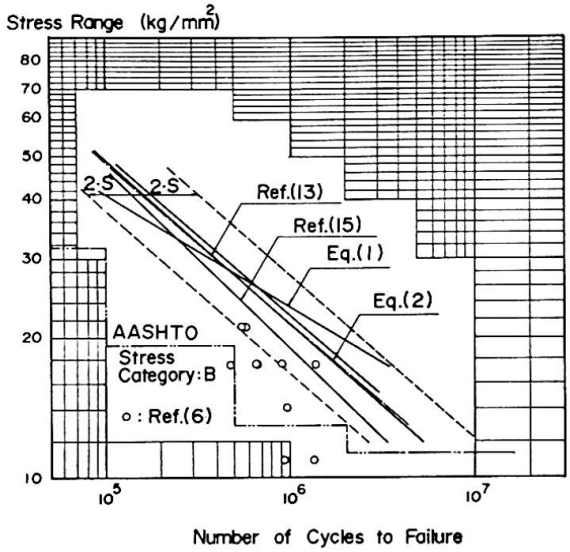

Fig. 9 Comparison of related S-N curves with design stress

The regession analysis of all the available test results by the method of least squares gives

$$\text{Log } N_f = 9.720 - 2.800 \text{ Log } S_r \qquad \cdots\cdots (2)$$

and fatigue strengths at 2×10^6 cycles of web-to-flange fillet weleded joints consisting of 80kg/mm² class high stregth steel in flanges are estimated at 16.7kg/mm² (mean) and 12.9 kg/mm² (95% confidence limit) in stress range. Shown in Fig. 9 is all the available S-N curves related to longitudinal fillet weldments in web-to-flange junctures, using the mean regression lines and the limits of dispersion correspoding to the 95% confidence limits in comparison with fatigue allowable stresses specified in AASHTO Specifications.

It will be resonable, if Toprac's result is ignored, that the clause in AASHTO(10,17) provides that web to flange weld connections in hybrid girders shall be designed for preventing fatigue based on the flange steel and that allowable fatigue stresses are given in terms of stress ranges.

III–3 Fatigue Behavior Prediction by Fracture Mechanics

The relation betwee the fatigue crack-growth rate and the change in the stress intensity factor is presented in the form of

$$da/dN = C(\Delta K)^m \qquad \text{(mm/cycle)} \qquad \cdots\cdots (3)$$

where a is a half length of fatigue crack and ΔK the variation of the stress intensity factor $(K_{max} - K_{min})$; C and m are material constants. And, the stress intensity factor usually takes the form

$$K = \sigma\sqrt{\pi a}\cdot f(a) \qquad \text{(kg/mm}^{-3/2}\text{)} \qquad \cdots\cdots (4)$$

where σ and f(a) respectively represent remotely applied stress and a correction function to which the dimensions of the plate, the distance to a free edge or surface and the shape of cracks are introduced. From eqs. (3) and (4), the fatigue life N is given as

$$N = \frac{1}{C(\Delta\sigma)^m}\int_{a_i}^{a_f} \frac{da}{a^{m/2}\cdot\pi^{m/2}\cdot f^m(a)} \qquad \cdots\cdots (5)$$

where a_i and a_f are the initial and final crack sizes, respectively. On the other hand, the conventional S-N relation is represented as follows

$$\text{Log } N = C' - n \cdot \text{Log}(\Delta\sigma) \quad \cdots\cdots (6)$$

where N and $\Delta\sigma$ are the fatigue lives and the applied stress ranges respectively and C' and n are material constants. Fisher et al.(14) introduced the relationship among these constants, in eqs. (3) and (6) that characterize the fatigue crack growth rate and the S-N curve, respectively, as follows.

$$m = n \quad (7\text{-a})$$

and

$$C' = \text{Log}\left[\frac{1}{C}\cdot\frac{(a_i^{-\alpha} - a_f^{-\alpha})}{\alpha \cdot f^m(a)\pi^{m/2}}\right] \quad (7\text{-b})$$

where, $\alpha = m/2 - 1$.

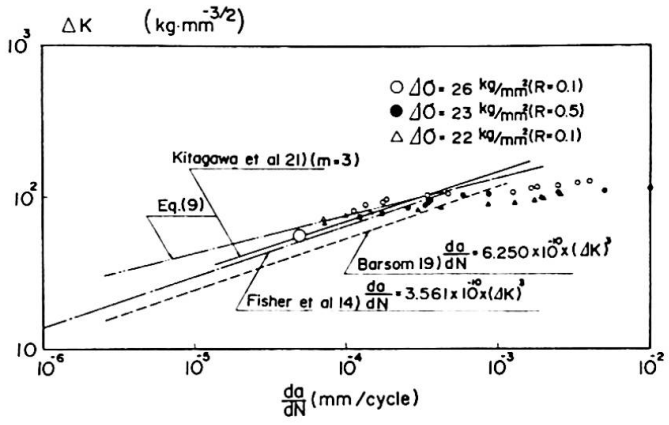

Fig. 10 Fatigue crack-growth rate

This relationship is based on an approximate assumption as the correction function f(a) does not vary under constant amplitude stress.

The relationship among the material constants represented in the form of eq.(7) is obtained for homogeneous beams where the crack growth rate is isotropic. All the previous works conducted on fatigue crack growth rates dealt with almost homogeneous materials. Accordingly, it was questionable whether such relation could be applied to hybrid members consisting of different steel grades, since Gurney (19) indicated the relation of m and Log C to be linear functions of yield stress of the material. The fracture surfaces observed in the present test, however, suggest the possibility of the application of the above relation, because it is recognized that the fatigue fracture surfaces indicate concentric circles as is typically shown in Fig. 8 and the fatigue crack growth rate may be isotropic.

Fisher et al. (14) also made an assumption to evaluate the crack growth constants, C and m, that the porosity was assumed to be described by a disc-like penny-shaped crack with a constant correction factor, f(a), over the interval of integration of $2/\pi$.

In the present work, the initial crack radius, a_i, for the evaluation of the crack-growth constants, C and m, was assumed 0.5mm that is the mesured tip radius of elongated worm-holes. The final crack radius, a_f, was assumed to be the flange thickness, The equation of the mean regression line from the method of least squares applied to the test data for specimens failing from embedded weld defects in the longitudinal fillet weld is

$$\text{Log } N_f = 11.388 - 3.895 \text{ Log } S_r \quad \cdots\cdots (8)$$

Thus, the material constants corresponding to C' and n in eq.(6) are 2.443×10^{11} and 3.895. From the above mentioned assumptions and eq.(7), the crack-growth constants, C and m, are evaluated and the fatigue crack growth-rate are represented numerically as

$$da/dN = 5.0 \times 10^{-12} \times (\Delta K)^{3.9} \quad \cdots\cdots (9)$$

Eq. (9) as descrided from the mean regression curve of fatigue test data is shown in Fig. 10 and compared with the data points for the measured crack-growth rates on inside surface of the flange for growth as a three-ended crack. The data points are compared well with the estimated curve up to the ΔK of about 100 kg/mm$^{-3/2}$ where crack penetrates the extreme fiber of flanges. The derived crack-growth relationship given by Fisher *et al.*(14) and a conservative upper bound for growth-rates on ferrite-pearlite steels proposed by Barsom (18) are also compared with the present test results. These works gave the m-value of 3 and the one obtained by the present test was about 4 that is the preliminary proposed value by Paris (21). Kitagawa *et al.* (20) found a convenient correlation between C and m for a number of data obtained by different investigators. The correlation curve is expressed in the form of

$$C = A/B^m \quad \cdots\cdots\cdots\cdots\cdots\cdots \quad (10)$$

where A and B are constants for some range of materials ; $A = 0.5 \times 10^{-4}$, $B = 55$ for steels and $A = 10^{-4}$, $B = 55$ for aluminium alloys. The crack-growth relationship derived from eq. (10) in case of $m = 3$ is also shown in Fig. 10. It seems that the correlation given by eq. (10) is compared well with the one by Fisher et al. and predicts the conservative relation for the present test results. Despite the lack of data in the slower crack-growth rate region, these predictions give similar relations.

References

1) R. W. Frost and C. G. Schilling, ASCE, Proc., Vol. 90, No. ST3, June, 1964
2) H. S. Lew and A. A. Toprac, S. F. R. L. Tech. Rpt., p550−11, Janu., 1968
3) P. S. Carskaddan, Tech. Rpt. 57, 019-904(4), Applied Research Lab. U. S. Steel Corp.
4) R. W. Frost, Tech. Rpt., 57, 19-904(1), Applied Res. Lab., U. S. Steel Corp., Nov. 4, 1963
5) A. A. Toprac, Weld. J., May, 1969, 195-s 202-s
6) A. A. Toprac and M. Natarajan, ASCE, Proc., Vol. 97, No. ST4, 1971
7) Y. Maeda and Y. Kawai, 18th Conf. of Bridge and St. Eng. in Japan, p137
8) F. Nishino, M. Ito, M. Hoshino, JSSC, Vol. 7, No. 71, 1971 (in Japanese)
9) Y. Maeda, M. Ishiwata, Y. Kawai, IIW, Doc. XIII-734-74, April, 1974
10) Specs. for Highway Bridges, AASHTO, 1973
11) AISC Spec., Section 1.10, 1969, AISC
12) T. R. Gurney, Brit. Weld. J., July, 1962, p446
13) H. S. Reemsnyder, Weld. J., Oct., 1965, 458-s 465-s
14) M. A. Hirt, J. W. Fisher, Eng. Frac. Mech., 1973, Vol. 5, p415-429
15) J. W. Fisher, K. H. Frank, M. A. Hirt and B. M. Mcnamee, N. C. H. R. P., Rpt. No. 102, 1970
16) Y. Kikuchi and K. Yamada, JWS, Proc., Vol. 41, No. 9, 1972, p1085-1093
17) Interm Specs., Bridges, AASHTO., 1974
18) J. M. Barsom, U. S. Steel Corp., Applied Res. Lab., 1971
19) T. R. Gurney, Metal Const. and Brit. Weld. J., Feb., 1969, p91-96
20) H. Kitagawa et al., JSME, J, Vol. 75, 1972, p1068
21) P. C. Paris and F. Erdogan, ASME Trans., Vol. 85, Series D, No. 4, 1963

SUMMARY

The data of fatigue strength of Type 3 crack in hybrid girders which initiate at tension flanges were explored and fatigue crack propagation behaviour at tension flanges and webs was studied by fracture mechanics analysis.

RESUME

Les données de la résistance à la fatigue du Type 3 crack dans les poutres hybrides commençant par des brides de tension ont été explorées et le comportement propagateur de craquelage par fatigue aux brides de tension et âmes a été étudié par l'analyse mécanique de fracture.

ZUSAMMENFASSUNG

Die Daten über Dauerfestigkeit des Anrisses vom Typ 3 an Hybridbalken, welche am Zuggurt beginnen, werden erörtert und das Ausbreitungsverhalten der Ermüdungsrisse an Zuggurten und Stegen werden mittels der Bruchmechanikanalyse untersucht.

Behaviour of Inelastic Beams under Cyclic Loading

Comportement de poutres sous l'effet de charges répétées

Verhalten von Trägern unter wiederholten Belastungen

SHOHKEN OGURA
Engineer
Izumi Sohken Engr.
Tokyo, Japan

YASUNAGA FUKUCHI
Associate Professor
Nagoya Institute of Technology
Nagoya, Japan

TADAO NAKAGOMI
Graduate Student
Tokyo Institute of Technology
Tokyo, Japan

HIROFUMI AOKI
Associate Professor
Yokohama National University
Yokohama, Japan

MORIHISA FUJIMOTO
Professor
Tokyo Institute of Technology
Tokyo, Japan

1. INTRODUCTION

In order to use higher strength steels advantageously in structures, many investigations have been carried out heretofore(1),(2). However, most of them have been on the strength and deformation capacity of the members under monotonous loading. In the countries which suffer from earthquakes frequently, such as Japan, the structural steel members are subjected to cyclically repeated loads. From this standpoint, the design methods which take into consideration the energy absorption due to plastic deformation should be adopted to design the structures economically and rationally. For this purpose, it is important to grasp thoroughly the inelastic behaviors of steel members subjected to extreme load reversals such as those which may occur during an earthquake. Investigations on the behavior of structures or structural members under cyclically repeated loads have been done considerably(3), especially in Japan(4). However, there has been little research done under such loads, relating to the phenomena of flange local buckling and lateral buckling, and little work, relating to the steels which have a yield point exceeding that of SM58 class steels.

This paper is a report of laboratory investigation of steel beams subjected to cyclically reversed loads under moment gradient, relating to flange local buckling and lateral buckling.

2. INELASTIC LOCAL BUCKLING BEAMS UNDER CYCLIC LOADING

2.1 SELECTIONS OF THE SPECIMENS

In Ref. 6, the limitation of width-thickness ratio b/t(where, b=one-half of flange width, t=thickness of flange) of wide-flange sections in the plastic designs is given as 6.00 for SM58(A572) class steels. In the case of beams under moment gradient, M.G. Lay has proposed next equation(8);

$$b/t=1.78/\sqrt{\sigma_y(3+1/Y)(1+E/5.2E_{st})E} \qquad (2.1)$$

where, $Y=\sigma_y/\sigma_u$= yield ratio of material(σ_u=tensile strength)

In Ref.7, the limitation of the ratio b/t in the elastic design is given as b/t= 11.85 for SM58(A572) class steels. The mechanical properties of materials are shown in Table 2.1, where ε_{st}=strain at initial strain hardening. Using the values of this table, b/t=4.20 is obtained from Eq.(2.1).

From the basic data as described above, for the width-thickness ratio b/t of the test specimens, The values of 4.2,6.0,9.0,and 12.0 were used.

2.2 EXPERIMENTAL ARRANGEMENT AND METHOD

Local buckling tests were carried out on single-span simply supported beams with central concentrated loads applied on the top flanges, as shown in Fig. 1.1 (a). The test specimens are beams having the cross section shown in Fig. 1.1 (b). In Fig. 1.1 (a), the notation S shows the lateral support.

Unsupported length of a beam, L, is designed as the value of L/r_y is less than that recommended in Ref.6, i.e. $L/r_y=43.9$ for the steels of $\sigma_y=5.32^{t/cm^2}$. The sectional dimensions of the test beams are given in Table 2.2, where, I=geometrical moment of inertia, and Z=section modulus. The program was made refering to experimental results in Ref.5.

According to Ref.5, in the beams having the same width-thickness ratio b/t, rotation capacity of the beam on which a monotonous loading test was performed showed the maximum value for all methods of loading, while the value of the beam subjected to cyclically repeated loads by controlling the deformations of the beam had the minimum value. In this report, therefore, three welded built up beams having the same ratio b/t were used (See Table 2.2). In Table 2.2, each beam is refered to by a code number such as SM9-3, in which SM stands for the materials of SM58, 9 means a width-thickness ratio of 9.0, and 3 means the third beam. The first beam test was carried out under monotonous loads, the second, under cyclically repeated loads by controlling the loads of the beam, i.e. the ratio of the positive moment to negative one was the ratio of 1:0.6 (See Fig. 2.2, 2.4 and 2.6), and the third, under cyclically repeated load by controlling the deformations of the beam (See Fig. 2.3, 2.5, 2.7 and 2.9).

Each so-called plastic cycle is defined here as the process of loading the beam downward until reaching $\delta/\delta_p=2.5$ (where, δ =the deflections of the beam section at the midspan), unloading, then reverse loading the beam upward until reaching $\delta/\delta_p=-2.5$, in the case of the third beam. From the second excursion, in every process of loading the beam downward, the deflection of the beam at the midspan was increased with $\delta/\delta_p=0.5$. The deflections and the rotations of the beam at the midspan were measured with the dial gages and the strains were measured by means of wire strain gages for plastic region.

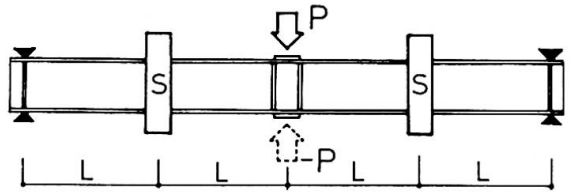

(a)

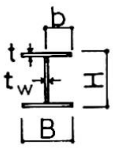

(b)

S shows the lateral support.

Fig. 1.1

Table 2.1
Mechanical Properties of Materials

σ_y t/cm²	σ_u "	σ_y/σ_u	ε_y %	ε_{st} "	E t/cm²	E_{st} "	E/E_{st}
5.32	6.19	.86	.252	2.06	2,111	25.2	83.7

Table 2.2
Sectional Dimensions

		H cm	B "	t "	t_w "	b/t	I cm⁴	Z cm³
SM12-2	1	21.76	21.56	.90	.61	11.98	4,629	425.4
	2	21.80	21.59	.91	.61	11.86	4,695	430.7
	3	21.73	21.56	.89	.62	12.11	4,580	421.5
SM9-2	1	21.80	16.17	.92	.61	8.79	3,649	334.8
	2	21.83	16.18	.92	.62	8.79	3,669	336.0
	3	22.30	16.17	.92	.62	8.79	3,845	344.8
SM6-2	1	21.86	10.79	.91	.60	5.93	2,559	234.1
	2	21.77	10.77	.92	.62	5.85	2,564	235.6
	3	21.83	10.78	.92	.60	5.86	2,569	235.4
SM4-	1	9.74	7.58	.90	.59	4.21	292	60.0
	3	9.76	7.57	.90	.58	4.21	293	60.0

Table 2.3 Experimental Results

		P_m t	P_{mp} "	P_m/P_{mp}	δ_m cm	δ_p "	δ_m/δ_p	θ_m/θ_p
SM12-2	1	53.7	50.03	1.07	2.54	.86	2.95	1.99
	2	53.0	50.65	1.05	2.13	.86	2.48	1.86
	3	53.4	49.63	1.08	2.15	.86	2.50	1.93
SM9-2	1	45.1	39.75	1.13	3.15	.87	3.62	2.54
	2	43.7	40.20	1.09	3.01	.87	3.46	2.42
	3	44.1	41.32	1.07	2.99	.86	3.48	2.22
SM6-2	1	32.5	28.17	1.12	4.49	.90	4.99	3.40
	2	32.1	29.82	1.10	3.80	.90	4.22	3.31
	3	33.0	29.22	1.14	3.30	.90	3.67	2.50
SM4-	1	19.6	15.44	1.23	9.76	.62	15.74	5.93
	3	17.8	15.44	1.15	3.75	.62	6.05	3.69

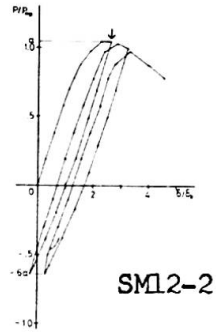
SM12-2

Fig. 2.2

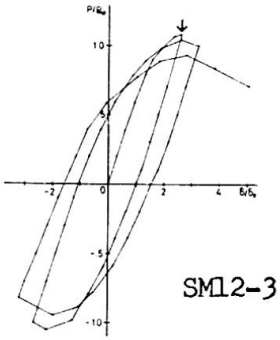
SM12-3

Fig. 2.3

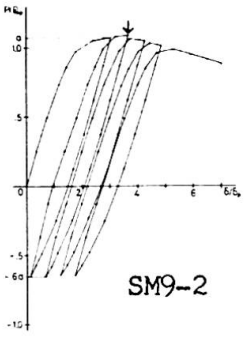
SM9-2

Fig. 2.4

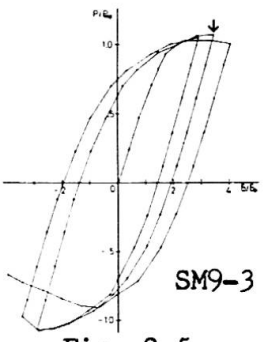
SM9-3

Fig. 2.5

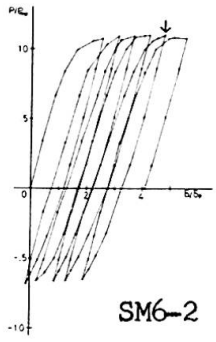
SM6-2

Fig. 2.6

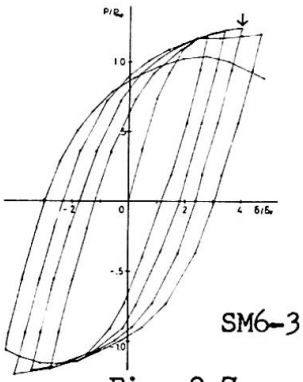
SM6-3

Fig. 2.7

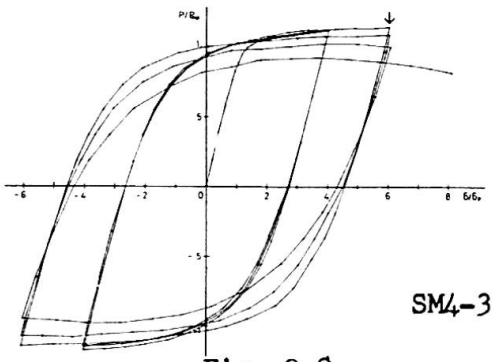
SM4-3

Fig. 2.8

2.3 EXPERIMENTAL RESULTS

Experimental results are shown in Table 2.3, where P_m=maximum load, δ_m and θ_m= the deflection and rotation corresponding to P_m, respectively, P_{mp}=the load corresponding to full plastic moment, δ_p and θ_p= elastic deformation and rotation corresponding to P_{mp}, respectively. The P-δ curves are shown in Fig. 2.2 to Fig. 2.8. In each figure, the arrow shows the point of beam failure. From these figures, the rotation capacity of the beam in the plastic range was found to be very small. Especially, the negative slope of P-δ curves in the third beam became steep comparing with that of the first beam (monotonous loading test).

In Fig. 2.9 , the relationshops between R and $(b/t)\sqrt{\sigma_y}$ are shown together with the experimental results of SS41 class steels. Fig. 2.9 shows that the rotation capacity of SM58 class steels is extremely small than that of SS41. In the case of the beams having the ratio b/t exceeding 6.0, as shown in Fig. 2.9, the rotation capacity of the beams decreases linearly as b/t becomes larger. However, in the case of the beam having the ratio b/t=4.2, the rotation capacity of the beams under monotonous loading was found to be 4.9, and 2.7 under cyclically repeated load. Therefore, the investigations relating to the beams having the ratio b/t between 4.2 and 6., need to be performed further. The rotation capacity of the beam under cyclically repeated loads was found to be very small, compared with that under monotonous loading. From the results, it is presumed that there are many problems in regard to the use of high strength steels to earthquake-proof strutures.

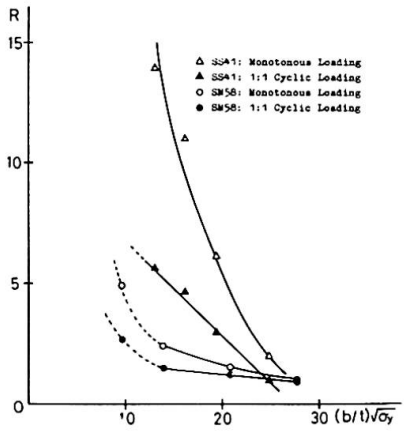

$R=\theta_m/\theta_p-1$= rotation capacity

Fig.2.9 Relationships between R and $(b/t)\sqrt{\sigma_y}$

It is very practically important to know the behavior of the members consisting of high strength steel and further research in this field is needed.

3. INELASTIC LATERAL BUCKLING UNDER CYCLIC LOADING

3.1 SPECIMENS AND EXPERIMENTAL METHOD

In this chapter, experiments of cyclic bending beams in which deformation capacity is determined by the combination of local and lateral buckling are presented. The experiments reported in this chapter were made by the Working Group of Fatigue in Low and High Cycle Range in Metals Subcommittee (The chairman is Prof. Morihisa Fujimoto) in Research Committee on Safety of Structural Materials (RCSSM, the chairman is Prof. Takeo Naka). Beam specimens were made of three kinds of structural carbon steel. Properties of the material are given in Table 3.1. Beam specimens were built up with steel plate of 9 mm by welding and the scope of the welding is illustrated in Fig. 3.1. After the specimens were welded, they were not treated by stress relief annealing. Dimensions of the specimens are given in Table 3.2. Ratio of width to thickness of flange, b/t, is restricted to one on each grade of steel, taking into consideration the experiments by G.H. Lay(9), T. Suzuki and so on, and recommendations of ASCE(6) and AIJ(7). Ratio of width to thickness of web, d/t_w is determined by the loading equipment, but it is within the values of the above recommendations.

The experimental purpose is to discuss the evaluation of deformation capacity of inelastic beams under cyclic loading, changing the variables such as slenderness factor $\lambda(=l_b/i_y)$, grade of steel and loading type. Conditions of loading and supporting are illustrated in Fig. 3.2. The specimen supported on rollers was loaded with a single concentrated load applied at the center, and deformable except for restricting to fall down sideways at loading and supported points. In fact, lateral buckling occured symmetrically in all of specimens in two half-waves and the load reached maximum.

3.2 EXPERIMENTAL RESULTS

Fig. 3.3(SM50, λ=55) shows M/M_p-θ/θ_p curves in cyclic loading as the amplitude was a rotational angle θ_m at maximum load M_m by monotonous loading, where M is applied moment, M_p, full plastic moment of the specimens, θ, rotation measured at supported point and θ_p, elastic rotation corresponding to M_p. And M/M_p-θ/θ_p curve in cyclic loading between θ_m and $-0.6\theta_m$ is plotted in Fig. 3.4. And the curves in the case of SM50, λ=45 are plotted in Fig. 3.5 and 3.6. The M/M_p-θ/θ_p curves (SM58, λ=50 and λ=40) in cyclic loading between $(1/2)\theta_m$ and $-(1/2)\theta_m$ are also plotted in Figs. 3.7 and 3.8. The endurance of beam in the case of SM58, λ=50 did not fall after 8 cycles loading, and that of SM58, λ=40 reached the maximum load in each cycle. M/M_p-θ/θ_p curves (HW70, λ=40 and λ=30) under cyclic loading with amplitude between $(1/2)\theta_m$ and $-(1/2)\theta_m$ are plotted in Figs. 3.9 and 3.10.

After local buckling occured at flange portion of every specimen, lateral buckling occured. At the maximum load, local buckling the web portion was observed. It seems that the negative slope of M/M_p-θ/θ_p curve after reaching the maximum load is determined by local buckling at web portion, especially under cyclic loading. The above experimental results indicated that the stability of hysteresis loop and deformational capacity of inelastic beams under cyclic loading are related to d/t_w as well as λ and b/t, when deformation capacity is prescribed by the combination.

Table 3.1
Chemical composition and Mechanical properties of Materials

Grade of steel	Chemical Composition (%)											Tension Test			Check Test				
	C	Si	Mn	P	S	Cu	Cr	Mo	V	B	Ceq	Y.P.	T.S.	El.	σ_y	σ_B	Est	Eu	Est
	x100			x10000		x100				x10000	x100	kg/mm²		(%)	kg/mm²		(%)		kg/mm²
SM 50	16	34	130	17	18							33	51	28	36.2	51.3	2.08	2.23	4559
SM 58	14	24	140	22	6						38	62	69	25	60.9	66.7	1.75	7.44	2760
HW 70	11	27	89	11	3	24	91	32	4	1	53	84	88	25	84.0	88.9		7.58	

Table 3.2 Dimension of Specimens and Experimental Results

Grade of steel	Specimen NO.	t(t_w) mm	R mm	b mm	b/t	d mm	d/t_w	l_b mm	i_y mm	l_b/i_y	M_p t m	θ_p 10⁻²Rad	M_u/M_p	θ_u/θ_p	Loading condition
SM50	H5755M	8.86	9.8	63.0	7.10	282	31.9	1378	24.6	56.0	19.2	0.90	1.18	4.79	Monotony
	H5755C1	8.86	9.1	63.0	7.10	282	31.9	1378	24.7	55.9	19.0	0.90	1.16	4.47	θ_u – $-\theta_u$
	H5755C2	8.86	10.5	63.2	7.13	282	31.9	1378	24.7	55.8	19.3	0.90	1.16	4.26	θ_u – $-0.5\theta_u$
	H5745M	8.86	10.3	63.1	7.12	282	31.9	1130	24.7	45.8	19.3	0.74	1.22	7.77	Monotony
	H5745C1	8.86	10.2	62.9	7.10	283	31.9	1130	24.6	46.0	19.2	0.74	1.24	6.81	θ_u – $-\theta_u$
	H5745C2	8.86	10.4	63.2	7.13	282	31.8	1130	24.7	45.7	19.2	0.74	1.22	6.36	θ_u – $-0.5\theta_u$
SM58	H6650M	9.40	9.4	54.1	5.76	198	21.1	1130	22.3	50.7	19.5	1.79	1.05	3.51	Monotony
	H6650C3	9.40	9.2	54.4	5.79	198	21.1	1130	22.4	50.4	19.5	1.79			$0.7\theta_u$ – $-0.7\theta_u$
	H6640M	9.40	10.2	53.9	5.73	198	21.1	904	22.1	40.9	19.6	1.43	1.10	5.53	Monotony
	H6640C3	9.40	10.7	53.9	5.73	198	21.1	904	22.1	41.0	19.7	1.43			$0.6\theta_u$ – $-0.6\theta_u$
HW70	H7540M	9.48	11.7	45.4	4.79	126	13.3	805	19.6	41.0	14.4	2.63	1.06	4.88	Monotony
	H7540C3	9.48	10.4	45.3	4.78	126	13.3	805	19.7	41.0	14.0	2.60			$0.6\theta_u$ – $-0.6\theta_u$
	H7530M	9.48	10.7	45.3	4.78	126	13.3	604	19.7	30.6	14.1	1.95	1.15	7.24	Monotony
	H7530C3	9.48	8.8	45.2	4.76	126	13.3	604	19.7	30.6	13.7	1.96			$0.6\theta_u$ – $-0.6\theta_u$

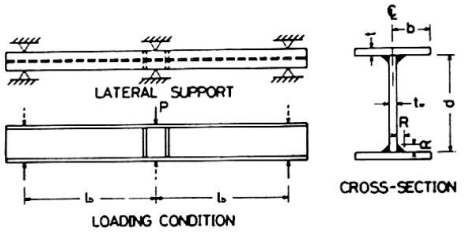

Fig. 3.1

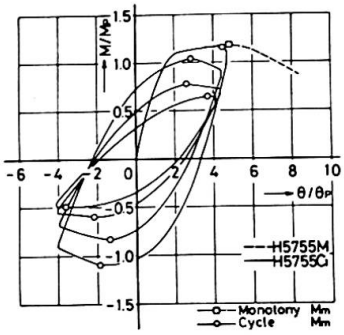

Fig. 3.3

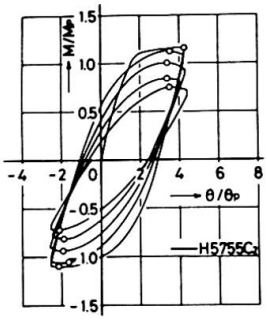

Fig. 3.4

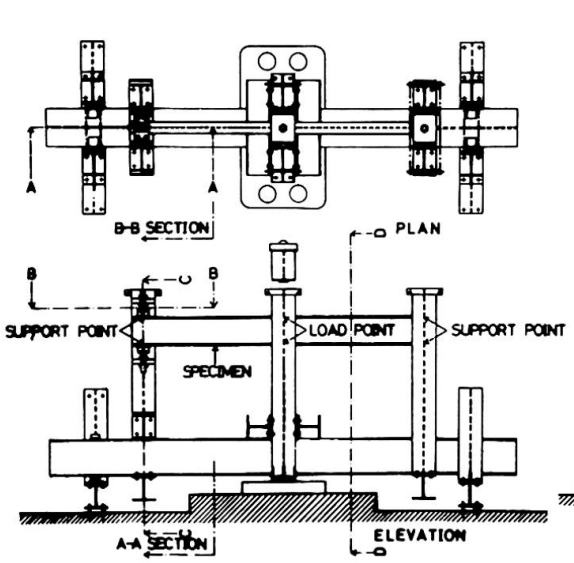

Fig. 3.2

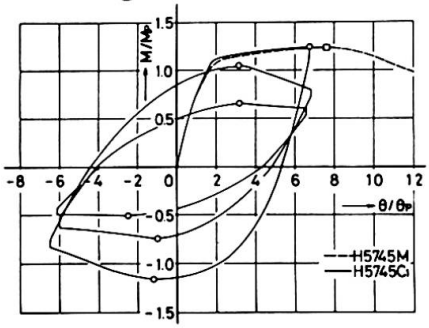

Fig. 3.5

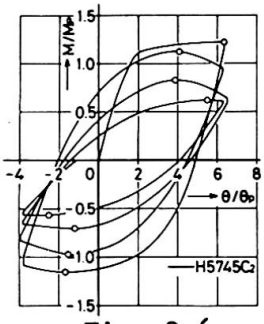

Fig. 3.6

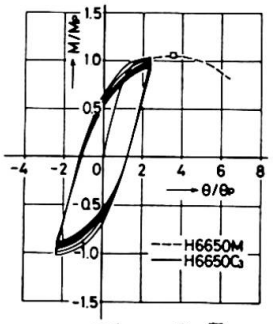

Fig. 3.7

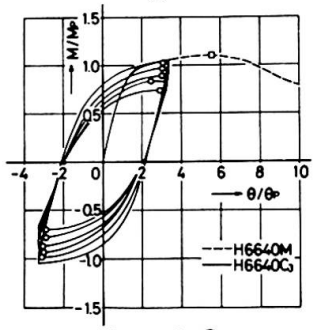

Fig. 3.8

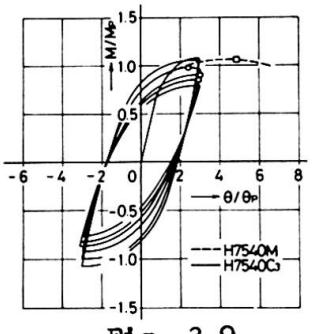

Fig. 3.9

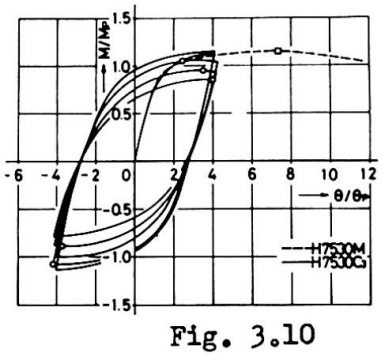

Fig. 3.10

ACKNOWLEDGEMENT

The authors wish to extend their appreciation to Prof. Ben Kato for his guidance.

REFERENCES

1. Adams,P.F., Lay,M.G. and Galambos,T.V. " Experiments on High-Strength Steel Members", WRC. Bulletin NO.10, Nov. 1965
2. Suzuki,T. and Ono,T. " Experimental Studies on the Plastic Design of High-Strength Steel Beams", Trans. AIJ. NO.219, May 1974,(in Japanese).
3. e.g. Bertero,V.V. and Popov, E.P. " Effect of Large Alternating Strains of Steel Beams", Proc. of ASCE, ST1, Feb. 1965
4. e.g. Suzuki,T., Tamamatsu,K., Kubodera,I. and Okuta,K. " Experimental Study on the Elasto-Plastic Behavior of Tensile Braced Frames", Tran. AIJ. NO.228 Feb. 1975,(in Japanese).
5. Fukuchi,Y. and Ogura,S. " Experimental Studies on Local Bucklings and Hysteretic Characteristics of H-Shape Beams", Trans. AIJ. NO.228, Feb. 1975, (in Japanese).
6. Plastic Design in Steel, A Guide and Commentary, 2nd Edition ASCE, 1971
7. AIJ. Specification for Design of Steel Structures, 1970
8. Lay, M.G. " Flange Local Buckling in Wide-Flange Shapes" J. of the Structural Division, Proc. of ASCE, ST6, Dec. 1965
9. Lay, M.G. and Galambos,T.V. " Inelastic Beams under Moment Gradient", J. of Structural Division Proc. of ASCE, ST1, Feb. 1967

SUMMARY

It was confirmed experimentally that rotation capacity of structural steel members, both mild and high strength steels, was influenced considerably by cyclic loading. The rotation capacity for beams of high strength steels with high yield ratio as compared with that of mild steels is small. The figures indicate that the rotation capacity of beams under cyclic loading is still lower. Therefore, it is desirable that the existing values L/r_y and b/t for high strength steels should be limited even more strictly.

RESUME

L'expérience confirme l'influence considérable de charges répétées sur la capacité de rotation d'éléments en acier doux et même à haute résistance. La capacité de rotation des poutres en acier à haute résistance et à haute limite d'élasticité est plus petite que celle de l'acier doux. Les figures montrent que la capacité de rotation des poutres sous charges répétées est encore plus petite. Par conséquent, il vaux mieux que les valeurs L/r_y et b/t en vigueur pour l'acier à haute résistance soient limitées sévèrement.

ZUSAMMENFASSUNG

Durch Versuche wurde festgestellt, dass die wiederholte Belastung auf die Rotationskapazität von Stäben sowohl aus leichtem wie aus hochfestem Stahl eine starke Wirkung ausübt. Die Rotationskapazität von Balken aus hochfestem Stahl mit hohem Streckungsverhältnis ist geringer als jene des weichen Stahls. Die Abbildungen zeigen, dass die Rotationskapazität der Balken unter widerholter Belastung noch kleiner ist. Somit ist der bestehende Wert von L/r_y und b/t für hochfesten Stahl noch strenger zu begrenzen.

High Strength Steel Composite Beams with Formed Steel Deck

Poutres mixtes en acier à haute résistance avec platelage métallique

Hochfeste Verbundträger mit Stahlblechdecke

JOHN A. GRANT, Jr.
Research Assistant

JOHN W. FISHER
Professor of Civil Engineering

ROGER G. SLUTTER
Professor of Civil Engineering

Fritz Engineering Laboratory, Lehigh University
Bethlehem, Pennsylvania, USA

1. INTRODUCTION

During the past forty years, formed steel deck has become the most common floor system used in high rise steel frame structures. A natural consequence of this floor system was the development of composite action between the steel beam and the concrete slab by means of shear connectors welded through the deck to the beam flange. However when the corrugations of the deck run perpendicular to the beam, experimental results have shown that a reduction in beam capacity may ensue.

Initial studies of this condition were made on a proprietary basis for specific products in building applications and thus were uncoordinated. Consequently considerable variance among controlled parameters existed, making it difficult to draw any general conclusions. In 1967 a detailed study by Robinson(1) showed that for high, narrow ribs the shear capacity of the connector is a function of the rib geometry and is substantially less than the capacity of connectors embedded in a composite beam with a solid slab. In 1970, Fisher(2) summarized the investigations that had been conducted to date and proposed design criteria. Fisher concluded that composite beams could be modeled as having a haunched slab, equal in thickness to the solid part of the slab above the rib, except that the shear capacity of the connector is reduced. He modeled this reduction in shear capacity by the following formula:

$$Q_{rib} = A \cdot \frac{w}{h} \cdot Q_{sol} \leq Q_{sol} \qquad (1)$$

where: Q_{rib} = shear strength of connection in a rib
A = numerical coefficient (0.5 for beam)
w = average rib width
h = height of rib
Q_{sol} = shear strength of a connector in a solid slab

With the many uncontrolled and ill defined variables in these early investigations, there was a need for additional research in this area. Also there was virtually no experimental work done which considered the effect of high strength steel beams and the resulting effect of increased slab force on connector and beam capacity. A research program was initiated at Lehigh University in 1971 involving 17 full scale beam tests, 15 of which utilized high strength steel beams. The work reported herein includes a detailed analysis of these 17 composite beams. Additionally, this analysis is supplemented by an evaluation of 39 other beam tests reported by previous investigators. The work is described in detail in Ref. 3.

This report provides an evaluation of the shear capacity of stud connectors embedded in composite beams utilizing high strength steel with formed steel deck, as well as the flexural capacity of the composite beams themselves. Additionally the stiffness of composite beams with or without formed steel deck is evaluated for service loads.

2. DESCRIPTION OF TESTS

The experimental program at Lehigh consisted of tests on 17 simple span composite beams. The program was designed in accordance with the recommendations suggested in Refs. 2 and 4.

Series A consisted of six beams. It served as the basic series in the program, with average rib width - height ratios of 1.5 and 2. The beams were designed for partial shear connection. Series B consisted of two mild steel beams, as all other beams were high strength steel. Series C consisted of five beams with low degrees of shear connection (below 50%). Series D consisted of four beams with larger rib slopes as their major variable.

The test beams consisted of steel beams on simple spans of 24 or 32 ft. (7.31 to 9.75 m), acting compositely with concrete slabs cast on formed steel deck. All of the steel beams except two were W16 x 40 or W16 x 45 sections with yield strengths between 55 and 70 ksi (379.5 and 483.0 N/mm^2). The two exceptions were both W16 x 58 sections with 36 ksi (248.4 N/mm^2) yield.

The slabs of the beams were made with structural lightweight concrete conforming to the requirements of ASTM C330 (Specification for Lightweight Aggregates for Structural Concrete). The concrete strength and modulus of elasticity where maintained as constants within fabrication tolerances at 4.0 and 220 ksi (27.6 and 151800 N/mm^2) respectively. Minimal reinforcement for all of the beams consisted of 6 x 6 - #10/10 welded wire fabric placed at mid-depth of the slab above the ribs. The thickness of the solid part of the slab was a constant 2-1/2 in. (63.5 mm) for all of the beams. The slab widths were proportioned as 16 times the full thickness of the slab plus the flange width of the steel beam. All slabs were cast without shoring.

The slabs were cast on 20 gauge galvanized steel deck without embossments. The rib heights of the deck were 1-1/2, 2 or 3 in. (38.1, 50.8 or 76.2 mm) for average rib width - height ratios of 1.5 and 2. The slopes of the ribs were a nominal 1 to 12 except for the series D beams which had 1 to 2 and 1 to 3 slopes. The steel deck was fabricated in widths of 24 or 36 in. (609.5 or 914.4 mm) with corresponding rib modules of 6 and 12 in. (152.4 and 304.8 mm).

Composite action between the steel beam and the slab was provided by the placement of 3/4 in. (19 mm) shear connectors. All studs conformed to ASTM A108 specification and were welded through the steel deck to the beam flange in a staggered pattern. All welds were tested by "sounding" the studs with a hammer. Questionable studs were given a 15 degree bend test. Faulty studs were replaced and retested. One or two studs were placed in a rib. The stud spacing was adjusted to accommodate the varying rib geometry but never exceeded 24 in. (609.5 mm). All studs were embedded 1-1/2 in. (38.1 mm) above the rib.

Four point loading was used on all of the beams to provide shear and moment conditions comparable to uniform load conditions. The loads were about equally spaced, but varied slightly so that loads were applied over a rib and not over a void. Figure 1 shows a typical test setup.

The beams were loaded in increments up to their estimated working load, then cycled ten times. After cycling the beams were reloaded in increments to near the ultimate load. Near ultimate, load was applied to produce fixed increments of deflection. Loading was terminated once the plateau of the load-deflection curve was established and deflections became excessive.

The beams were instrumented to measure the deflection at midspan, the slip

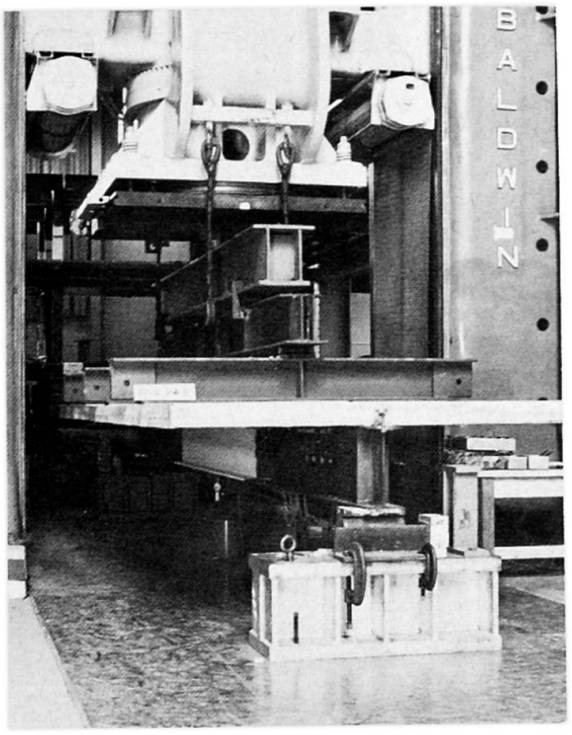

Fig. 1

at various points along the span, and the strain in the steel beam at various points along the span.

3. THEORETICAL CONSIDERATIONS

The flexural capacity of the test beams reported herein was determined essentially from the model suggested by Slutter and Driscoll(4) for composite beams with flat soffit slabs. However, the slab force was assumed to act at the centroid of the solid portion of the slab, above the top of the ribs and not at the center of the concrete stress block.

In many instances, the location of the slab force made little difference in the computed flexural capacity. For beams designed fully composite with the concrete slab governing the shear connection, the center of the stress block coincides with the centroid of the solid portion of the slab. However, for beams with low degrees of partial shear connection and/or high ribs, the location of the stress block has a significant influence on capacity.

For composite beams, with or without formed steel deck, there is loss of interaction or slip between the slab and the steel beam before developing the flexural capacity. This slip has little effect on the shear capcity of the connectors. However, it does effect the location of the slab force. Without any connection at all the compressive stress resultant would lie somewhere in the upper half of the full slab depth. However, with the bottom of the slab constrained by the presence of shear connectors the location of the stress resultant in the slab drops. The assumption that the stress resultant acts at the centroid of the solid portion of the slab seems to more adequately account for all cases involving composite beams with formed steel deck.

Robinson(5) has compared this difference in the assumed location of the slab force for a beam with 3 in. ribs and about 30% partial shear connection. He found that applying the method in Ref. 4 directly, provided an estimated capacity 3% higher than the test data and, that assuming the slab force to act at the center of the solid slab above the ribs, underestimated the capacity. However, he did not include the force on the shear connector directly under the load point, which falls at the edge of the shear span. Had this connector been included, the beam capacity would be overestimated by 9%. With the slab force acting at the center of the solid slab above the rib the capacity would be overestimated by 1%. Strain measurements on this beam confirm the location of the stress resultant in the slab as near the mid-depth of the solid portion of the slab. A similar conclusion was drawn from the Lehigh test beams.

4. BEHAVIOR OF COMPOSITE BEAMS WITH METAL DECK

4.1 Ductility - A significant aspect of these beams is their ductility. This ductility is demonstrated by the large deflections shown in the load-deflection plots in Fig. 2, even for beams with low degrees of partial shear connection. Also shown on the plots are two idealized elastic-plastic load-deflection curves. The elastic portion of the stiffer curve assumes complete interaction between the slab and the beam. The plastic plateau of that curve is the ultimate load for a partial shear connection with a reduced connector capacity defined in Eq. 1. The lower idealized curve is adjusted to account for an effective moment of inertia in the elastic range, which will be discussed later. The plastic plateau for that curve reflects a modified connector capacity as will be discussed later.

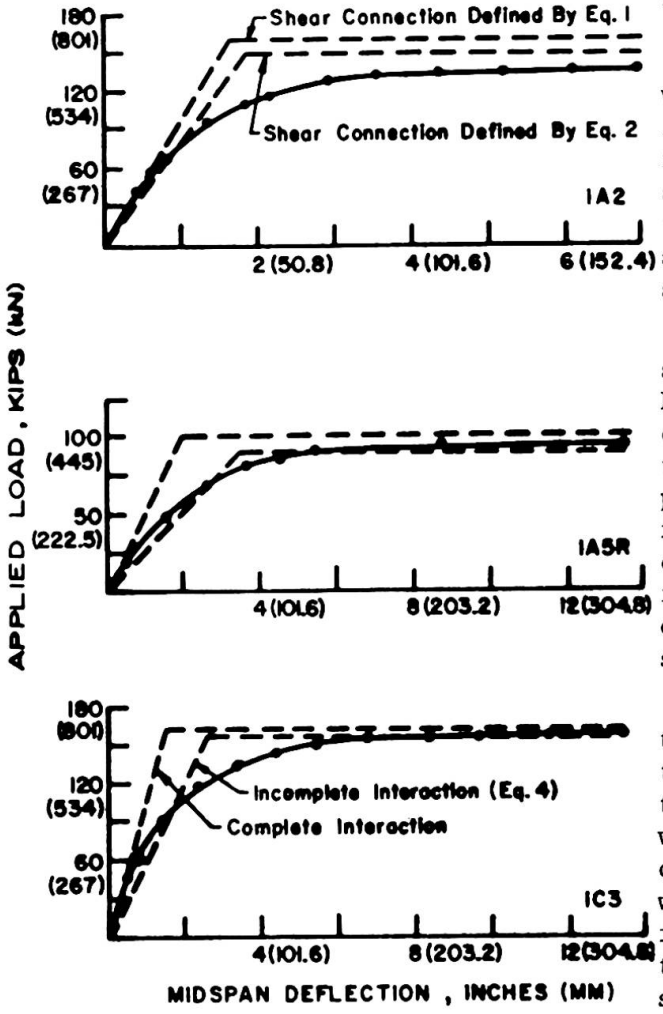

Fig. 2

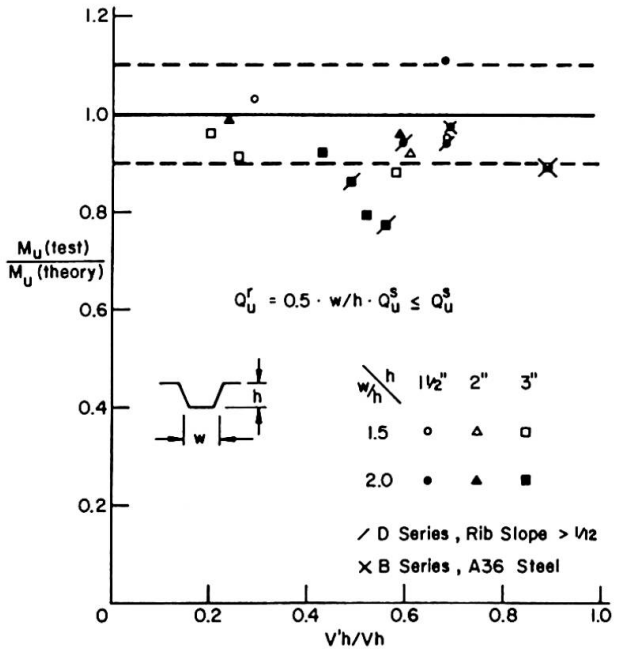

Fig. 3

All of the test beams sustained maximum deflections between 8 and 22 in. (203 to 560 mm). These deflections correspond to more than ten times the deflection at working load in all but two cases. Such large deflections were permitted by the formation of a plastic hinge near the midspan in all of the beams. The formation of these plastic hinges which produced the desired ductility could only have been possible with a ductile shear connection.

Shear connectors were instrumented at selected points along each of the beams. Data on a few of the beams was analyzed and confirms the ductility of the shear connection. All exhibited ductile behavior which permitted the redistribution of the slab force along the span and thus a ductile composite beam. This redistribution of forces permits the prediction of an average connector capacity for the beam, such as suggested in Ref. 2.

The reason for the ductile behavior of the shear connector can be attributed to the relative wide slabs used in the Lehigh test beams. In these tests the slab widths were taken as 16 times the full thickness of the slab, including rib height, plus the width of the steel beam flange. Previous investigators(2,6) have suggested using this slab width for beam tests and for design because it provides an upper limit connector ductility and capacity and more closely simulates the slab-beam interaction in an actual structure. Strain measurements across the slab width have indicated that shear lag is no more severe in a ribbed slab than in a solid slab(3).

4.2 Flexural and Connector Capacity - Unfortunately, the connector model suggested in Ref. 2 (see Eq. 1) for determining the flexural capacity of the composite beams proved unsatisfactory. Figure 3 shows the variation between test moment and theoretical moment using this model for all of the 17 beams. The test moment is nondimensionalized by the predicted moment and plotted against the degree of partial shear connection. Despite the obvious fact that several of the beams fall below their predicted capacity, the plot also shows that several beams with very low degrees of partial shear connection can obtain their predicted capacity. The observation has been made by Robinson(6) as well. Similarly rib slope and yield strength of the steel beam did not appreciably effect the beam capacity, as can be seen in Fig. 3. It is apparent that the connector model must consider other variables.

One such variable was found to be the height of the rib. A reexamination of all available test data, indicated that all of the beams with 3 in. (76.2 mm) deck except one had a stud embedment length greater than 1-1/2 in. (38.1 mm) above the rib. Although not considered as a variable in the Lehigh test program, it was obvious that embedment length is a key parameter in connector capacity. This observation has also been made by Robinson(6).

Thus additional modifications to the connector capacity model proposed in Ref. 2 are required. Besides the average rib width - height ratio, the height of the rib and the embedment of the connector must be taken into account to correctly predict the flexural capacity of composite beams with formed steel deck. To reflect these additional governing parameters, the following revised model was developed:

$$Q_{rib} = 0.6 \cdot \frac{H - h}{h} \cdot \frac{w}{h} \cdot Q_{sol} \leq Q_{sol} \qquad (2)$$

where: Q_{rib} = strength of stud shear connector in a rib
w = average rib width
h = height of rib
H = heigh of stud shear connector
Q_{sol} = strength of a stud shear connector in a solid slab

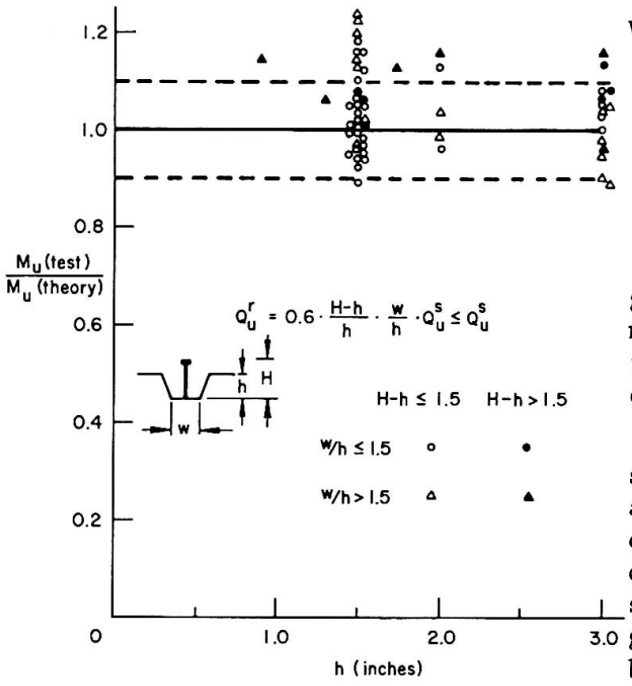

Fig. 4

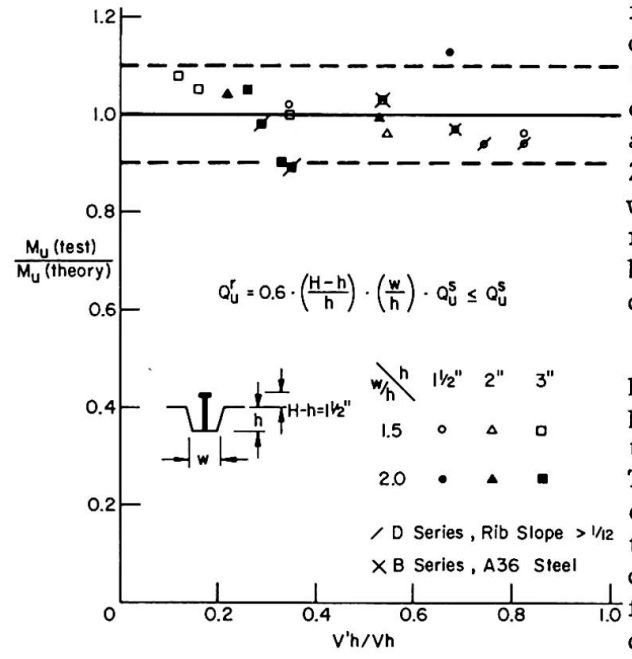

Fig. 5

Several recent tests on beams having greater connection embedment length were made at the University of Texas(7). These tests have further confirmed the applicability of Eq. 2.

Figure 4 shows all 56 beam test results in terms of test moment nondimensionalized by theoretical moment as a function of rib height. Equation 2 was used in predicting beam capacity. Figure 5 shows the same moment ratio as a function of the degree of partial shear connection, V'h/Vh, but for the 17 Lehigh tests only. The plots indicate that the connector capacity defined by Eq. 2 provides a better estimate of flexural capacity for beams with 3 in. (76.2 mm) deck. About the same flexural capacity is provided for beams with 1-1/2 and 2 in. (38.1 and 50.8 mm) deck. Equation 2 continues to account for the varying width - height ratios as indicated by the relatively even dispersion of the test beams for all rib heights. Further details of this study are given in Ref. 3.

4.3 Stiffness - The load-deflection plots shown in Fig. 2 show that beams with partial shear connection are less stiff than assumed for full composite action. This is due to the loss of interaction accompanying partial shear connection. For the Lehigh test beams with the least amount of shear connection, the stiffness was found to be between 70 and 80% of that calculated for full composite action at the working load level.

Early studies at the University of Illinois (8) and more recent studies at the University of Missouri (9) have shown that composite beams with flat soffit

slabs designed for full composite action have 85 to 90% of their calculated stiffness at the working load level. This loss in stiffness can be attributed to the fact that the shear connectors are flexible. Thus the connectors permit some slip or loss of interaction between the slab and the steel beam of a composite member, even though they will take all the force required for full composite action.

The shear connectors in a composite beam with formed metal deck behave similarly. Thus one would expect the same sort of difference to exist between actual and assumed stiffness of such beams designed for full composite action. The Lehigh test beams with the lowest degree of partial shear connection exhibited 20 to 30% loss of the stiffness which is about twice as much as experienced for full composite action in flat soffit slabs(8,9). On the other hand, these same beams provided at least twice the stiffness of a non-composite system. Thus a low degree of partial shear connection is very efficient in terms of stiffness.

Because of the complexity of the nonlinear variation of stiffness with the degree of partial shear connection, several emperical relationships have been examined(3). A relationship of the form:

$$I_{eff} + I_s + \frac{V'h}{Vh}^{\alpha} (I_{tr} - I_s) \qquad (3)$$

where I_{eff} = effective moment of inertia
I = moment of inertia of the steel section
I_{tr} = moment of inertia of the transformed composite section
α = numerical exponent

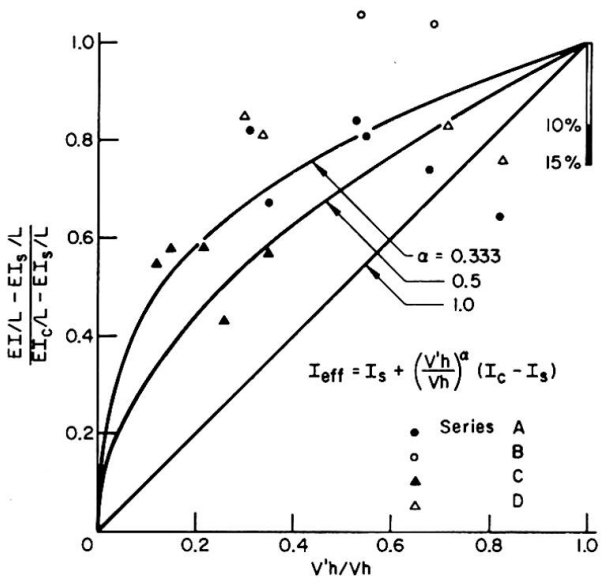

Fig. 6

was found to provide a reasonable fit to test data when α was taken equal to 1/2 or 1/3 as is demonstrated in Fig. 6. The stiffness provided by the 17 test beams is plotted for comparative purposes. With no shear connection, the stiffness is essentially that of the steel beam alone. A composite beam with full composite action (as provided by 100% shear connection will be assumed to have the stiffness of a transformed section with no loss of interaction between slab and beam. The straight line running from 0 to 1 in Fig. 6 would represent a linear variation of stiffness with α equal to 1. The solid vertical line at V'h/Vh equal to 1.0 shows the possible 15% variation between actual and assumed stiffness for a fully composite member. The plot clearly shows that the variation provided by the exponent α equal to 1/2 is generally conservative yet representative. The maximum deviation occurs as the degree of shear connection approaches unity. In no case is the loss of interaction greater than expected for a full shear connection.

Studies at the University of Missouri showed comparable behavior for composite beams with flat soffit slabs(9). A comparison of this data indicated general agreement with Eq. 3 when α was taken as 1/2.

5. CONCLUSIONS

The following conclusions may be drawn from the analysis reported herein:

1. The capacity of one or two stud shear connectors in the ribs of composite beams with formed steel deck may be determined from the following emperical expression:

$$Q_{rib} = 0.6 \cdot \frac{H - h}{h} \cdot \frac{w}{h} \cdot Q_{sol} \leq Q_{sol}$$

where H is the height of a stud shear connector in the rib, h is the height of the rib, w is the average rib width and Q_{sol} is the strength of the stud shear connector in a flat soffit slab.

2. The flexural capacity of a composite beam with formed steel deck can be more accurately and conservatively estimated if the slab force is considered to act at the mid-depth of the solid portion of the slab above the ribs, rather than at the centroid of the concrete stress block.

3. The flexural capacity of a composite beam utilizing high strength steel is not adversely affected by the increased slab force and can be predicted provided that the connector capacity is known.

4. The deflection of a composite beam with partial shear connection, with or without formed steel deck, may be estimated with the following expression for an effective moment of inertia:

$$I_{eff} = I_s + \frac{V'h}{Vh} (I_{tr} - I_s) \quad (4)$$

where I_s is the moment of inertia of the steel beam, I_{tr} is the moment of inertia of the transformed composite section, V'h is the total horizontal shear to be resisted by connectors providing partial composite action and Vh is the total horizontal shear to be resisted by connectors under full composite action.

6. ACKNOWLEDGMENTS

The testing described in this report was conducted at Fritz Engineering Laboratory, Lehigh University. The contribution of the Fritz Laboratory staff is gratefully acknowledged.

7. REFERENCES

1. Robinson, H. - TESTS OF COMPOSITE BEAMS WITH CELLAR DECK, Journal of the Structural Division, ASCE, Vol. 93, No. ST4, August 1967.
2. Fisher, J. W. - DESIGN OF COMPOSITE BEAMS WITH FORMED METAL DECK, AISC Engineering Journal, AISC, Vol. 7, No. 3, July 1970.
3. Grant, J. A., Jr., Fisher, J. W. and Slutter, R. G. - COMPOSITE BEAMS WITH FORMED STEEL DECK, to be published, AISC Engineering Journal, AISC.
4. Slutter, R. G. and Driscoll, G. C. - FLEXURAL STRENGTH OF STEEL-CONCRETE COMPOSITE BEAMS, Journal of the Struc. Div., ASCE, Vol. 91, No. ST2, April 1965.
5. Robinson, H. - COMPOSITE BEAM INCORPORATING CELLULAR STEEL DECKING, Journal of the Structural Division, ASCE, Vol. 95, No. ST3, March 1969.
6. Robinson, H. and Wallace, I. W. - COMPOSITE BEAMS WITH PARTIAL CONNECTION, Meeting Preprint No. 1549, ASCE Annual Conf., St. Louis, Mo., Oct. 18, 1971.
7. Furlong, R. W. and Henderson, W. D. - REPORT OF LOAD TESTS ON COMPOSITE BEAMS OF LIGHTWEIGHT CONCRETE IN THREE-INCH METAL DECK WITH STUD LENGTH AS THE PRINCIPAL VARIABLE, University of Texas at Austin, August 1975.
8. Siess, C. P., Viest, I. M. and Newmark, N. M. - SMALL-SCALE TESTS OF SHEAR CONNECTORS AND COMPOSITE T-BEAMS, Bul. 396, Exp. Sta., U. of Ill., Urbana, Ill., 1952.
9. McGarraugh, J. B. and Baldwin, J. W. - LIGHTWEIGHT CONCRETE-ON-STEEL COMPOSITE BEAMS, AISC Engineering Journal, AISC, Vol. 8, No. 3, July 1971.

SUMMARY

This report presents the results of 17 composite beam tests conducted at Lehigh University incorporating formed steel deck. These results were analyzed in conjunction with 39 additional tests conducted by previous investigators. The purpose of this report was to evaluate shear connector capacity and beam flexural capacity and behaviour, particularly for beams utilizing high strength steel.

RESUME

Ce rapport contient les résultats de 17 essais réalisés à l'Université Lehigh sur des poutres mixtes avec platelage métallique incorporé. Ces résultats ont été analysés conjointement avec 39 autres essais réalisés auparavant par d'autres chercheurs. Le but de ce rapport était d'évaluer la résistance au cisaillement des boulons et la résistance à flexion des poutres, particulièrement pour les poutres en acier à haute résistance.

ZUSAMMENFASSUNG

Dieser Bericht enthält die Ergebnisse von 17 Tests an Verbundträgern, die an der Lehigh Universität durchgeführt wurden, an denen ein Stahlblech eingearbeitet war. Die Resultate wurden anhand 39 zusätzlicher Tests analysiert, die vorher von anderen Forschern ausgeführt wurden. Zweck dieses Berichtes war, die Tragfähigkeit der Verbundmittel und des Trägers selber, sowie das Verhalten, besonders für Tragbalken aus hochfesten Stählen, zu berechnen.

Vb
Problèmes de conception
Entwurfsprobleme
Design Problems

Leere Seite
Blank page
Page vide

An Application of High Strength Steels to Earthquake Resistant Buildings

Utilisation des aciers à haute résistance dans des bâtiments résistants aux tremblements de terre

Anwendung hochfester Stähle in erdbebensicheren Bauten

HIROSHI AKIYAMA
Associate Professor
University of Tokyo
Tokyo, Japan

1. INTRODUCTION

One of the structural performances requisite for earthquake resistant structures is absorption capacity of vibrational energy exerted by earthquakes. Sources of energy absorption are found in inelastic deformations of structural members and other damping effects and to evaluate the inelastic deformation is essentially necessary to economically proportion steel structures.

Ordinary structural steel can develop considerable amount of inelastic deformation, provided that the structural members are properly kept from any types of instability . High-strength steels, however, show less inelastic deformability as stated in Theme report Va. Therefore it seems less advantageous to make use of the poor inelastic deformability of high-strength steels. It may be rather more efficient to make use of the large elastic deformability and high strength of them.

Combined use of high-strength steels and usual steels may allow preferable structural performances in earthquake resistant structures, especially in tall buildings. In such composite structures where high-strength steels form a continuous structural component besides usual steels, the structural component composed of high-strength steels can behave elastically, while components composed of usual steels with less elastic deformability may undergo plastic deformations and can absorb vibrational energy. As a whole, the co-existence of these two different steels is likely to facilitate to evenly disperse plastic deformations over the whole structure, preventing the collapse of the structure caused by concentration of damages into one story. Only confined use of high-strength steels may be sufficient to attain the aim.

2. ASSESSMENT OF INELASTIC DEFORMABILITY OF HIGH-STRENGTH STEELS

In Fig.1 the simplified structural model for a multi-storied structure subjected to seismic forces is shown, where deformable elements are represented by columns clamped by rigid beams. As shown in Fig.1(b), structural behavior of the structure is reduced to that of the cantilever column with the length of one half of the story height. The inelastic behavior of the cantilever steel column can be well predicted by a simple theory allowing for the strain-hardening of the steel(1). Stress-strain relationship of the steel may be expressed by a tri-linearized relation as shown in Fig.2(a). Moment-curvature relationship for usual sectional shapes such as H-shapes and structural tubes can be readily obtained from $\sigma - \varepsilon$ relation, the inelastic part of which is expressed by a

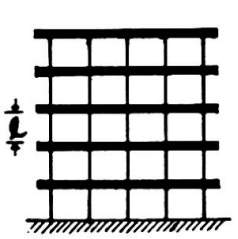

(a) (b)

Fig.1 Simplified Structural Model

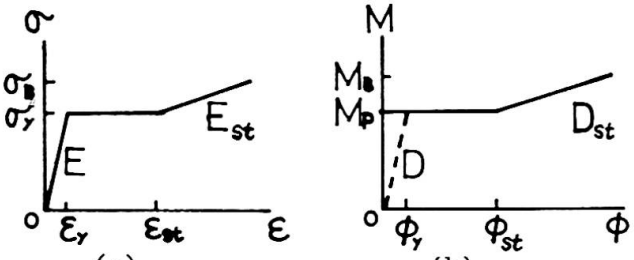

(a) (b)

Fig.2 Properties of Steels

bi-linear relation as shown in Fig.2(b). In Fig.2(b) M_p and M_B mean the fully plastic moment and the ultimate moment capacity of a section respectively and can be expressed as

$$M_p = A \times M_{p0}(1-p), \qquad M_B = A \times M_{p0}(1/Y-p), \tag{1}$$

where M_{p0}=fully plastic moment under pure bending, $p=P/P_y$, P=axial force, P_y=yield axial force, Y=yield ratio of the material= σ_y/σ_B, A=constant.

Flexural rigidity in plastic range, D_{St} and the curvature at the onset of the strain-hardening, ϕ_{st} can be determined as

$$\begin{aligned} &\text{for } p \le 0.5, \quad D_{St} = DE_{St}(1+2p)/E, \quad \phi_{St} = \phi_o, \\ &\text{for } p > 0.5 \quad D_{St} = 2DE_{St}/E, \quad \phi_{St} = \phi_o/(2-2p), \end{aligned} \tag{2}$$

where $\phi_o = \phi_y(\varepsilon_{st} - \varepsilon_y)/\varepsilon_y$, D=flexural rigidity in elastic range=EI, $\phi_y = M_p/D$.

Then the inelastic deformation of the cantilever column can be calculated from the following formula.

$$\delta_p = \left(\frac{\alpha-1}{2}\frac{D}{D_{St}} + b\right)\left(\frac{\alpha^2-1}{2\alpha^2}\right)\frac{\ell^2\phi_y}{2}, \qquad Q_e = \frac{2\alpha M_p}{\ell}, \quad \alpha \ge 1, \tag{3}$$

where $b = \phi_{st}/\phi_y$, α=stress increase ratio beyond M_p, and the maximum value of α at the ultimate state can be written from Eq(1) as

$$\alpha_m = M_B/M_p = (1/Y-p)/(1-p) \tag{4}$$

Since for most of structural steels $Q_e - \delta_p$ relation becomes almost linear, $Q_e - \delta$ relation may be simply expressed by a bi-linear relation. Thus by non-dimensionalizing Q_e by $Q_{ye}(=2M_p/\ell)$ and δ by $\delta_y(=Q_y\ell^3/12D)$, $Q_e - \delta$ relation is obtained as shown Fig.3(a), where μ_m means dimensionless ultimate plastic deformation capacity(ductility) and μ_m is given by the following equation.

$$\mu_m = \frac{\delta_p}{\delta_y} = 3\left(\frac{\alpha_m-1}{2}\frac{D}{D_{St}} + b\right)\left(\frac{\alpha_m^2-1}{2\alpha_m^2}\right) \tag{5}$$

For an example two typical structural steels(a mild steel and a high-strength steel) are compared in their structural behavior in the inelastic range. Material properties of them are tabulated in Table 1.

Grade	σ_y t/cm²	σ_B t/cm²	Y	ε_{st}	E_{st}
mild steel (SS41)	2.4	4.1	0.59	11 ε_y	E/30
high strength steel(SM58)	5.0	6.0	0.83	5 ε_y	E/50

Table 1. Mechanical Properties of Steels

High-strength steel is characterized by it's high yield ratio.

In Fig.3(b) and 3(c) the results of calculation are shown. In Fig.3(b) the slope of inelastic range relative to that of elastic range is shown. In Fig.3(c) the ductility is plotted. From these figures it can be seen that the slope of the inelastic range is not likely to be affected by the difference of the steels, ranging about 5% of the slope in elastic range and consequently the ductility is considerably affected by the yield ratio of the material.

Thus the ductility of the high-strength steel will be considerably reduced according to the increase of the yield ratio and should not be reliable sources of energy absorption during earthquakes. On the contrary mild steels can develop fairly large ductility even under high axial compression.

Substantial horizontal resistance of the column is affected by P-δ effect and is expressed by

$$Q = Q_e - P\delta/\ell \tag{6}$$

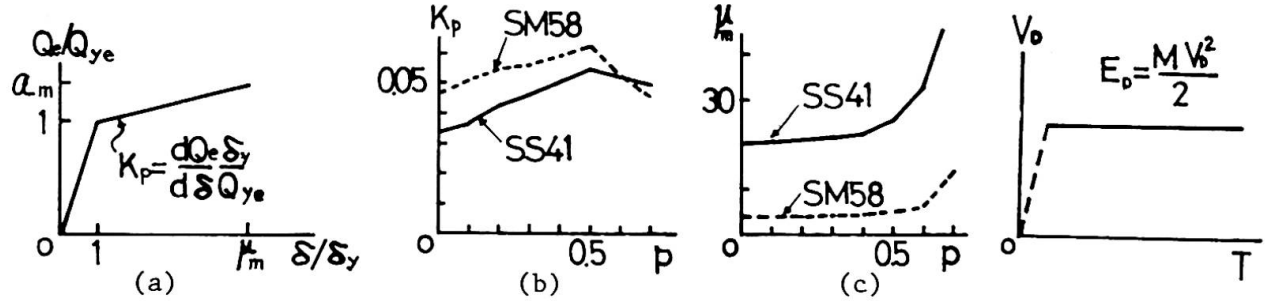

Fig.3 Behavior of Cantilever Columns

Fig.4 Energy Input

3. GENERAL BEHAVIOR OF BUILDINGS UNDER EARTHQUAKES

Housner assumed that energy input contributable to structural damages exerted by an earthquake can be approximately expressed by

$$E_D = 0.5M\dot{y}_{e\,max}^2, \tag{7}$$

where E_D=energy input causing damages, M=total mass of the structure, $\dot{y}_{e\,max}$=velocity response spectrum of elastic system(2).

A general law on vibrational systems can be written as

$$W_e + W_p + W_h = W_E \tag{8}$$

where W_E=total energy input exerted by an earthquake, W_p=energy absorption due to accumulated plastic work(structural damages), W_h=energy absorption due to damping, W_e=elastic vibrational energy.

E_D may correspond to W_p+W_e. Through vast amount of numerical analyses on inelastic vibrational systems with various types of restoring force characterisyics, each energy component in the above equation was evaluated and Housner's assumption was verified to be applicable to general structures(3). Consequently the amount of energy contributable to structural damages is scarecely affected by the difference of the structural forms and averagingly E_D, when expressed in a velocity through conversion given below, may be considered to be constant over a wide range of fundamental natural periods of the structures except a narrow range of shorter natural period as shown in Fig.4.

$$V_D = \sqrt{2E_D/M} = \sqrt{2(W_p+W_e)/M} \tag{9}$$

To controle vertical distribution of damages is one of the essentials in the aseismic design of multi-storied buildings subjected to a certain amount of energy input. When the vertical strength distribution is well balanced, the damages may be evenly dispersed. Otherwise, the damages concentrate into relatively weak stories. Since distribution of damages are seriously dependent on the vertical strength distribution, the effect of probable deviation of the strength distribution from the aimed one must be taken into account and the structural robustness of the tall building must be examined under such a disadvantageous condition encountered by the decrease of strength in a story.

4. BEHAVIOR OF COMPOSITE STRUCTURES UNDER EARTHQUAKE

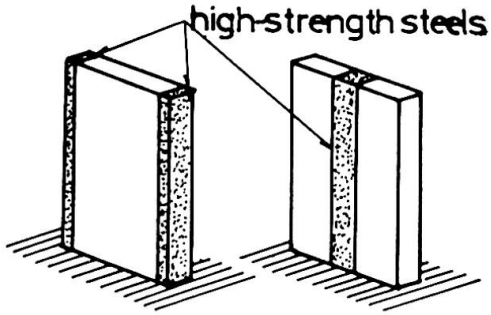

Fig.5 Composite Structure

A possible combination of usual steel components and high-strength steel components is illustrated in Fig.5. High-strength steel components extending vertically are tightly connected to mild steel components through rigid slabs.

Restoring force characteristics for high-strength steels may be considered to be elastic within the limit determined by their yield strength. P-δ effect being a negative linear action as seen in Eq(6) can be included in the property of high-strength steel components. Thus the characteristics for high-strength steels involving P-δ effect may be depicted as shown in Fig.6(a) where δ and Q denote relative story displacement and restoring force in the story. The restoring force characteritics for mild steels can be readily constructed from the bi-linear load-deflection relation under monotonic loading as shown in Fig.6(b), where the broken line

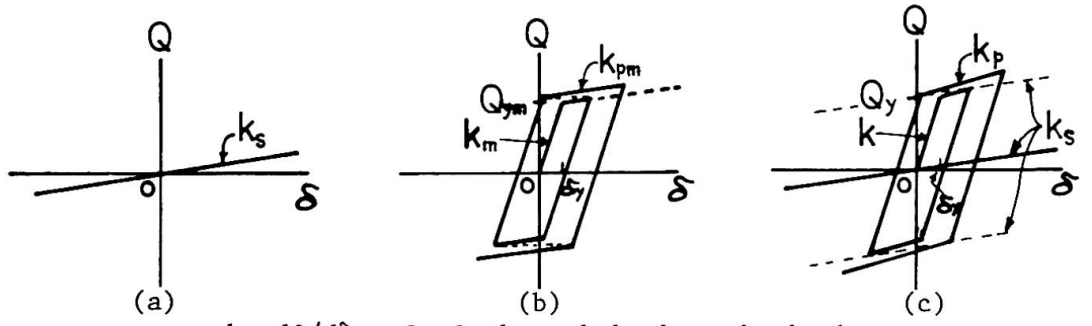

$k = dQ/d\delta$, $Q_y = Q_{ym} + k_s\delta_y$, $k = k_m + k_s$, $k_p = k_{pm} + k_s$

Fig.6 Restoring Force Characteristics of Composite System

shows the monotonic Q-δ relation. These are drawn according to the rule that the inelastic parts in each cycle of loading in one loading domain(negative or positive) connected sequentially should coinside with the inelastic curve in the monotonic loading(4). Overall restoring force characteristics in one story may become like that shown in Fig.6(c).

According to the conventional numerical technique, the dynamic responses of composite structures were carried out. Applied models are five-mass systems with 1 sec of fundamental natural period and the used accelerogram is of El Centro May 1940-NS Component, maximum value of which is 320 gals. No other damping source except inelastic deformations was considered.

Parameters used in analyses are specified in Table 2 where α denotes yield shear coefficient defined below.

$$\alpha = Q_y / W \quad , \tag{10}$$

where W=total gravity load above the story considered,

Q_y=yield strength of the story.

m_i/m_1	α_2/α_0	α_3/α_0	α_4/α_0	α_5/α_0	k_2/k_1	k_3/k_1	k_4/k_1	k_5/k_1	comment
1.0	1.1	1.25	1.56	2.0	0.87	0.73	0.6	0.4	common for all cases

Case	No.1	No.2	No.3	No.4	No.5	No.6
k_{pi}/k_i	0.0	0.1	0.2	0.05	0.15	0.25
k_{si}/k_i	0.0	0.1	0.2	0.0	0.1	0.2
comment	elastic -plastic	composite without strain hardening		composite with strain hardening		
α_1/α_0	1.0, 0.8, 0.7 for all cases					

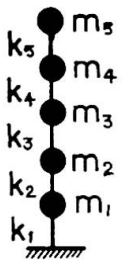

Table 2. Parameters Used in Response Analysis

Dynamic responses of those models were calculated by varing α_0 from 0.1 to 0.6. Special attention was paid to the responses of the first story where the yield strength was changed in three steps as shown in Table 2. Maximum story displacement and accumulated plastic deformation in both positive and negative directions were obtained and non-dimensionalized responses were defined as

$$\mu_{1\pm} = |\delta_{1\pm}| / \delta_{y1}, \quad \eta_{1\pm} = \Sigma\,|\Delta\delta_{p\pm}| / \delta_{y1} \tag{11}$$

where δ_1 =maximum deflection of the first story into one direction,

$\Delta\delta_p$=plastic deformation increment of the first story into one direction.

In Fig.7 some typical responses for composite structures are shown. In Fig.7(a) the greater value of $\mu_{1\pm}$ are plotted. It can be seen that when the strength of the story is reduced by 30%, the maximum deflection of non-composite elastic-plastic system increases considerably. The composite structure, however, can be kept in small increase of deflection by only 10% of cooperative action of high-strength steels(k_s/k=0.1 in No.5).

In Fig.7(b) the greater value of $\eta_{1\pm}$ is plotted. The decrease of strength of the first story produces severe energy concentration in elastic-plastic system and the composite structures without strain-hardening are also likely to undergo the remarkable energy concentration comparable to that in non-composite structures. The composite structure with strain-hardening, however, can do without suffering such a large energy concentration, and only 10 or 15% of the

cooperative action of the high-strength steels with mild steels enables the enrgy concentration to reduce by half.
In Fig.8 the correspondence between $(\mu_+ + \mu_-)/2-1$ and $(\eta_+ + \eta_-)/2$ is shown. This relation may be generally used to estimate μ from η and vice versa as mentioned afterward.
It can be concluded that the hazardous energy concentration induced by the probable decrease of the strength may be overcome by the robust nature of the composite structure.

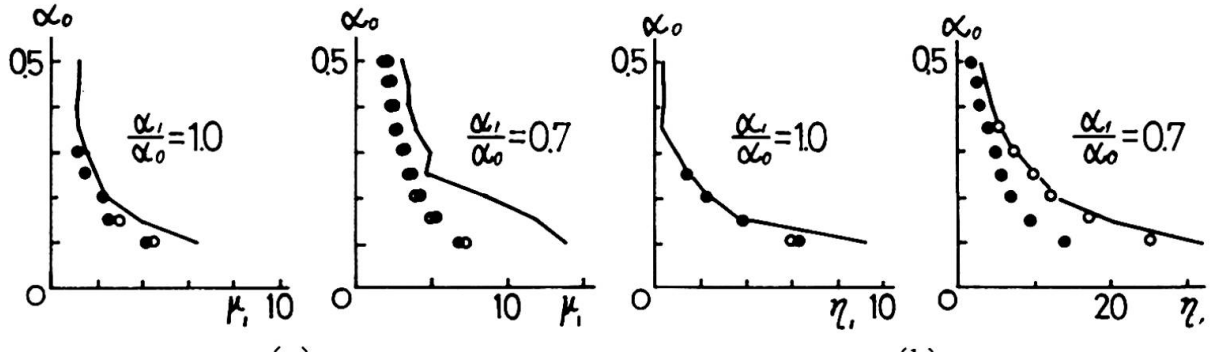

o k_p/k =0.2, k_s/k =0.2 (No.3)
● k_p/k =0.15, k_s/k =0.1 (NO.5)

Fig.7 Responses of Composite Structures

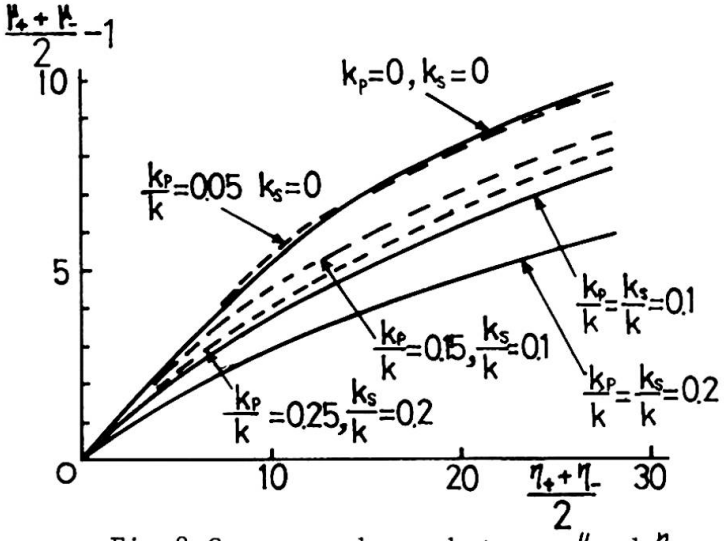

Fig.8 Correspondence between μ and η

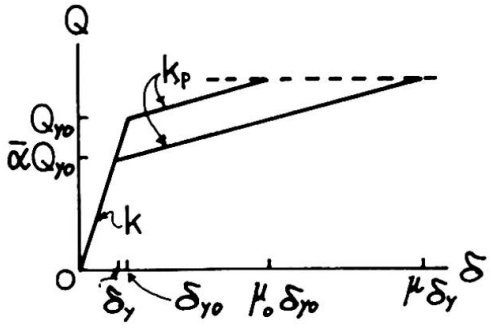

Fig.9 Maximum Deflection

5. ESTIMATION OF RESPONSES OF COMPOSITE STRUCTURES

The response of the composite structures may be estimated from that of the elastic-plastic system with same strength distribution by making an assumption that $\mu_+ = \mu_-$ and $\eta_+ = \eta_-$.
By taking account of the equivalence in accumulated plastic energy into two systems with same strength, η of the composite system can be converted from the response of the elastic-plastic system, η_{ep} through the following equation.

$$\eta\left(1-\frac{k_p-k_s}{k-k_s}\right)\left[2\left(1-\frac{k_s}{k}\right)+\eta\frac{k_p-k_s}{k}\right]=2\eta_{ep}, \qquad (12)$$

where k, k_p and k_s are rigidities defined in Fig.6.
μ can be readily obtained from Fig.8.
The maximum displacement of the story where some decrease of the strength happened to occur can be estimated from the original undegraded system under the assumption that the maximum lateral force of the degraded system does not exceed that attained by the original system. Referring to Fig.9, the possible maximum response of the degraded story can be obtained as

$$\mu=\frac{k}{k_p}\frac{1}{\bar{\alpha}}\left[\frac{k_p}{k}(\mu_0-1)+1-\bar{\alpha}\right]+1, \quad \mu_0 \geq 2.0,\ k_p/k \geq 0.1. \qquad (13)$$

η can be also determined from Fig.8. For smaller values of μ, the above equation will give overestimation. However, for smaller value of η, $\alpha - \eta$ relation can be extrapolated from the already obtained by the next equation(3).

$$\alpha^2 \eta = \text{constant} \qquad (14)$$

Thus alternatively smaller values of μ can be determined again from Fig.8.
To verify the above mentioned procedure, the response of the composite structure was predicted by using only the averaged response of the elastic-plastic system(No.1), $(\mu_{1+}+\mu_{1-})/2$ and $(\eta_{1+}+\eta_{1-})/2$. Predicted values are compared with the actual responses in Fig.10 and are found to be in good agreement with them.

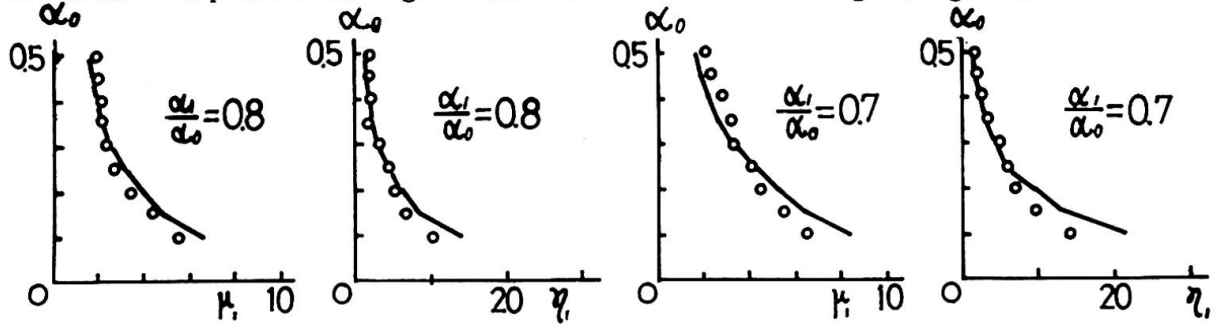

—— prediction o Responses of No.5(k_p/k =0.15, k_s/k=0.1)

Fig.10 Predicted responses of Composite Structure

REFERENCES

(1) Kato,B. and Akiyama,H., Inelastic Bar Subjected to Thrust and Cyclic Bending, Proc. ASCE, ST1, January 1969
(2) Housner,G.W., Limit Design of Structures to Resist Earthquakes, 1st WCEE,1956
(3) Kato,B. and Akiyama,H., Energy Input and Damages in Structures Subjected to Severe Earthquakes, Trans. AIJ, No.235, Sept. 1975(in Japanese)
(4) Kato,B. and Akiyama,H., Theoretical Prediction of the Load-Deflection Relationship of Steel Members and Frames, IABSE Sym. Lisboa 1973

SUMMARY - It is required for earthquake resistant tall buildings to be equiped with large energy absorption capacity and to be prevented from hazardous energy concentration. The proposed hybride structure consisting of principal mild steel components and secondary high-strength steel components was found to exhibit preferable robustness during earthquakes. It was also shown that the response of the composite structure can be well predicted taking into account the response of the fundamental elastic-plastic systems.

RESUME - Les maisons hautes susceptibles de résister aux tremblements de terre doivent être capables d'absorber de grandes quantités d'énergie tout en évitant leur concentration . La construction hybride proposée dans cet article, composée d'éléments principaux en acier doux et d'éléments secondaires en acier à haute résistance, a présenté la meilleure résistance lors de tremblements de terre. Les réactions de la construction hybride peuvent être déterminées à l'avance en fonction du comportement élasto-plastique du système.

ZUSAMMENFASSUNG - Die erdbebensicheren Hochhäuser müssen grosse Energiemengen absorbieren, welche sich nicht konzentrieren dürfen. Das im Bericht beschriebene hybride Tragwerk aus Hauptelementen aus Stahl St 37 und Nebenelementen in hochfestem Stahl, hat das beste Verhalten gegen Erdbeben gezeigt. Die Widerstandsfähigkeit des hybriden Tragwerkes kann im voraus anhand des elastoplastischen Verhaltens des Systems berechnet werden.

Stützen aus hochfestem Baustahl StE 47 in einem Hochhaus in Frankfurt am Main

Columns in High-yield Steel StE 47 in a Tall Building in Frankfurt

Colonnes en acier à haute résistance StE 47 dans un immeuble de grande hauteur à Francfort

F.W. GRAVERT
Dr.-Ing., Partner
Ingenieursozietät BGS
Frankfurt am Main, BRD

Das Hochhaus wurde geplant für zwei Kellergeschosse, ein Erdgeschoß und 31 Obergeschosse mit einer Höhe von 147 m über dem Gelände. Den Grundriß eines Normalgeschosses zeigt Abb. 1. Der Lasteinzugsbereich beträgt bei den am höchsten belasteten Eckstützen rund 13o m². Die Nutzlasten in den Geschossen reichen von 5 kN/m² bis zu 17 kN/m². Die größte Stützenlast beträgt 59 MN.

Das Bauwerk wird durch zwei am Gebäuderand stehende Kerne ausgesteift. Die Decken wirken als Scheiben und geben über Doppelunterzüge in den Stützenachsen ihre Vertikallast an Stützen und Kerne ab. Die Stützen erhalten daher Momente nur aus den auskragenden Unterzügen und infolge der unterschiedlichen Senkung der Deckenauflager. Die Momentenbeanspruchung beträgt maximal 1 MNm.

Die Stützen sollten ursprünglich wie die Bodenplatte, Decken, Unterzüge und Kerne in Stahlbeton ausgeführt werden. Eine Vordimensionierung ergab bei Stahlbetonstützen zahlreiche Querschnittsänderungen und eine maximale Querschnittsfläche von F_B = 1,5ox 1,5o = 2,25 m² bei Bn 45o und μ = 8 %. Die mehrfachen Querschnittssprünge waren wie die großen Abmessungen in den unteren Geschossen unerwünscht. Darum wurden zum Vergleich Hohlkastenstützen aus Stahl untersucht, wobei die Wanddicke zunächst mit 1o % der Seitenlänge angesetzt wurde, Abb. 2.

Untersuchte Stähle:	St 37-2	St 52-3	StE 47	StE 7o
Streckgrenzen /N/mm²/:	24o	36o	47o	7oo

Die Untersuchungen ergaben, daß im unteren Gebäudeteil Stahlstützen mit Außenabmessungen o,8o x o,8o = o,64 m² und im oberen Gebäudeteil o,6o x o,6o = o,36 m² ausgeführt werden können. Je nach Belastung und Knicklänge wurden außerdem

Stahlgüte und Wanddicke der Hohlkästen variiert. Für die meisten Stützen wurde der hochfeste Feinkornbaustahl StE 47 gewählt. Die Blechdicken reichen von 26 bis loo mm.

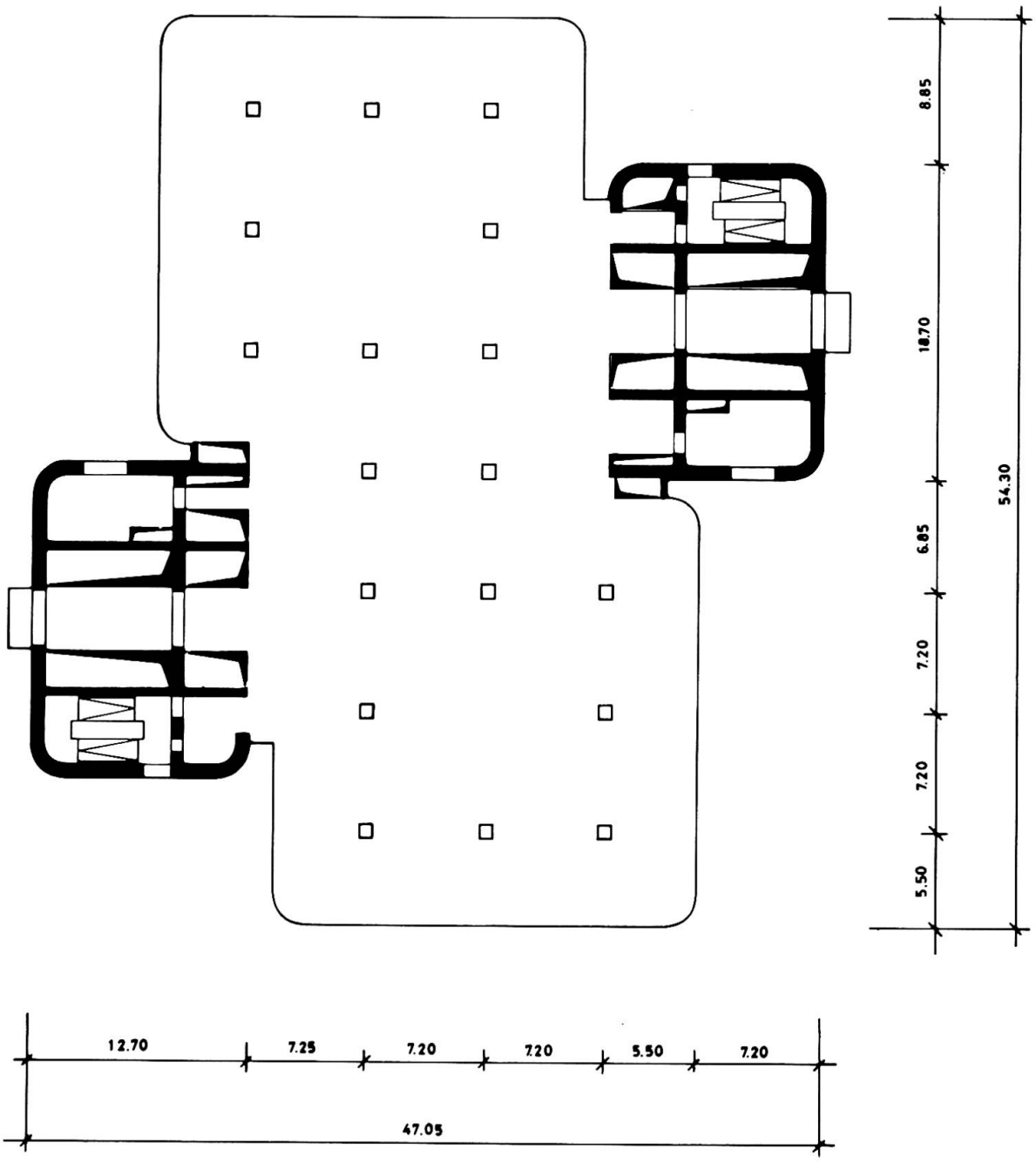

Abb. 1: Normalgeschoßgrundriß

Die Kosten für die Stahlstützen waren einschließlich des Brandschutzes fast doppelt so hoch wie für Stützen gleicher Tragfähigkeit aus Stahlbeton. Dem war gegenüberzustellen: schnelle und einfache Herstellung der Stützen beim Rohbau, da sie montagefertig angeliefert wurden; in zwei Gebäudebereichen identische Elemente beim Ausbau, da alle Querschnitte 8o x 8o cm oder 6o x 6o cm ausgeführt wurden; ein Nutzflächengewinn von rund 3oo m², Abb. 3.

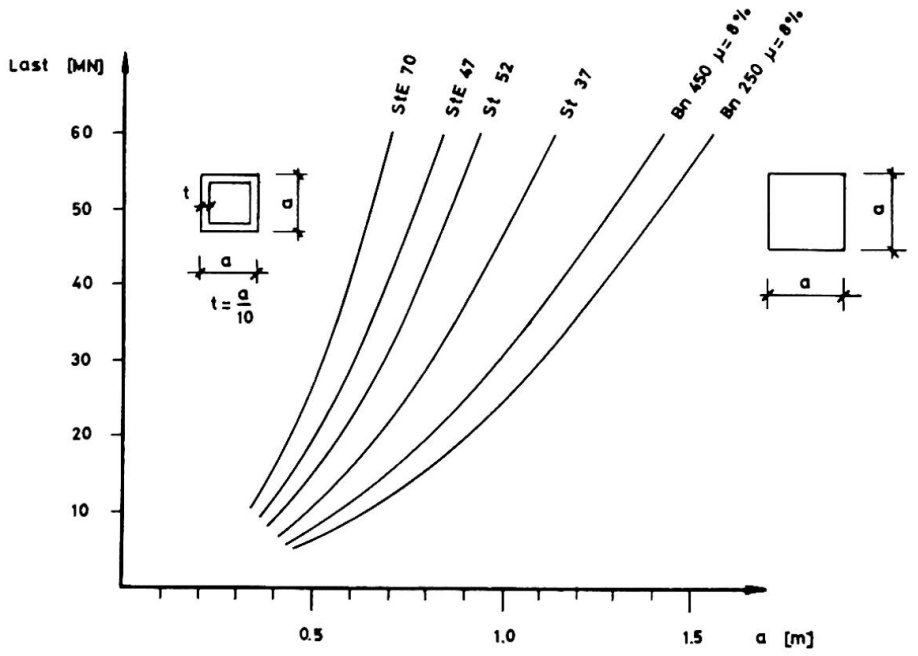

Abb. 2: Flächenbedarf von Stützen

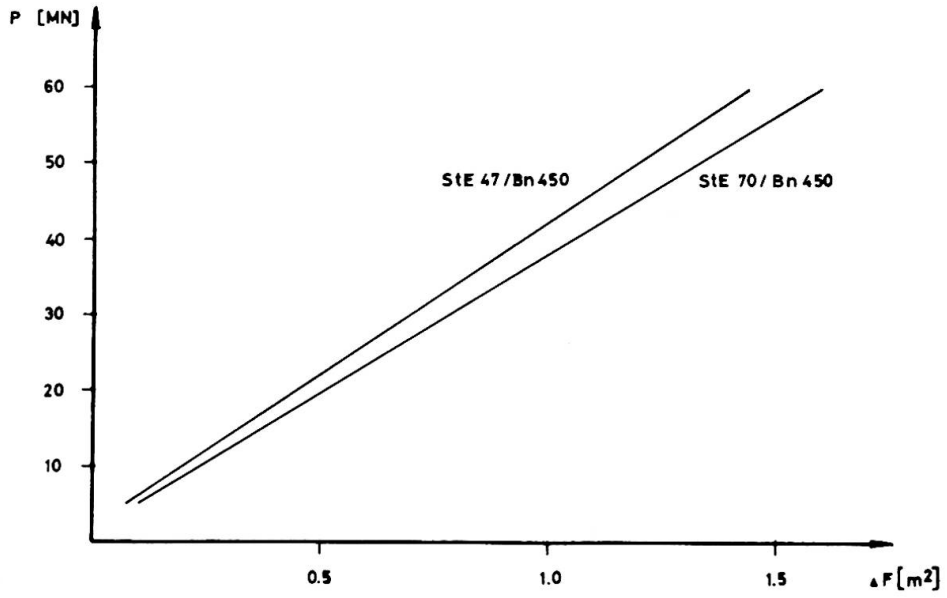

Abb. 3: Nutzflächengewinn bei Stahlstützen gegenüber Betonstützen

Der Zeitgewinn bei Roh- und Ausbau und der finanzielle Vorteil des Einbaus identischer Ausbauelemente bei abgehängten Decken und Einbauwänden sowie des Nutzflächengewinns haben den Mehrkostenaufwand gerechtfertigt.

Nachdem dies feststand, konnten die Stützen endgültig dimensioniert werden. Für die geringer belasteten Stützen aus genormtem St 37-2 und St 52-3 brauchten keine Spannungsüberlegungen angestellt zu werden. Bei den hoch belasteten Stützen aus StE 47 wurde die zulässige Spannung im Lastfall Hauptlasten für

Blechdicken bis 6o mm gemäß DAST-Richtlinie 011 mit 28o N/mm² angesetzt. Für die größeren Blechdicken wurde die zulässige Spannung linear so abgemindert, daß bei loo mm Blechdicke gegenüber der Streckgrenze eine Sicherheit von ν = 1,71 eingehalten wird. Damit beträgt die zulässige Spannung bei dieser Dicke 24o N/mm², Abb. 4

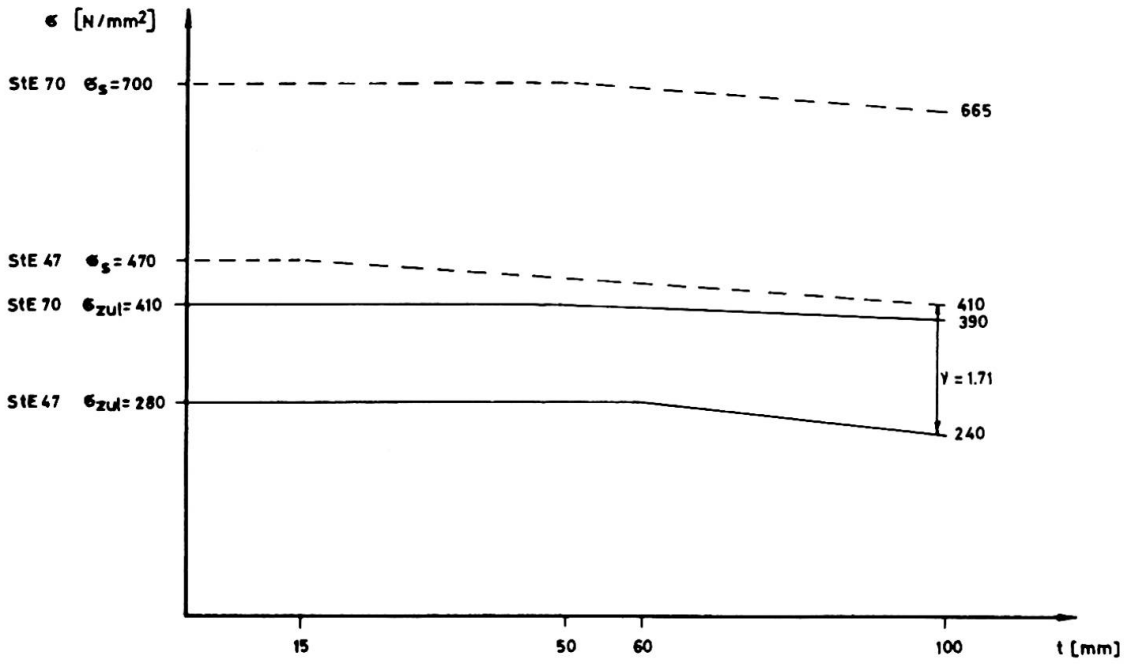

Abb. 4: Spannungen hochfester Stähle

Der Einsatz des noch tragfähigeren StE 7o wurde nicht erwogen, da er außer zu größeren Schlankheiten besonders zu erheblich größeren Stützenstauchungen geführt hätte.

Die Stahlstützen wurden aus Blechen zu quadratischen Hohlkästen mit Kopf- und Fußplatte zusammengeschweißt. Die die Einzelbleche zum Kasten verbindenden Längsnähte müssen Normalspannungen und Schubspannungen in Nahtrichtung übertragen. Versuche ergaben, daß diese Schubspannungen nicht abgemindert werden müssen. Die vorgesehenen Schweißlagen konnten verringert werden.

Blechdicke	≧ 6o	<6o /mm/
Dicke a der Längsnaht Seitenblech/Seitenblech	15	1o /mm/
Dicke a der Kehlnaht Seitenblech/Kopf- und Fußplatte	2o	15 /mm/

Die Kopf- und Fußplatten sind für die Lasteintragung aus den Stahlbetondoppelunterzügen in die Stahlstützen dimensioniert, Abb. 5.

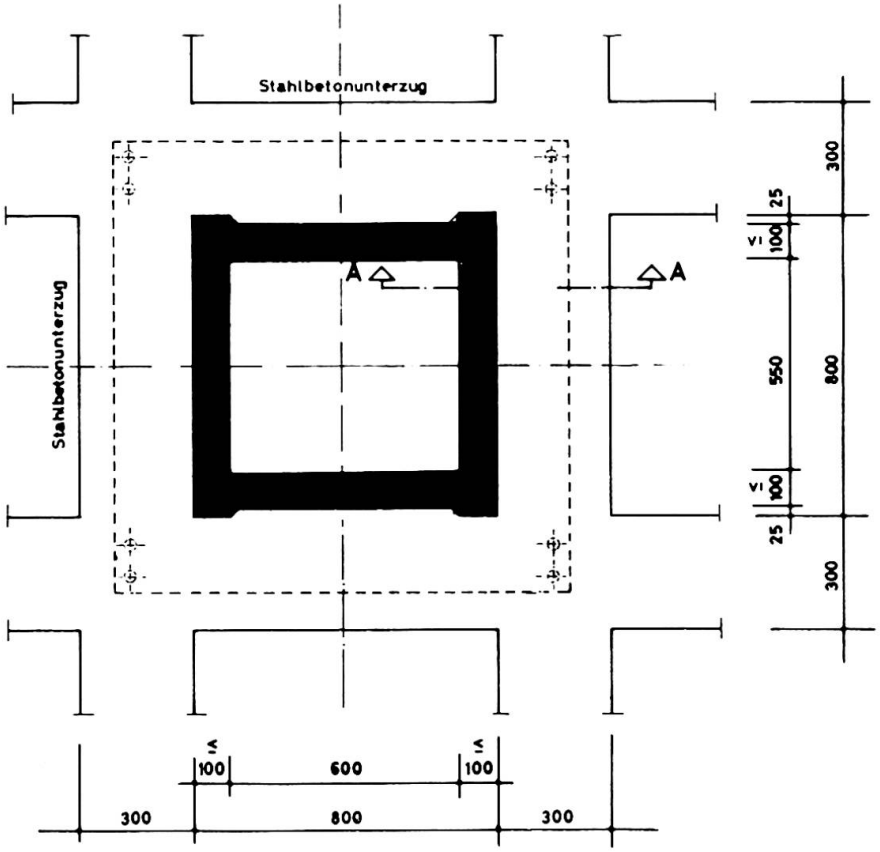

SCHNITT A - A

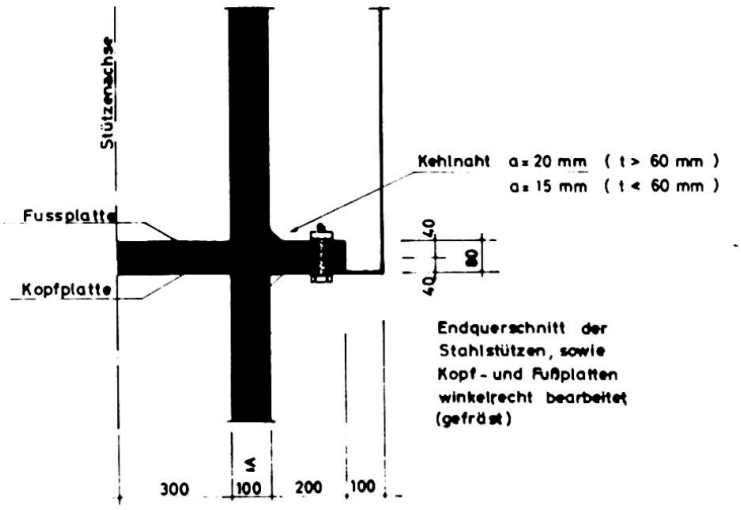

Abb. 5: Ausführung der Stützen in StE 47

Zur Montagesicherung werden die Platten an den Ecken mit je zwei HV-Schrauben verbunden. Damit kann auch ein Moment aus unplanmäßiger Horizontalbelastung der noch nicht einbetonierten Stütze aufgenommen werden. Die Lastabgabe in die 4 m dicke Bodenplatte erfolgt über loo mm dicke Stahlplatten in Form einer Stufenpyramide. Ebenso erfolgt die Lastübertragung vom Stützenquerschnitt 6o x 6o mm auf den 8o x 8o mm durch eine 2oo mm dicke Lastverteilungsplatte. Zum Brandschutz für F 18o wurden die Stahlstützen mit einer Spezialmineralwolle und einer Blechhaut umgeben.

Die Stahlstützen haben ein anderes Stauchungsmaß als die Betonkerne. Darum waren die Stauchungsunterschiede, die in den durchlaufenden Decken Schnittgrößen erzeugen, zu ermitteln. Sie errechnen sich zu $\ddot{U}^G_r = \ddot{U}^G_{Sr} - \ddot{U}^G_{Br}$ mit folgenden Bezeichnungen und vereinfachenden Ansätzen:

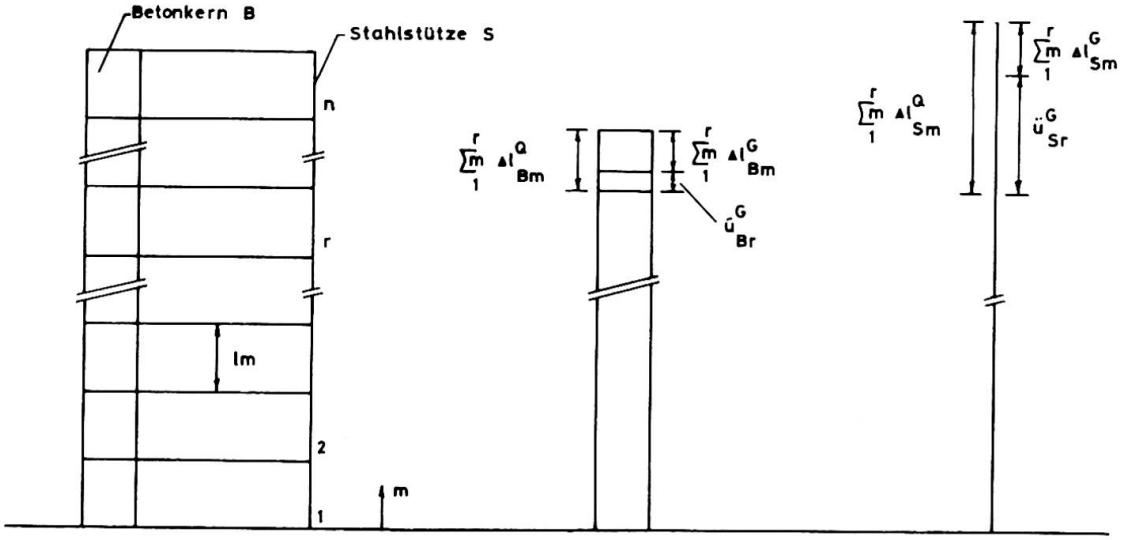

Die Gesamtzahl der Geschosse ist n; die Geschosse werden fortlaufend von unten nach oben mit m bezeichnet: $1 \leqq m \leqq n$; ein bestimmtes Geschoß wird mit r gekennzeichnet; alle Geschoßhöhen l_m sind gleich: l_m = const. = h; die Stützen bestehen in ihrer ganzen Länge aus dem gleichen Baustoff: E_m = const. = E_B für Beton, E_S für Stahl; die Betonkerne haben in allen Geschossen gleichen Querschnitt F_{Bm} = const. = F_B; die Betonkerne erhalten aus jedem Geschoß die gleiche Last Q_{Bm} = const. = Q_B und somit den gleichen Spannungszuwachs $\sigma^Q_B = \frac{Q_B}{F_B}$; die Stahlstützen haben im Gebrauchszustand in allen Geschossen die gleiche Spannung $\sigma^Q_{Sm} = \frac{Q_{Sm}}{F_{Sm}}$ = const. = σ^Q_S. Die Belastung im Gebrauchszustand ist Q, im Rohbauzustand G; es gilt G_S = o,5 Q_S, G_B = o,9 Q_B. Eine Setzungsmulde tritt nicht auf.

$$\ddot{U}^G_{Sr} = \sum_1^r {}_\Delta l^Q_{Sm} - \sum_1^r {}_\Delta l^G_{Sm}$$

$$= r \frac{h}{E_S} \sigma^Q_S - \frac{h}{2 E_S} \sigma^Q_S \sum_1^r \frac{r - m + 1}{n - m + 1}$$

$$\ddot{U}^G_{Br} = \sum_1^r {}_\Delta l^Q_{Bm} - \sum_1^r {}_\Delta l^G_{Bm}$$

$$= \frac{h}{E_B} \sigma^Q_B \sum_1^r (n - m + 1) - o{,}9 \frac{h}{E_B} \sigma^Q_B \sum_1^r (r - m + 1)$$

Mit den Zahlenwerten: $n = 34$

$E_S = 21oooo$ N/mm²

$E_B = 34ooo$ N/mm²

$h = 46oo$ mm

$\sigma^Q_S = 23o$ N/mm² in jedem Geschoß vorhanden

$\sigma^Q_B = o{,}3$ N/mm² aus jedem Geschoß im Kern

wirksam, wobei der plastische Verformungsanteil gleich dem elastischen gesetzt wurde, folgt Abb. 7.

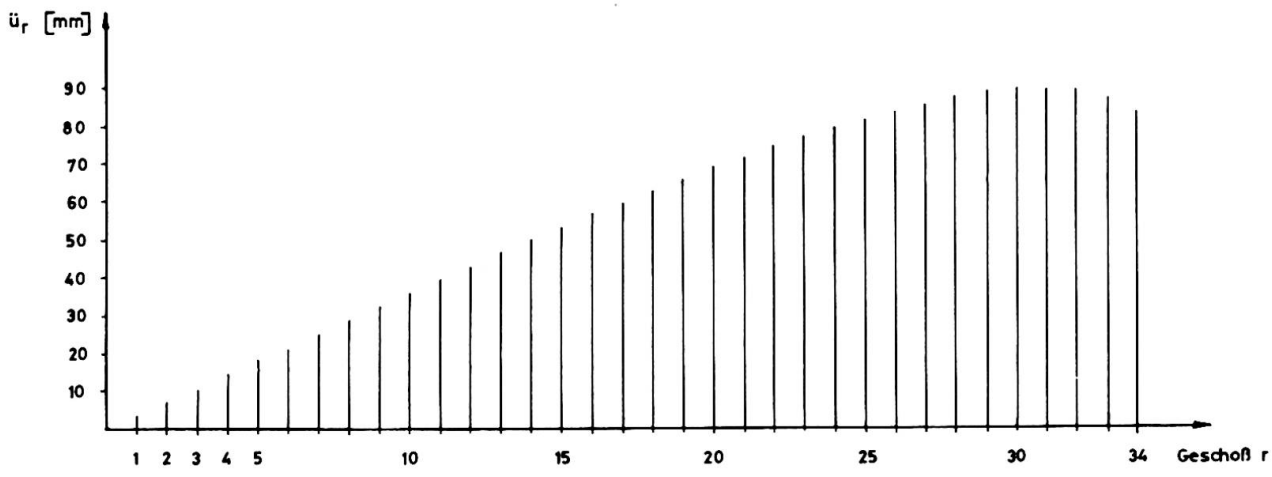

Abb. 7: Überhöhung der Geschoßdecken im Rohbauzustand $\ddot{U}^G_r$

Die Verwendung von Stützen aus hochfestem Feinkornbaustahl StE 47, die im Hüttenwerk montagefertig zusammengeschweißt wurden, hat sich bewährt. Die Rohbauausführung wurde beschleunigt. Die Justierung nach Höhe und Schiefe wurde durch laufende Vermessungen überwacht, eventuelle Korrekturen wurden durch Fräsen der Fußplatten erreicht. Die Montage erfolgte durch Baustellenkräne.

ZUSAMMENFASSUNG

Bei einem Hochhaus bestehen die Aussteifungskerne aus Beton, die Stützen wegen der hohen Belastung grösstenteils aus StE 47. Sie wurden aus Blechen bis zu 100 mm Dicke zu Hohlkastenprofilen zusammengeschweisst. Die Wahl des Werkstoffes, Bemessung und konstruktive Ausbildung werden erläutert. Die Berechnung der Auflagerüberhöhungen der durchlaufenden Decken infolge der unterschiedlichen Stauchungen zwischen Stahlstützen und Betonkernen wird dargestellt.

SUMMARY

In a tall building the cores providing stability are in reinforced concrete, the columns, because of the high loads, mostly in steel StE 47. They are built up with steel plates up to 100 mm thick, welded together to form hollow sections. The choice of the material, the design and the construction method are commented. The calculation of the height adjustment of the supports to the continuous slabs, because of the differential compression between the steel columns and the reinforced concrete cores, is illustrated.

RESUME

Dans un immeuble de grande hauteur, les noyaux assurant la stabilité sont en béton armé; les colonnes, en raison des charges élevées sont pour la plupart en acier StE 47. Elles sont faites de plaques d'acier, jusqu'à 100 mm d'épaisseur, soudées pour former des sections creuses. Le choix des matériaux, les calculs et la méthode de construction sont commentés. Le calcul pour l'ajustement des niveaux d'appuis pour les planchers continus est nécessaire à cause des différents degrés de compression des colonnes d'acier et des noyaux de béton.

Application of High Strength Steels of Class S 60 to Long Span Highway and Railway Bridges

Application de l'acier à haute résistance, de classe 60, aux ponts-route et ponts de chemin de fer de grande portée

Anwendung hochfester Stähle S 60 in weitgespannten Strassen- und Eisenbahnbrücken

K.P. BOLSHAKOV
Candidate of technical sciences

A.A. POTAPKIN
Candidate of technical sciences

CNIIS of the Ministry of Transport Construction
Moscow, USSR

1. General

There is a good number of theoretical, technological and constructive problems to be solved in connection with the application of high-strength steels in bridges. Special attention should be paid to the investigation of steels supplied by industry, to establishment of design specifications for them and development of technology of structures manufacture (including welding).

Consideration of analysis, design and practical application of high-strength steels in bridges are presented below.

The class of steel is being established according to a rated value of conditional yield stress $\sigma_{0,2}$ in kgf/mm^2. Thus, for example, yield stress of class S 60 steel is $\sigma_{0,2} \geqslant 60$ kgs/mm^2.

2. General Designing Specifications

The accepted in the USSR limit design method provides the satisfaction of the following inequality

$$S_{max} \leqslant \Phi_{min}$$

Here S_{max} - is maximum probable force in element; $S_{max} = \sum S_{i,r} n_i \xi$;
Φ_{min} - is minimum bearing capacity of element equal to $\frac{\gamma_{cm}}{K_H}$ FR - when its strength is analysed; $\frac{\gamma_{cm}}{K_H}$ RF - when fatigue strength is analysed; $\frac{\varphi_m}{K_H}$ RF - when overall stability is analysed.

The values of design resistance R for steels of S 40, S 50 and S 60 classes are respectively equal to 3200, 3800 and 4350 kgf/cm^2.

a) Strength analyses are made on the basis of the criterion, proposed by the authors /1/, i.e. limited residual plastic strain $\varepsilon_{p_1 max} \leqslant 0{,}0025$.

The new methods, allowing estimation of strainstress state of complex systems, were developed by the authors on the basis of strain plasticity theory.

For example, the strength of bending element is calculated from the formula

$$M_{max} \leqslant \frac{\gamma_{cm}}{K_H} W_{nt} R .$$

For box element with two axes of symmetry C is obtained from the formula

$$C = \frac{1-\theta}{K_\sigma} + \theta \frac{3+6\alpha-K_\sigma^2}{2+6\alpha},$$

where $K_\sigma = \frac{1}{1+\frac{E}{\theta\sigma_s}\varepsilon_{P_1 max}}$.

The corresponding formulas are derived for the case of compound bending when shearing stresses are taken into account.

The value of rasidual strain $\varepsilon_{P_1 i}$ for strength analysis of sections providing local stability of section elements is obtained from the formula (fig.1)

$$\varepsilon_{P_1 i} = \varepsilon_{cr,i} - \frac{\sigma_{cr,i}}{E}.$$

b) Fatigue strength analysis /2/ is made for rated service loads by the following formulas

- under tension and compression $N_r \leqslant \frac{\gamma_m}{K_H} FR$;
- under bending in one of main planes $M_r \leqslant \frac{\gamma_c \cdot m}{K_H} W_{nt} R$, etc.

The factors of design resistance reduction γ of elements base metal and of the metal o f their joints (welds, rivets, high-strength bolts) are derived from the formula

$$\gamma = \frac{1}{(a\rho+b)-(a\rho-b)\rho} \leqslant 1.$$

The values of parameters "a" and "b" for steels of different classes are: for S 40-a=0,74; b=0,18; for S 50-a=0,84; b=0,23; for S 60-a=1,00; b=0,24.

c)Overall stability analysis of axially compressed bars is made by the formula

$$N_{max} \leqslant \frac{\varphi m}{K_H} F_{br} R.$$

The buckling factors φ for steel S 60 are calculated in respect with initial imperfections, and the factor φ^* - for welded and wide flange rolled elements of H-section and in respect with residual stresses (table 1).

Table 1

λ	φ	φ^*	λ	φ	φ^*	λ	φ	φ^*
0	0,93	0,93	70	0,49	0,46	140	0,14	0,13
10	0,92	0,92	80	0,40	0,36	150	0,12	0,12
20	0,89	0,89	90	0,32	0,28	160	0,11	0,11
30	0,86	0,86	100	0,25	0,22	170	0,09	0,09
40	0,76	0,75	110	0,21	0,19	180	0,08	0,08
50	0,67	0,65	120	0,18	0,17	190	0,08	0,08
60	0,58	0,56	130	0,16	0,15	200	0,07	0,07

The value of φ for steel of lower classes may be calculated on the basis of conventional flexibility

$$\lambda_1 = \lambda\sqrt{\frac{\sigma_{s,1}}{\sigma_{s,60}}} .$$

A method accounting for values of φ for axially compressed bars is proposed for bending and torsional analysis /3/.

d) Local stability analysis of plate elements is obtained from the formula

$$\sigma_{i_{max}} \leqslant \frac{1}{m^* K_H}\sigma_{cr},$$

where σ_{cr} for isotropic plates is derived by generally known methods, and for elastic plastic stage - by Ilyushin - Stowell theory.

The factor m^* is determined from the expression

$$m^* = \bar{\alpha} + \frac{\bar{\beta}}{(\sigma_s - \sigma_\pi)^2}(\sigma_{cr} - \sigma_\pi)^2,$$

where $\bar{\alpha}$ and $\bar{\beta}$ for welded structures from steel S 60 are equal to 1.1 and 0.28. For steels of other classes

$$\bar{\beta} = \frac{\sigma_s}{R} - 1.1 .$$

The safety factor K_H is equal to 1.0 for webs of girders being bent and to 1.1 for compression chord of a box girder.

Critical compressive stress in a box girder chord may be derived from the formula, developed by the author on the basis of anisotropic plates theory using Shenly's conception

$$\sigma_{cr} = \min \frac{\pi^2}{B^2\delta_x'}\varphi_s\,(\gamma' D_x \frac{1}{\lambda^2} + D_y\lambda^2 + 2D_{xy}),$$

where $\gamma' = \frac{3}{4}\frac{\varphi_t}{\varphi_s} + \frac{1}{4}$; $\lambda = \frac{A}{mB}$;

m - is a number of semi-waves which should be varied.

It is necessary that local stability of stiffeners and a plate in a compression chord and berides the stability of longitudinal stiffeners under bending and torsion should be determined.

The specifications of the USSR don't allow the performance of plate elements of bridges in a post critical stage.

The moment of inertia of a cross girder of compression chord of a box girder is determined proceeding from the equality between the free length of longitudinal ribs and the distance between cross girders by the value of critical stress of longitudinal ribs σ_{cr}.

This relationship may be written in the following form

$$J_{cr} = 2\left(\frac{\pi}{\alpha}\right)^4\left(\frac{b}{A}\right)^3\frac{\sigma_{cr}}{\sigma_{cr}^*}\cdot\frac{b}{b_0}\pi^2 J_{lng}\left(1+\cos\frac{\pi}{K}\right),$$

where α - is factor of restraint of a cross girder ($\alpha = \pi$ in the case of hinged bearing);

b_0 - is distance between longitudinal ribs;

K - is a number of longitudinal ribs spans on the section of compression chord;

σ_{cr}^* - is critical stress of longitudinal ribs in the case of inlimited elasticity.

e) Linear and corner girders displacements in an elastic-plastic stage is obtained from the formula

$$W = \int \chi(x) M_i(x)\,dx,$$

where $\chi(x)$ - is curvature of girder axis from prescribed load M;

M_1 - is bending moment from the corresponding single force.

Within the strain theory of plasticity and the method of analysis in elastic stage the general relationship between curvature and bending moment may be written as

$$\chi(x) = \frac{M + \Delta M'}{EJ\psi_M'},$$

where

$$\psi_M' = \frac{1}{J}\int_F \frac{y^2}{1 + \frac{\omega\varepsilon_p}{\varepsilon_s}}\,dF; \quad \Delta M' = \sigma_s(1-\omega)\int_F \frac{\varepsilon_p y}{\varepsilon_s + \omega\varepsilon_p}\,dF; \quad \omega = \frac{\varepsilon_{p,1}}{\varepsilon_p};$$

$\varepsilon_{p,1}$ - is a part of residual plastic strain, changing elasticity parameters.

The given relationship reflects a combined method /4/ of plasticity theory for the case of validity of Prandtle diagram.

The method of additional loads by A.A.Ilyushin is valid when $\omega = 0$, while the method of variable parameters of elasticity by by I.A.Birger is valid when $\omega = 1$.

3. The Results of Trial Designing

Trial designing of three steel bridges was carried out to show up the effectiveness of the use of high-strength steels.

Bridge 1 - a railway continuous truss bridge with a composite action of the deck (spans are of 132 + 154 + 132 m size). Truss depth is 15 m, panel length is 11 m, the deck is analysed by the procedure /6/.

Bridge 2 - highway box-girder bridge with steel orthotropic deck (spans are of 90 + 3 x 148 + 90 m size). There are two boxes of 3.6 m depth in a cross section.

Bridge 3 - highway box girder bridge with concrete deck. There are two boxes of 3.6 m depth in a cross section.

The weight of metal for spans made of different steel classes is given in Table 2. Steels of class S 50 and S 60 were used for the most loaded elements.

Table 2

Bridge span	Steel class of the most loaded elements		
	S 40	S 50	S 60
N 1	100%	98%	94%
N 2	100%	95%	94%
N 3	100%	-	80%

The efficiency of high-strength steel used for spans of bridge 1 has been found to be lower than predicted because of the same sections sizez of box welded elements (depth, width). In this case however, available templates may be used in the process of manufacture.

Reduction of metal weight for spansof bridges 2 and 3 results from shortening of horisontal plates thickness. Here essential reduction of metal consumption is achieved in composite spans where high-strength steel should be used in the first place.

4. Constructed Bridges Examples

a) Highway stiffened bridge with flexible arch (fig.2). The arches (2) are of constant H-section along the whole length. Horizontal plates are of 530 x 32 mm size, while vertical oues are of 1120 x 50 mm. Arches are manufactured from steel of class S 50.

Continuous stiffening girder consist of four main web girders of 2,5 m depth. The bridge deck consist of a reinforced concrete slab (concrete - M400) with a composite action of beams. Beams are made from steel S 35.

Weldel structures were connected by high-strength bolts during the erection.

Metal consumption per 1 m^2 of the deck in a main spen is 365 kg/m^2, of approach spans - 201 kg/m^2; concrete consumption 0,16 m^3/m^2.

b) All-welded highway box-girder orthotropic tied bridge (fig.3). Steel of class S 60 is used for lower chords of box-girders. Other elements were manufactured from steel of class S 35. Steel consumption was 320 kg/m^2.

c) Composite steel welded deck with spans of 81 + 135 + 81 m (fig.4).

The span in its cross section has two boxes, connected by reinforced concrete slab (concrete M500). Steel members of the span were supposed to be manufactured from steel of class S 40, but practically a metalurgical plant delivered steel as strong as steel of class S 60. The thickness of webs varied from 14 to 32 mm, while the thickness of horizontal plates achieved 40 mm.

The consumption of rolled steel reached 285 kg/m^2, and reinforced concrete - 0,32 m^3/m^2.

Conclusion

The application of high-strength steels of classes higher than class S 40 in bridges may result in essential technical-economical effect provided the development of new design approaches to spans.

Though the considered above examples represent highly modern structures and progressive methods have been used for their analysis (including three - dimentional analysis method), the application of steels of classes S 50 and S 60 hasn't appeared to bring sufficient effect.

The use of high-strength steels has been found to be the most effective for tensile and compression members in the case of small values of flexibility.

These steels are not effective for members under vibration load, as the increase of fatigue limit falls behind strength growth.

High frost-resisting property of steels under review should be mentioned as positive.

Notation

S_{ir} - force in member from rated load i;
n_i - overload factor of load i;
γ_i - factor of loads combination;
c - factor of conditional increase of design resistance as a result of plastic strains;

m - service factor of member;
R - design resistance;
F - design geometrical parameter of section;
K_H - factor ofsafety (equal to 1.1 when studying structure failure);
γ - fatigue ratio;
C'' - fatigue factor with regard to gradient of stresses (in the case of bending in one plane C'' = 1.05; skew bending C''_{max} = 1.25);
φ - factor of longitudinal bending;
W_{nt} - effective section resistance (netto);
E - Joung's modulus;
E' - modulus of strain hardening;
$\theta = 1 - \frac{E'}{E}$ - parameter of weakening (fig.1);
$\alpha = \frac{\Sigma F_\rho}{\Sigma F_w}$ (ΣF_ρ - total area of flanges; ΣF_w - total area of box webs);
σ_s - yield point;
ε_ρ - residual plastic strain;
ε_{cr} - critical value of strain;
σ_{cr} - critical stress;
F_{nt} - area of effective cross section (netto);
β - effective factor of stresses concentration;
$\rho = \frac{\sigma_{min}}{\sigma_{max}}$ - factor of asymmetry of variable stresses cycle;
λ - flexibility of bar;
σ_π - limit of proportionality;
σ_i - intensity of stresses from design loads;
δ'_x - reduced depth of anisotropic plate;
B and A - width and length of anisotropic plate;
$\varphi_s = \frac{E_s}{E}$ - relative value of secant modules;
$\varphi_t = \frac{E_t}{E}$ - relative value of tangent modulus;
J_{lng} - moment of inertia of longitudinal rib;
J_{cr} - moment of inertia of cross rib.

References

1. Potapkin A.A. Teoria i raschot stalnych i stalegelezobetonnych mostov na prochnost s uchotowi nelinejnych i plasticheskich detormacyi. Trudy CNIIS, N 84. M., Transport, 1972.
2. Bolshakov K.P. Raschot stalnych mostov na vynoslivost. - "Transportnoe stroitelstvo", 1966, N 6.
3. Bolshakov K.P., Potapkin A.A. Sovershenstvovanie norm projektirovanija stalnych mostov i metodov ih raschota na prochnost i ustojchyvost. Sbornik trudov CNIIS, N 90. M., Transport, 1974.
4. Potapkin A.A. K raschotu stalnych mostov v uprugo-plasticheskoj stadii. Sbornik trudov CNIIS, N 94. M., Transport, 1975.

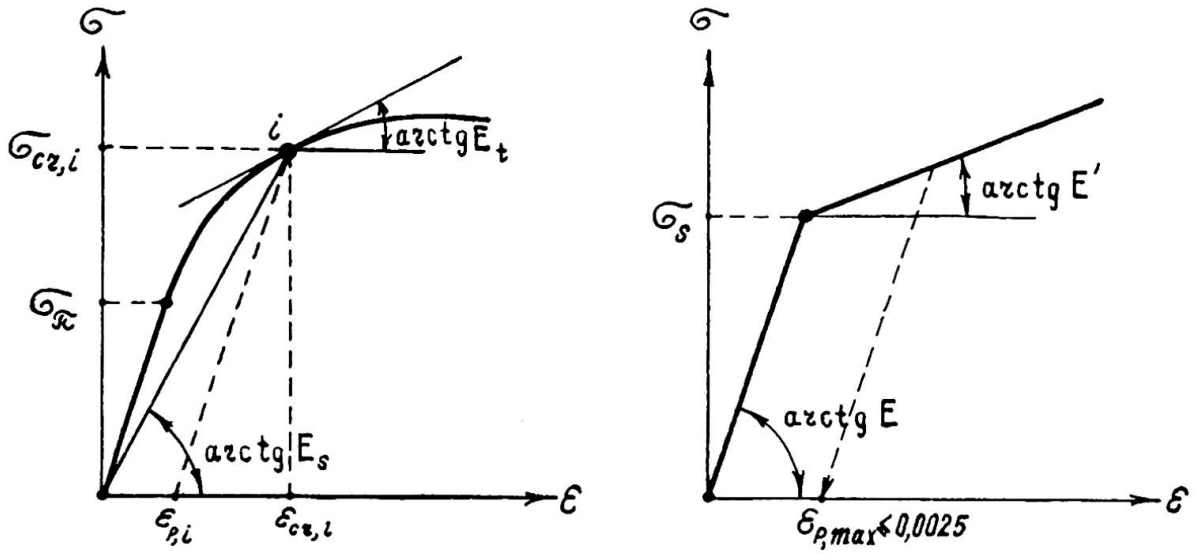

Fig. 1

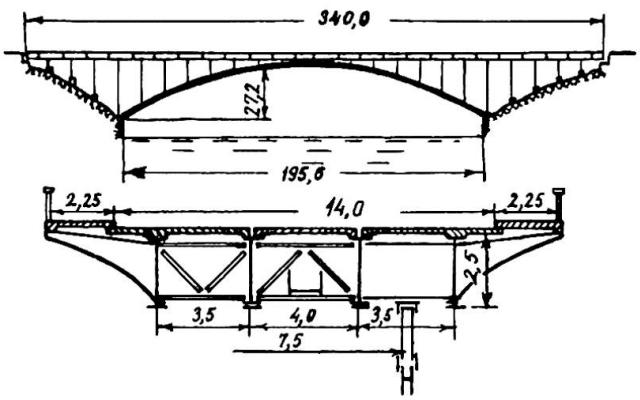

Fig. 2

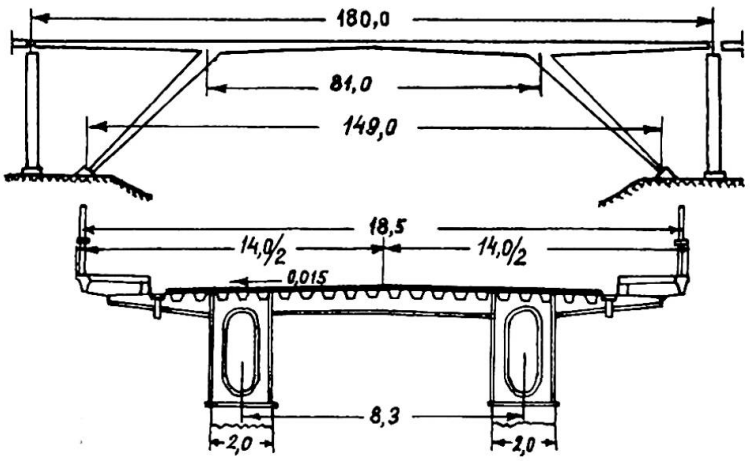

Fig. 3

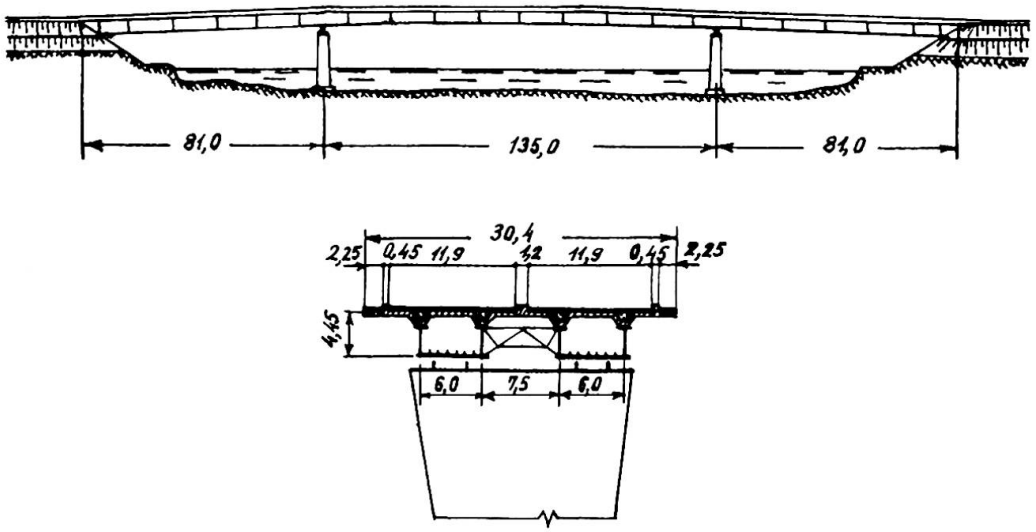

Fig. 4

5. Gurnaly - "Transportnoje stroitelstvo", 1971, N6; 1974, N 2; 1975, N 2.
6. Potapkin A.A. Truss Railway Bridges with a Composite Action of a Bridge Deck and the Main Trusses. Symposium JABSE - Steel and Composite Structures for User Needs - Preliminary Report. Dresden, 1975.

SUMMARY

The problems of effectiveness of high-strength steel application on bridges are analysed on the basis of specifications developed by the authors and used in the process of trial designing. The examples of constructed bridges are presented. The conclusion is drawn that research should be directed to development of new structural forms to make application of steels highly effective.

RESUME

On traite des questions de l'emploi efficace d'aciers à haute résistance pour les ponts sur la base de spécifications élaborées par les auteurs. Des exemples de ponts réalisés sont présentés. On conclut qu'il est nécessaire de rechercher de nouvelles formes de construction pour mieux utiliser les qualités des aciers à haute résistance.

ZUSAMMENFASSUNG

Die Probleme der wirkungsvollen Anwendung hochfester Stähle im Brückenbau werden aufgrund der vom Verfasser erarbeiteten Vorschriften und Berechnungsmethoden untersucht. Es werden Beispiele ausgeführter Brückenbauten vorgeführt. Man schliesst daraus, dass die wirkungsvolle Anwendung hochfester Stähle das Suchen nach neuen gestalterischen Formen im Brückenbau erfordert.

Mitwirkung der Längsträger mit den Hauptträgergurten bei Eisenbahnbrücken

Cooperation of Longitudinal Beams for Combined Action with Truss Chords of Railway Bridges

Collaboration des poutres longitudinales et des membrures de poutres de ponts de chemin de fer

N.N. STRELETZKIJ
Dr. d.t. Wiss.
ZNIIprojektstalkonstruktzija
Moscow, USSR

Die Perspektiven der Anwendung von hochfesten Stählen für Eisenbahnbrückentragwerke stellen viele komplizierte Probleme, die mit der Sicherstellung erforderlicher Steifigkeit, Dauerfestigkeit, Standsicherheit der Elemente, ihrer Wirtschaftlichkeit u.s.w. verbunden sind. Im Zusammenhang mit der Stahlfestigkeitserhöhung bei gleichem Elastizitätsmodul kommt der Fahrbahnsicherheit grosse Bedeutung zu, wobei die Verformungen in der Fahrbahnlage der Hauptbindergurtungen vergrössert werden.

Die sich in der Brückenfahrbahnlage befindlichen Bauteile, wurden in drei Etappen ausgearbeitet. In der ersten Etappe wurden diese Konstruktionen ohne Berücksichtigung der Verbundwirkung von Längsträgern und Bindergurtungen der Eisenbahnbrücken entworfen; als Folge ergaben sich zahlreiche Zerstörungen der Konstruktionen, hauptsächlich der Nietverbindungen. Die zweite Etappe ist durch das Streben gekennzeichnet, die Längsträger von der Verbundwirkung mit den Bindergurtungen zu befreien. Die Längsverbände wurden zu den Längsträgern beweglich aufgehängt; es wurden auch Bremsverbände angewandt. Bei den Feldern von über 80m wurden in den Längsträgern Abstände mit den längs-beweglichen Stützungen eingerichtet. Aber trotz allen Vervollkommnungen wurden die Längsträger in Verbundwirkung mit den Bindergurtungen durch die auf Ausbiegung in horizontaler Ebene beanspruchten Querträger etwas eingeschlossen. Dabei entstanden ziemlich grosse Überspannungen, die in Bezug auf die Dauerfestigkeit und Kaltbrüchigkeit schädlich sind. Die längsbeweglichen Stützungen für Längsträger zeigten sich im Betrieb als ungünstig.

Die dritte heutige Etappe in der Entwicklung obengenannter Konstruktionen erweist sich als zweckmässig, da sie die vollständige Einschliessung der Längsträger in Verbundwirkung mit den Bindergurtungen ermöglicht, wenn das Brückentragwerk als Raumeinheit nach dem Prinzip der Funktionsvereinigung der Konstruktionsteile projektiert wird. Das war unter folgenden Bedingungen möglich:

— Benutzung der modernen Elektronenrechentechnik;
— Ausarbeitung der Methodik der Grenzzustände;
— Anwendung der Montageverbindungen mit hochfesten Bolzen.

Die vom Autor vorgeschlagenen und in "Giprotransmost" ausgearbeiteten neuen Konstruktionsschemas der Eisenbahnbrückentragwerke mit einer Verstärkung der Verbundwirkung der Fahrbahn und der Hauptbinder (s. Bild I) unterscheidet sich sehr wenig von den früher verwendeten Konstruktionen mit einer Entspannung dieser Verbundwirkung. Die unteren Längsverbände des Kreuzschemas liegen in der Ebene der Fahrbahnträgeruntergurtungen und der unteren Ränder der Binderuntergurtungen.

In den neuen Konstruktionen sind die Diagonalen und Verstrebungen der Längsverbände in allen Kreuzungen mit den Längsträgeruntergurtungen durch hochfeste Bolzen verbunden. Zwischen einigen Kreuzungen der Diagonalen und der Längsträger werden zusätzliche (kurze) Verstrebungen angebracht. Diese Vertstrebungen verwandeln die entsprechenden Kreuzverbändeplatten in die unveränderlichen, steifen, gitterförmigen, den Längsträgern axiale Verlängerungen verleihenden Horizontalaussteifungen, die den Verlängerungen den Bindergurtungen nahe sind. Dadurch werden die Längsträger in eine intensive Verbundwirkung mit den Bindergurtungen eingeschlossen, was die letzten entsprechend entlastet.

Die Querträger, deren Steifheit in der Horizontalebene natürlich um das Mehrfache der Steifheit der gitterförmigen Horizontalaussteifungen weniger ist, befreien sich dabei in gewissem Masse von einer Biegung in der Horizontalebene.

Die Anzahl von kurzen, gitterförmigen Horizontalaussteifungen bildenden Verstrebungen wird in den nicht durchlaufenden Brückentragwerken, in Abhängigkeit von der Feldhöhe, so gehalten: für 33 und 44m- 2St.; für 55 und 66m- 4St.; für 77m- 6St.; für 88m- I2St.; für IIOm- I6St. (s. Bild I). Es ist vollkommen nicht rationell, kurze Verstrebungen in allen Kreuzungsknoten der Diagonalverbände mit den Längsträgern anzubringen. Ausser dem unnötigen Metallverbrauch und einer grossen Bolzenanzahl für Verstrebungen und deren Befestigung, würde das eine unbegründete Anschlussbefestigung der Untergurte aller Querträger und der Diagonalen erfordern, da die Wirkung der Horizontalaussteifungen zusammen mit den Querträgern unter der örtlichen senkrechten Belastung intensiv , aber wenig effektiv ist.

Im rechnerischen Modell des Brückentragwerkes mit Verbundwirkung der Hauptbinder, Fahrbahn und Verbindungen wird folgendes berücksichtigt: Widerstand der Elemente den Axialkräften, der Biegung in beiden Ebenen und der Verdrehung, alle konstruktiven Exzentrizitäten, Steifheit der Hauptbinderknoten und der meisten Fahrbahnknoten, Verkürzung der Elementenlänge wegen der konstruktiven Knotenbesonderheiten. Zugleich wurde eine Reihe von wesentlichen Vereinfachungen angenommen.

Die Biegebeanspruchung in der Horizontalebene jeder Fahrbahnträgergurtung wird trotz der Steg- und gegenseitigen Gurtwirkung berücksichtigt. Annähernd wird die Wirkung von Quer- und Längsoberverbindungen zwischen den Bindern und die Wirkung von Längsträgerverbindungen berücksichtigt. Die Quer- und Verdrehungsfestigkeit von Verbändeelementen, die Verdrehungsfestigkeit von H-Binderelementen u.s.w. werden nicht berücksichtigt.

Das durch obengenannte Besonderheiten gekennzeichnete Raumrechenmodell erlaubte mit Hilfe von ERM „БЭСМ-4" viele genauere Berechnungen mit graphischer Darstellung von Einflusslinien verschiedener Kräfte durchzuführen. Auf Grundlage der Ergebnisanalyse dieser automatisierten Berechnungen wurden einige Verfahren ohne Hilfe von ERM ausgearbeitet und zur Einflussliniendarstellung einiger Kräfte in der statisch unbestimmten Raumkonstruktion vielfach verwendet.

In dem rechnerischen Untersuchungen der Verbundwirkung zwischen den Hauptbindern, der Fahrbahn und den Verbindungen ist der Einfluss von Horizontalaussteifungen dem Einfluss von Abständen in den Längsträgern entgegengezetzt (Bild I, a;b).

Die Längskräfteverteilung auf Binderuntergurte und Längsträger bei Nichtvorhandensein von Horizontalaussteifungen hängt hauptsächlich von der Feldlänge oder der Strecke zwischen den Abständen und der Horizontalsteifheit der Querträger ab. Bei Vorhandensein

von Horizontalaussteifungen hängt das im wesentlichen vom Querschnittsverhältnis der Längsträger und der Binderuntergurte ab.

Die Abstände in den Längsträgern vermindern die grössten Axialkräfte darin um 2,5-3mal, und die grössten horizontalen Biegemomente vermindern sie nur um 20-30%. Beim Nichtvorhandensein von Horizontalaussteifungen erfordern die Konstruktionen aus dem niedriglegierten Stahl für den Tragwerk von 66m nur einen Trägerabstand, für den Tragwerk von 88m- 2 Abstände, für den Tragwerk von II0m- 3 Abstände. Mit Verwendung von hochfesten Stählen wäre noch mehrere Anzahl von Abständen in den Längsträgern erforderlich.

Die Einrichtung von Horizontalaussteifungen anstatt des Trägerabstandes wird die Axialkräfte in den Längsträgern um 3-4 mal vergrössern (Bild I, a), was entsprechende Biegemomente in den Querträgergurten um 5-6 mal vermindert (Bild I, b).

Die Längsträger werden im senkrechter Ebene auf die Kombination von Biegung (als durchlaufende Träger auf den gegenseitig verbundenen Auflagern verschiedener Nachgiebigkeit -Bild I, d-), mit den Axialkräften beansprucht. Der Einfluss von durch Querträger übertragenen Drehmomenten ist gering, der Einfluss des aussermittigen Anschlusses der Horizontalaussteifungen ist dagegen bedeutend. Die Axialkräfte in den Längsträgern entstehen infolge der Verformungen von Binderuntergurten und der Begrenzung der Längsträgerverbiegung unter der örtlichen Vertikalbelastung, wobei diese Begrenzung von den senkrechten Exzentrizitäten abhängt. Der Spannungsanteil aus den Axialkräften in den vollen Fiberspannungen in einem Längsträger beträgt, wenn es keine Horizontalaussteifungen gibt, von I bis I2%, mit den Horizontalaussteifungen-- von 20 bis 30%. Die genaueren Berechnungen im Vergleich zu den elementaren stellen eine wesentliche Zeichenwechslung der Spannungen in der Reihe von Längsträgerbereichen fest, die auf die Dauerfestigkeit überprüft werden müssen.

Dank den Horizontalaussteifungen ist es nicht nötig, für die Axialkräfteübertragung durch Längsträger eine Erschwerung der Längsträgerquerschnitte auszuführen, denn äquivalente Belastungen, dynamische Beiwerte und Überlastungsfaktoren vermindern sich bei einer genaueren Berechnung. Die Längsträgerfische müssen unbedingt vervollkommnet werden (Bild I, e).

Die horizontalen Biegemomente in den Qerträgergurten entstehen sowohl aus den Knotenlängsverschiebungen der Binderuntergurte gegen Längsträgerknoten, als auch aus der durch Längsträger ausgelösten Querträgerverdrehung. Mit Einrichtung von Horizontalaussteifungen verschwinden Momente aus den Längsverschiebungen fast völlig, aber die Verdrehungsmomente bleiben, was in den Querträgergurten bedeutende Spannungen hervorruft (Bild I, f).

Mit Einrichtung von Horizontalaussteifungen beträgt die Entlastung der Binderuntergurte durch Längsträger in der Feldmitte in der Regel 25-35%. Die Entlastung durch Längsverbände beträgt für die unteren und oberen Binderuntergurte 3-6%.

Die genaueren Raumberechnungen der Brückentragwerke mit Verbundwirkung von Bindergurten, Längsträgern und Verbindungen zeigen Kräfte, die in den elementaren Berechnungen nicht berücksichtigt werden. Dementsprechend wurden in den vielen Elementen die vergrösserten Fiber- und Punktspannungen festgestellt. Aber das führt zur Erschwerung einer Konstruktion nicht, was der in der sowjetischen Rechenpraxis vorgesehenen genaueren Bestimmung als linker, sowie rechter Teil der Grenzungleichheiten der Grenzzuständemethodik zu verdanken ist. Bei der Prüfung von Fiber- und Punktspannungen erhalten die rechnerischen Widerstände die erhöhenden Beiwerte

"m_2" und "c", die die Entwicklung von plastischen Verformungen im Festigkeitsgrenzzustand berücksichtigen. Die m_2-Beiwerte zeigen entsprechende Kräfte- und Momentenverteilungen im Brückentragwerk. Die c-Beiwerte zeigen Festigkeitsreserve in den Elementenquerschnitten, und zwar im Intervall zwischen der Fiber- oder Punktfliessbarkeitsentstehung und dem Querschnittsgrenzzustand, der durch die relative restliche Grenzverformung in der Randfiber oder dem Randpunkt gekennzeichnet wird (mit dem Wert von 0,001 bis 0,0025).

Der Metallverbrauch für die neuen Brückentragwerke vermindert sich fast um 5%. Der Vorteil dieser neuen Konstruktionen besteht in der Erhöhung ihrer Betriebssicherheit, der Verbesserung ihrer Nutzungseigenschaften und ihrer Vereinfachung bei der Ablehnung von den beweglichen Verbindungen, den Bremseverbänden u.s.w.

Die Einschliessung von Längsträgern in Verbundwirkung mit den Bindergurten gibt die Möglichkeit, Längsträger als Verstärkungselemente für Binderuntergurte im Freivorbau zu benutzen und aufgelegte Sonderelemente als Gurteverstärkung zu beseitigen.

In der UdSSR ist eine Rehe von durchlaufenden und nicht durchlaufenden Brückentragwerken einer neuen Bauart aufgebaut. Sie haben eine untenliegende Fahrbahn mit dem Holzbelag und den Spannweiten bis 132m. Es werden analogische Konstruktionen ausgearbeitet, die durch den bettungslosen Belag auf einer Eisenbeton- und durchlaufenden Stahlplatte gekennzeichnet sind. Es werden auch Konstruktionen mit der obenliegenden Fahrbahn ausgearbeitet.

ZUSAMMENFASSUNG

Die Anwendung hochfester Stähle erfordert Sondermassnahmen für die Mitwirkung der Längsträger mit Gurten der Hauptträger. In den neuen Brückentragwerken aus niedriglegiertem Stahl wird diese durch gitterförmige Horizontalaussteifungen in der Untergurtebene erreicht. Es wurden die genaueren Berechnungen durchgeführt. Die Betriebssicherheit ist erhöht, die Nutzungs- und Montageeigenschaften sind verbessert, es ist Stahlersparnis erreicht.

SUMMARY

The use of high strength steels requires special measures to provide combined action of longitudinal beams and truss chords. In new spans this is successfully fulfilled by means of using through horizontal diaphragms in the planes of the lower braces. Refined calculations have been made. Safety has been increased, maintenance and erection quality improved, and steel saving achieved.

RESUME

L'Application des poutres longitudinales en acier à haute résistance exige des moyens particuliers pour qu'elles puissent supporter les efforts dans la même mesure que les membrures. La transmission des efforts des travées en acier à faible alliage est réalisée grâce aux diaphragmes horizontaux évidés placés dans les entretoisements inférieurs. On a fait les calculs avec une grande précision. On a ainsi augmenté la fiabilité, on a amélioré les conditions d'exploitation et d'assemblage, et on a obtenu une économie d'acier.

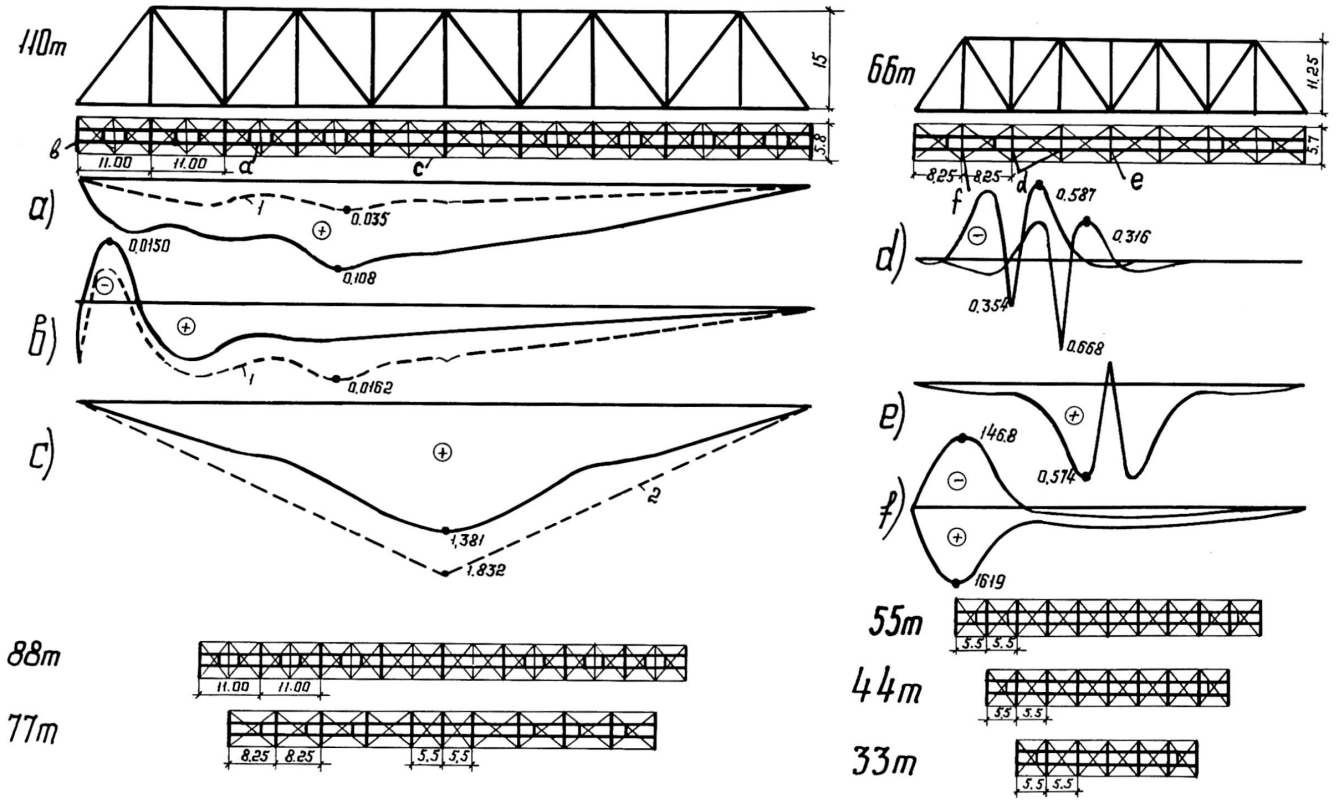

Bild I Schemas der Konstruktionen und der Einflußlinien: a=Axialkraft im Längsträger; b=horizontales Biegemoment im Querträgeruntergurt; c= Axialkraft im Binderuntergurt; d= Biegemomente im Längsträger; e= Kraft im Fisch; f= Beanspruchungen in den oberen und den unteren Querträgergurten; 1= bei einem Abstand in einem Längsträger; 2= in einem ebenen gelenkigen Binder.

Leere Seite
Blank page
Page vide

Vergleich zwischen den Paralleldrahtseilen und verschlossenen Seilen am Beispiel der Eisenbahnschrägseilbrücke über die Save in Belgrad

Comparison between Parallel Wire Bundles and Closed Ropes Illustrated on the Cable Stayed Railway Bridge over the River Save in Belgrade

Comparaison entre les câbles à fils parallèles et les câbles torsadés dans le cas du pont de chemin de fer haubanné sur la Save à Belgrade

NIKOLA HAJDIN
Prof. Dr. sc. techn.
Universität Beograd
Beograd, Jugoslawien

1. Einführung. Konstruktive Gestalltung der Brücke.

Die doppelgeleisige Eisenbahnbrücke über die Save in Belgrad, z.Zt. im Bau, besteht aus einem Brückenzug von etwa 2 km Länge.

Dominierter Teil ist die Strombrücke mit den Spannweiten 54 + 85 + 50 + 254 + 50 + 65 m.[☆]

Das System ist eine Schrägseilbrücke mit zwei vertikalen Pilonnen beidseits der Hauptöffnung von 254 m (Abb. 1).

Eine solche Eisenbahnbrücke, unseres Wissens die erste dieser Art für den reinen Eisenbahnverkehr, bietet eine Fülle von technischen und praktischen Problemen, unter denen die Seilverspannung eines der wichtigsten ist.

Der Versteifungsträger der Brücke besteht aus zwei druchlaufenden Kastenträgern mit der konstanten Bauhöhe von 4,45 m und der Beite von 3,2 m. Die Träger sind mit einer, etwa 70 cm unter dem Obergurt der Träger liegende orthotrope Platte verbunden.

Die vier Pilonen der Brücke überragen die Oberkante der Kastenträger um 55 m. Sie haben einzellige Rechteckquerschnitte. Die Pilonenbreite ist konstant und beträgt 1,90 m. Querschnittshöhe variiert linear; an der Kontaktstelle mit dem Kastenträger beträgt 3,10; an der Spitze jedoch nur 2,50 m.

Jeder Pilon ist in dem entsprechenden Kastenträger eingespannt und dient zur Aufnahme von 4 Abspannkabeln. Die zwei zur Strömoffung hin angeordneten Schrägkabel ergeben die erforderliche elastische Stützung des Kastenträger. Die landseitigen Kabel dienen als Rückverankerung.

Die, zwischen den Kastenträgern liegende orthotrope Platte hat eine Breite von 8,1 m.

Die Gesambreite der Brücke mit den beiden Dienstwegen (2x1,0 m) beträgt 16,5 m.

Die, im statischen Sinne etwas ungünstige Lage der orthotropen Platte unter der Oberkante der Kastenträger ist durch das Schotterbett bedingt. Schon zu Beginn der Projektierung wurde verlangt dass durch die entsprechende Auswahl des Oberbaues über den ganzen Brückenzug die Lärm infolge des Eisenbahnverkehers möglichst gedämpft werde. Bei den Zufahrtbrücken hat sich Schotterbett als sehr geeignet gezeigt.

Im Falle der Strombrücke hat sich ausserdem eindeutig herausgestellt, dass wegen der ungünstigen Verhältniss zwischen der Verkehrlast und dem Eigengewicht eine Erhöhung der ständigen Last erwünscht wäre. Die mittels Schotterbett erreichte Erhöhung des Eigengewichtes hat nur einen ganz unbedeutenden Einfluss auf die Gesamtkosten der Brücke. Diese Zusatzbelastung bringt praktisch keine Vergrösserung des Seilgewichtes (siehe die Reihe 7 in der Tabelle), da die

---

[☆]Entwurfverfasser: Prof. Dr. N. Hajdin, Dipl.-Ing. und Dipl.-Ing. Lj. Jevtović, Belgrad, Jugoslawien.

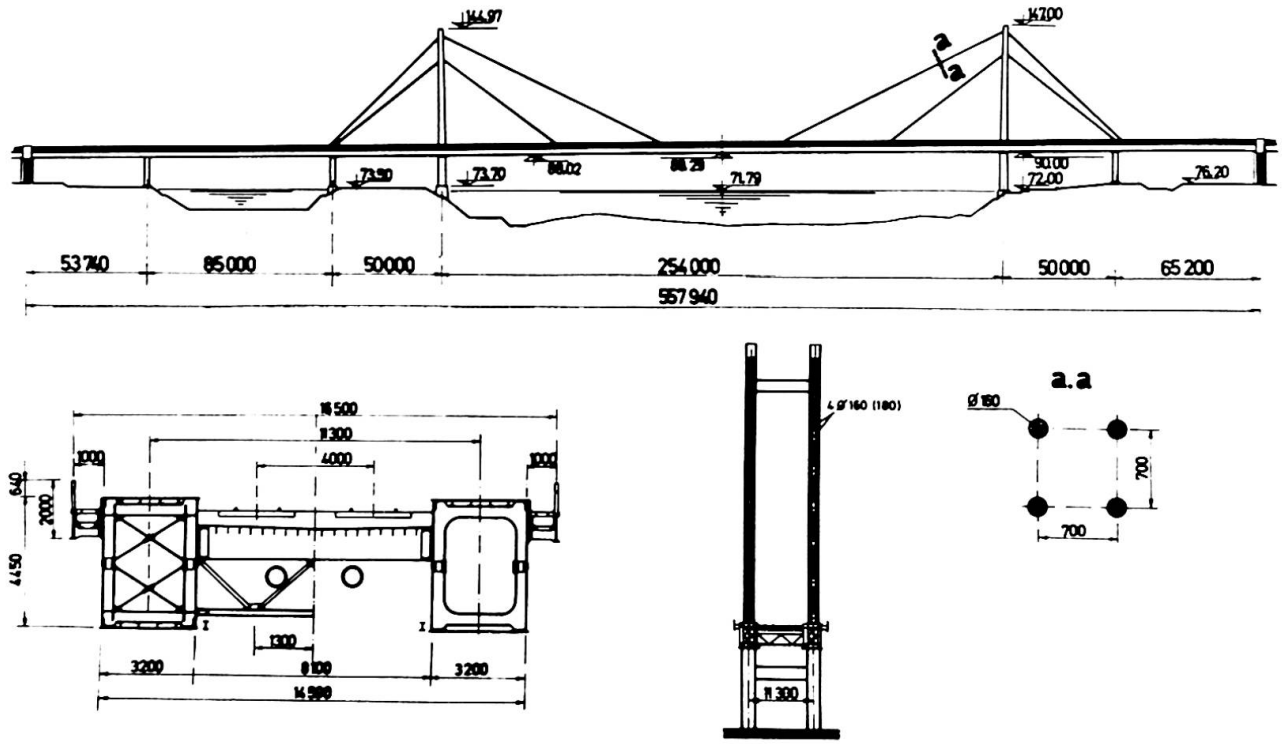

Abb. 1.

Dauerschwingfestigkeit für die Bemessung massgebend ist. Ein etwas grosseres Eigengewicht (infolge des Schotterbettes) hat auch praktisch keinen Einfluss auf das Gewicht der Kastenträger. Ein gewisses Mehrgewicht (etwa 1,7% des Gesamtgewichtes der Strombrücke) zeigt sich nur bei den Pilonen.

2. Kabel. Ein Vergleich zwischen dem verschlossenem Seil und dem Paralleldrahtbündel

Das Schrägkabel stellt ein von den wichtigsten Elementen einer Brücke dieses Systeme dar.

Der Hauptunterschied zwischen einer Strassenbrücke und einer Eisenbahnbrücke dieses Systems liegt im Verhältnis zwischen der beweglichen und ständigen Belastung. Dieses Verhältnis ist bei einer Eisenbahnbrücke beträchtlich grösser. Ausserdem ist die Haufigkeit des Auftretens der beweglichen Belastung höherer Intensität bei einer Eisenbahnbrücke meist grosser.

Bei einer Schrägseilbrücke ist die Durchbiegung und die Neigung wegen der Flexibilität des Systems verhältnismässig gross, was sich bei der Eisenbahnbrücke ungünstig auswirken könnte. Es ist zu erwarten, dass die dynamische Wirkung bei einer flexibilen Brücke mit grosser Durchbiegung mehr zum Ausdruck kommt.

Als Unterlage für Bemessung der Kabel wurde DIN 1073 benutzt. Gemäss dieser Vorschrift wird die Dauerschwingfestigkeit aufgrund der Schwingbreite zwischen der maximalen σ_o und minimalen σ_u Spannung für verschiedene Werte maximalen Spannung bestimmt, und zwar:

für Paralleldrahtbündel (PDB):

$$\text{zul } \sigma_o = \frac{2500}{1 - 0{,}895\varkappa}$$

für verschlossenes Seil (V.S.)

$$\text{zul } \sigma_o = \frac{2000}{1 - 0{,}896\varkappa} \qquad (1), (2)$$

wo $\varkappa = \sigma_u / \sigma_o$ ist. Die Formeln (1) und (2) sind für Bruchspannung von 16.000 kp/cm^2 gegeben. Bei Strassenbrücken müssen nur 50% der Spannungen aus Verkehrslast eingerechnet werden. Die Spannungen aus Lasten von Schienenfahrzeugen einschliesslich Schwingbeiwert müssen im vollen Betrag eingesetzt werden. Da es sich in unserem Fall praktisch nur um bewegliche Belastung infolge Eisenbahnverkehr handelt, wird die Dauerschwingfestigkeit mit volem Betrag der

entsprechenden Spannung berechnet. Das hat zur Folge (siehe Tabelle), dass für die Bemessung der Kabel überall die Dauerschwingfestigkeit massgebend ist.

In diesem Fall und auf Grund von Formeln (1) und (2) zeigen die Parallelendrahtbündel gegenüber den verschlossenen Seilen ein Ersparnis im Gewicht von 25%.

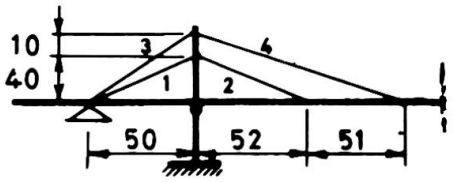

Nr	Seil		1		2		3		4	
			PDB	VS	PDB	VS	PDB	VS	PDB	VS
1	zul $\sigma_{0,1}$	kp/cm²	4771	3822	4518	3617	5179	4148	5389	4316
2	$\sigma_{u,1}$	kp/cm²	2532	2033	2254	1805	2994	2398	3228	2585
3	$\sigma_{s,1}$	kp/cm²	961	769	941	753	1004	803	974	779
4	$\varkappa_1$		0,532		0,499		0,578		0,599	
5	zul $\sigma_{0,2}$	kp/cm²	3960	3171	3698	2959	4355	3487	4584	3671
6	$\sigma_{u,2}$	kp/cm²	1632	1306	1339	1071	2073	1660	2329	1865
7	$\varkappa_2$		0,412		0,362		0,476		0,508	
8	F_1 / F_2		1,04		1,03		1,04		1,04	
9	$\frac{E_i F(1)\ [PDB]}{E_i F(1)\ [VS]}$		0,974		0,978		0,972		0,985	

In der Tabelle eingeführten Bezeichnungen haben die folgende Bedeutung:

Index 1 – bezieht sich auf die Lösung mit Schotterbett,

Index 2 – bezieht sich auf die Lösung ohne Schotterbett,

PDB – Paralleldrahtbündel , VS – Verschlossenes Seil,

$\sigma_{s,1} = G_s/F_1$ – Spannung infolge des Schotterbettgewichtes,

F_1, F_2 – Querschnittsfläche des Seiles.

Das Ersparnis im Gewicht und die anderen Gründe, worüber später berichtet wird, haben zur Wahl von Paralleldrahtbündeln geführt.

Wie aus der Abb. 1 ersichtlich, besteht jeder Kabelstrang im statischen Sinne aus 4 Drahtbündeln. Die Zahl der Drähte in den einzelnen Drahtbündeln variiert zwischen 240 und 290. Es werden Runddrähte mit Durchmesser von 7 mm und Festigkeit zwischen 150 – 170 kp/mm^2 ausgewählt. Die Drahtbündel einer Gruppe sind räumlich getrennt. Jedes Drahtbündel besteht aus den Drähten mit einer Litze umwickelt (Abb. 2) und einer äusseren Polyaethylenhülle der Stärke von 7 (8) mm und mit einem Aussendurchmesser von 160 (bzw. 180) mm. Es wurde die HiAm–Verankerung [1], [2] verwendet, welche bei schwingender Belastung die Ermüdungsfestigkeit des freien Drahtbündel erreicht.

Nach Ernst [3] kann die Dehnungssteifigkeit des Seiles wie folgt berechnet werden:

$$E_i F = \frac{E_0 F}{1 + \frac{1}{24} (\gamma' l^2) \frac{\sigma_0 + \sigma_u}{\sigma_u^2 \sigma_0^2} E_0} \tag{3}$$

wobei E_i – scheinbarer E – modul, E_0 – rechnerischer Modul des Seiles, γ' – spezifisches Gewicht des Seilmaterials mit Zuschlägen sind.

Bei den Paralleldrahtbündel ist mit einem E_0 – Modul von 2.050 Mp/cm^2 zu rechnen, bei den verschlossenen Seilen jedoch nur mit 1.700 Mp/cm^2.

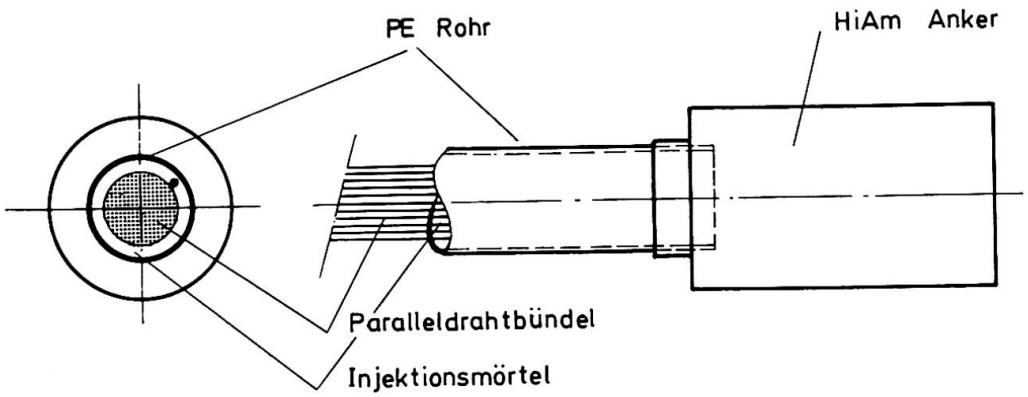

Abb. 2.

Der Wert γ' ist bei den Paralleldrahtbündeln in unserem Fall, wegen des Gewichtes von Polyaethylenrohren und Zementmörtel, etwa 8x1,25 = 10 Mp/m^3 gross. Bei den verschlossenen Seilen ergibt sich 1,05x8,0 = 8,40 Mp/m^3.

Wie aus der Tabelle ersichtlich, geben die Paralleldrahtbündel, mit dem um 25% kleineren Querschnitt, praktisch die gleiche Kabelsteifigkeit E_iF wie die verschlossenen Seile.

Die Längssteifigkeiten FE_i sind im Falle der Lösung mit Schotterbett etwa 5% grösser und der Durchhang des längsten Seiles für ständige Belastung um cca 40% kleiner als die entsprechenden Werte der Brücke ohne Schotterbett.

Andere Vorteile der Paralleldrahtbündel gegenüber dem verschlossenen Seil, welche hier nicht quantitativ gezeigt werden können, sind in unserem Fall die folgenden:

– Diese Art der Kabel ermöglicht die Bildung der Bündel grosser Durchmesser mit angepasster Anzahl Drähte. Das hat sich, wegen der Knappheit in den Verankerungsstellen im Pilon vorteilhaft erwiesen.

– Die räumlich getrennten und parallel geführten Bündel, haben keine Spreizstellen. Diese hätten eine negative Wirkung auf die Dauerschwingfestigkeit des Seiles. Aus diesen Gründen haben wir jede Änderung der Kabelrichtung inklusive Sattellager vermieden. Die Paralleldrahtbündel mit HiAm – Verankerung ermöglichen die Lösung dieses Problem und bieten gleichzeitig eine einfache Montage, Spannen und Kontrole der Kabelkräfte.

– Ein präzis vorausgegebener E_o – Modul der Bündel erleichert die Montage und ermöglicht eine genaue Berechnung der verschiedenen Durchbiegungen während der Montagezustände.

3. Bemerkungen zur Anwendung dieses Systems für weitgespannte Eisenbahnbrücken

Eine weitere Anwendung dieses Systems für die Eisenbahnbrücken sehr grosser Spannweiten wird stark von den Annahmen über Dauerschwingfestigkeit abhängen. Eine Berechnung mit αe – Werten aus nur einem Teil der Verkehrlast, wie bei den Strassenbrücken, was uns als berechtig scheint, würde die Verwirklichung der Eisenbahnbrücken sehr grosser Spannweiten ermöglichen. Wie stark αe– Werte, im Falle dass die Dauerschwingfestigkeit für die Bemessung massgebend ist, die untere Grenze $\sigma_o \approx \sigma_g$ des scheinbaren E_t–Modul beeinflüssen, zeigt die Abb. 3.

Wie aus Abb. 3 ersichtlich, wind die Seillängen über 150 bzw 200 m, ohne Versteifungseile, für αe– Werte unter 0,5, wegen des niedrigen E_i–Modul, kaum möglich.

Die Dauerversuchen mit den Paralleldrahtbündeln zeigen, dass eine Erhöhung der Schwingbreite um cca 25% durchaus zu vertreten wäre. Das würde viel der Wirtschaftlichkeit dieses Systems im Falle einer Eisenbahnbrücke beitragen.

Der Gewichtszuschlag infolge des Zementmörtels vergrössert bei den Paralleldrahtbündeln den Durchhang des Seiles und verkleinert E_i–Modul. Ein anderer Korosionschutz mit etwas kleinerem Gewicht würde noch mehr der Überlegenheit der Paralleldrahtbündel beitragen. –

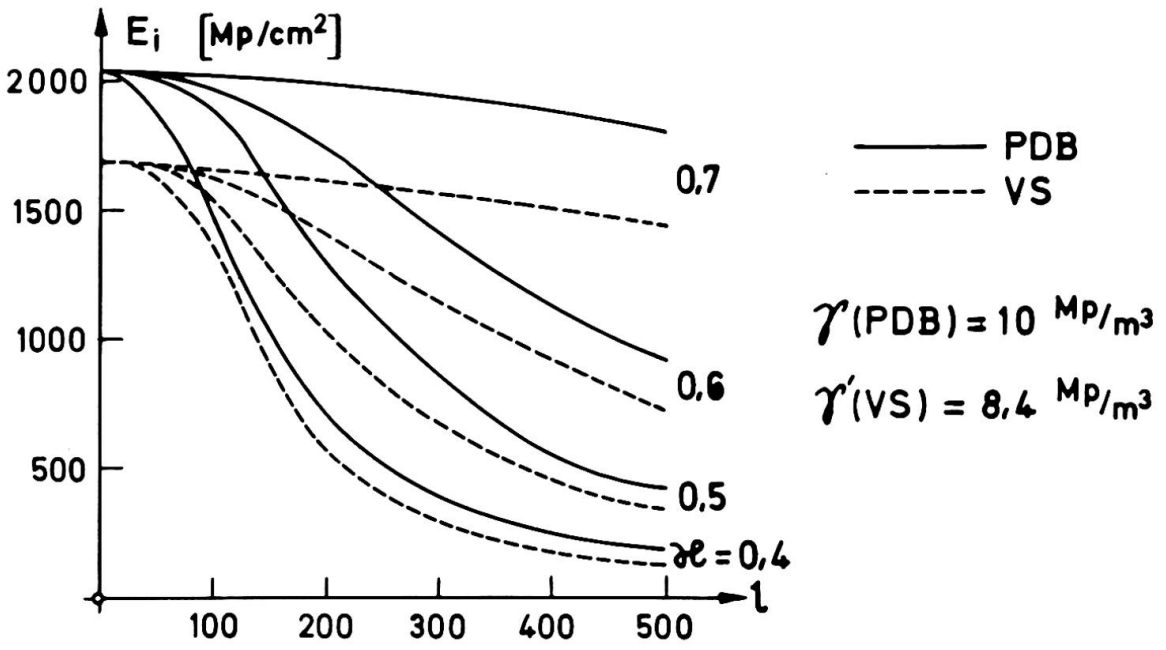

Abb. 3.

Literaturverzeichnis

[1] Andrä, W. und Zellner, W.: Zugglieder aus Paralleldrahtbündeln und ihre Verankerung bei hoher Dauerschwellbelastung. Die Bautechnik 46 (1969). H. 8. u. 9.

[2] Leonhardt F. und Zellner, W.: Vergleiche zwischen Hängebrücken und Schrägkabelbrücken für Spannweiten über 600 m. Abhandlungen IVBH, Bd 32–I, 1972.

[3] Ernst, H.J.: Der E–Modul von Seilen unter Berücksichtigung des Durchhanges.Der Bauingenieur 40(1965).

ZUSAMMENFASSUNG - Das Problem der Seilverspannung einer Eisenbahnschrägseilbrücke wird diskutiert. Bei einer reinen Eisenbahnbrücke dieser Art kommen der Dauerschwingfestigkeit und dynamischen Beanspruchung grössere Bedeutung zu als bei einer Strassenbrücke. Ein Vergleich zwischen den Paralleldrahtbündeln und dem verschlossenen Seil zeigt eine merkbare Ueberlegenheit der ersteren gegenüber verschlossenen Seilen.

SUMMARY - The submitted contribution deals with the problem of cable work on a cable stayed railway bridge. Fatigue resistance and dynamic effects in a railway bridge with the cable stayed system become more significant than in a road bridge with the same system. These effects have important influence on the dimensioning of the cables. Parallel wire bundles in comparison with closed ropes show a noticeable superiority of the former.

RESUME - On présente un problème posé par un pont de chemin de fer haubanné réalisé avec des câbles. Dans le cas d'un pont-rail typique, la résistance à la fatigue et aux sollicitations dynamiques sont plus critiques que dans un pont-route. Ces facteurs ont une influence significative sur le dimensionnement des câbles. Une comparaison entre le faisceau de fils parallèles et le câble torsadé montre une supériorité notable du premier par rapport au câble torsadé.

Leere Seite
Blank page
Page vide

Fatigue Design Criteria on Honshu-Shikoku Suspension Bridges

Le critère de la fatigue dans le cas des ponts suspendus entre Honshu et Shikoku

Kriterien für den Dauerfestigkeitsnachweis der Honschu-Schikoku Hängebrücken

JIRO TAJIMA
Dr., Manager

ATSUSHI OKUKAWA
Dr.

YOSHIHIRO TANAKA

Honshu Shikoku Bridge Authority
Tokyo, Japan

1. INTRODUCTION

In the construction of Honshu-Shikoku bridges, the use of 40 to 80 kg/mm^2 class steels is considered. Since allowable fatigue stresses for high strength steels have not been determined in any standard for structural design in Japan, they are required to be determined newly.

The Honshu-Shikoku bridges are designed as combined highway-railway bridges and so the width of main trusses is wider than usual railway bridges. The cross frames are designed rigidly in consideration of wind resistance. And these facts increase tortional rigidity of the stiffening trusses, and make it necessary to consider the fatigue effect by not only single track loading but also double track loading.

With the above mentioned background, the allowable fatigue stress for 60 to 80 kg/mm^2 class steels was determined and the cumulative effect of actual train load was discussed. This report is the outline of these studies.

2. ALLOWABLE FATIGUE STRESS

2.1. Classification of types of joints

Various types of joints were classified in accordance with Railway Bridge Standard[1] as shown in Table 1, that is, 4 groups (A ~ D) for normal stress and 3 groups for shearing stress (S_1 ~ S_3).

Tab1 Classification of joint

	Class	Types of joint
Tension or Compression	A	1.Base metal 2.Friction grip bolted joint 3.Groove welded joint (finished) 4.Longitudinal welded joint 5.Flange plate with gasset which is cut together with flange plate
	B	6.Base metal with a stiffener (finished) 7.Flange plate with groove welded gusset plate
	C or D	8.Base metal with a stiffener 9.Base metalwith a diaphram 10.Non load carrying fillet welded joint 11.Web plate with a gusset plate
Shear	S_1	12.Base metal
	S_2	13.Longitudinal fillet weld
	S_3	14.Load carrying fillet weld

2.2. General expression of allowable stress

Allowable fatigue stress for each group is given by the expression $\sigma_{ao}/(1-\alpha k)$, where σ_{ao} is a basic allowable fatigue stress, k is stress ratio, and α is a parameter which shows the effect of mean stress.

2.3. Effect of mean stress

Among various types of joints, longitudinal butt welded joints are considered to be affected mostly by the mean stress because stress concentration by the shape is considered comparatively small and the residual stress overlaps in

the direction of external force. Dots (·) in Fig. 1 show the result of fatigue tests on longitudinal butt welded joints with various mean stress conditions[2][3][4][5][6]. The inclination of the straight line connecting these points is about -1/6. Rewriting this inclination by the parameter α in 2.2, we obtain α = 0.7 in tension range and α = 1.4 in compression range.

In the other hand, recent test reports on welded joints like fillet welded joints and welded I beam show that test results are affected by mean stress very little, when mean stress is in the tension range[7][8]. Fig. 2 is fatigue test results on fillet welded joints carried out by us[9]. Here also mean stress in tension range affects the results very little.

Considering all these results, the values of α were determined as follows: α = 1.0, that is, no effect of mean stress when k $\geqslant$ 0.3 (tension), α = 0.7 when -1.0 $\leqslant$ k $\leqslant$ 0.3 (tension), and α = 1.4 when -1.0 $\leqslant$ k $\leqslant$ 1.0 (compression).

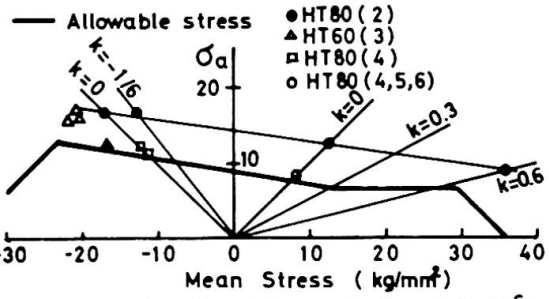

Fig.1 Longitudinal butt joint (2×10^6)

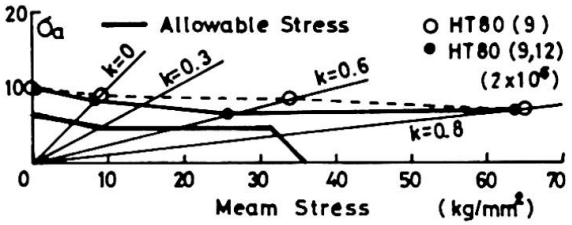

Fig.2 Nonload carying fillet welded joint

2.4. Basic allowable fatigue stress, σ_{ao}

We determined one value σ_{ao} for 60 to 80 kg/mm^2 class high tensile steel irrespective of the class of steels in convenience of practical usage. The followings are explanations on basic allowable fatigue stress for several typical welded joints.

1) Longitudinal butt welded joint

Fig. 1 shows fatigue strength for 80 kg/mm^2 class steels obtained from various fatigue tests. As shown in Fig. 1, fatigue strength of 80 kg/mm^2 class steels is about 15.6 kg/mm^2 (k = 0) and this value seems rather low. This is a result of approximation of S-N curve by

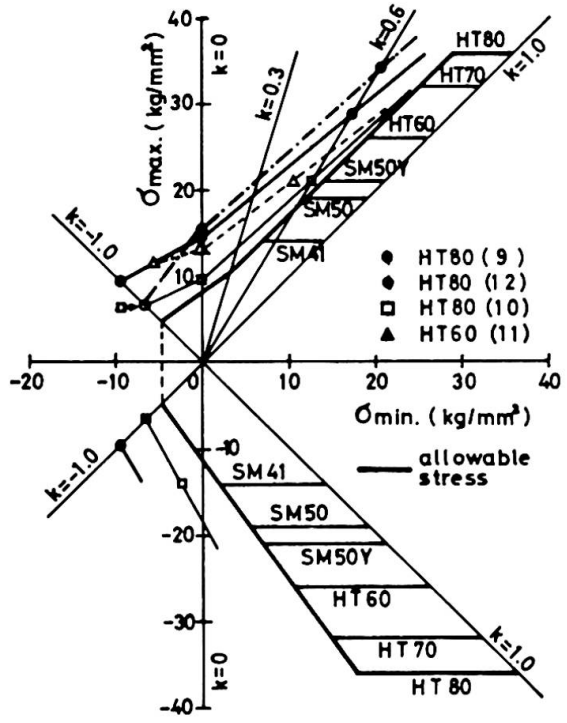

Fig.3 Fatigue strength of fillet welded joint at 2×10^6

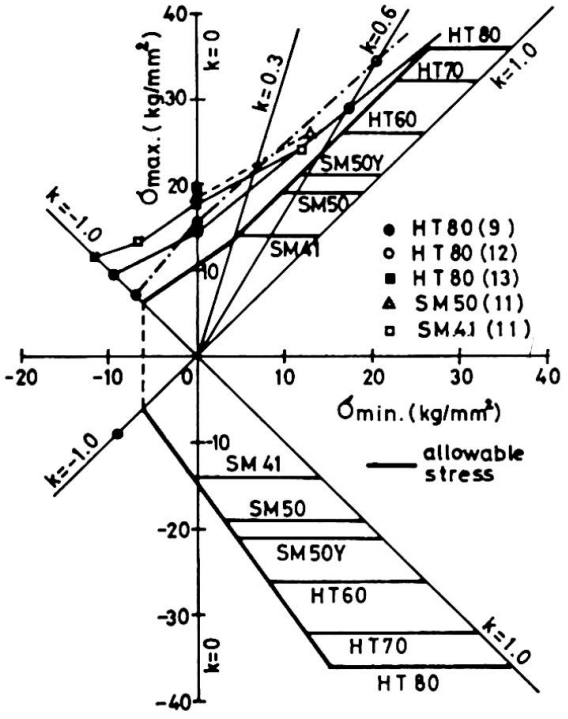

Fig.4 Fatigue strength of fillet welded joint at 2×10^6

a straight line, and there are actually no data which shows fracture by the stress amplitude of less than 16 kg/mm^2. Hence, as for basic allowable fatigue stress for longitudinal butt welded joints, the value σ_{a0} = 1530 kg/cm^2 recommended in Railway Bridge Standard seems appropriate and they are classified in A group.

Tab.2 Allowable fatigue stress (kg/cm^2)

Class	Tension		Compression
	$-1.0 \le k \le 0.3$	$0.3 \le k \le 1.0$	$-1.0 \le k \le 1.0$
A	$\frac{1530}{1-0.7k}$	$\frac{1355}{1-k}$	$\frac{2160}{1-1.4k}$
B	$\frac{1275}{1-0.7k}$	$\frac{1130}{1-k}$	$\frac{1800}{1-1.4k}$
C	$\frac{1050}{1-0.7k}$	$\frac{930}{1-k}$	$\frac{1480}{1-1.4k}$
D	$\frac{800}{1-0.7k}$	$\frac{710}{1-k}$	$\frac{1130}{1-1.4k}$
Shearing			
	$-1.0 \le k \le 0.3$	$0.3 \le k \le 1.0$	
S_1	$\frac{920}{1-0.7k}$	$\frac{815}{1-k}$	
S_2	$\frac{820}{1-0.7k}$	$\frac{725}{1-k}$	
S_3	$\frac{650}{1-0.7k}$	$\frac{580}{1-k}$	

(note) k=|σ|min./|σ|max. or |τ|min./|τ|max.
k>0 (in tension or compression only)
k<0 (between tension and compression)

2) Non-load carrying fillet welded joint

Relatively a large number of fatigue tests on this kind of joints have been carried out. The data of those tests are presented in Fig. 3[10][11]. This figure shows that fatigue strength of higher tensile strength steels tends to be of lower value. Fatigue strength of 80 kg/mm^2 class steels is about 9.8 kg/mm^2. From this result, basic allowable fatigue stress for non-load carrying fillet welded joints must be as low as σ_{a0} = 800 kg/cm^2.

Recently, however, several methods to improve fatigue strength of fillet welded joints have tried[9][12][13]. These method are dressing, finishing, blast treatment and usage of improved welding electrodes which give especially smooth bead. The effects of these methods are shown in Fig. 4. It is clear from Fig. 4 that fatigue strength of improved specimens is increased. So in conditions that the bead and the toe of the weld are well shaped, we can adopt a higher value for the basic allowable fatigue stress. From these results we determined the basic allowable fatigue stress for this type of joint as follows: σ_{a0} = 1050 kg/cm^2 for those in the conditions described above and classified in C group, and σ_{a0} = 800 kg/cm^2 for those without the conditions and classified in D group.

We have been determining basic allowable fatigue stresses for various type of joints listed up in Table 1 with as many test results as possible in the manner explained in this chapter. All the results are presented in Table 2.

3. CUMULATIVE DAMAGE BY TRAIN LOAD

A route (Honshi-Awaji line) of Honshu-Shikoku bridges is planned for double tracks of New trunk lines and D route (Honshi-Bisan line) for double tracks of both New trunk lines and ordinary lines. The total number of trains within 100 years of the service life length is 5.5 x 10^6 in A route and 9.5 x 10^6 in D route. In this chapter, we will discuss cumurative damage by actual load include of the effect of double track loading according to Miner's law based on fatigue strength at 2 x 10^6 loading cycles. Finally we will determine the amendment coefficient for allowable stress.

3.1. S-N curve

S-N curve used in Miner's law is expressed by the following equation and shown in Fig. 5;

$$\log \frac{\sigma}{\sigma_a} = -k_i \log \frac{N}{\bar{N}} \qquad (i = 1, 2) \qquad (1)$$

where σ is stress amplitude, N is loading cycle, σ_a is allowable fatigue strength at 2 x 10^6 and $\bar{N}$ = 2 x 10^6, k_1 = 0.2 ($N \leqslant \bar{N}$), k_2 = 0.1 ($N \geqslant \bar{N}$).

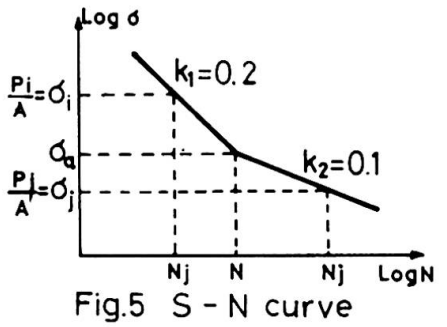

Fig.5 S - N curve

3.2. Cumulative damage by fatigue load[14]

When member force P_i, P_j is given as shown in Fig. 5 that is, n_i cycles of member force P_i where $\sigma_i = P_i/A \geqslant \sigma_a$ and n_j cycles of P_j where $\sigma_j = P_j/A < \sigma_a$, cross sectional area A must be determined so as to satisfy the relation of Miner's law;

$$\Sigma \frac{n_i}{N_i} + \Sigma \frac{n_j}{N_j} \leqslant 1 \qquad (2)$$

Rewriting σ in Eq. (1) by P and A and putting it into Eq. (2), we obtain

$$\frac{1}{(\sigma_a A)^{\frac{1}{k_1}}} \sum_i \frac{n_i}{N} P_i^{\frac{1}{k_1}} + \frac{1}{(\sigma_a A)^{\frac{1}{k_2}}} \sum_j \frac{n_j}{N} \cdot P_j^{\frac{1}{k_2}} \leqslant 1 \qquad (3)$$

P_i and P_j can be expressed as $P_i = f_i P_0$ and $P_j = f_j P_0$, where P_0 is a member force due to the design load. Solving Eq. (3) by A, we obtain

$$A = \beta \frac{P_0}{\sigma_a}, \beta = \left(\frac{C_1 + \sqrt{C_1^2 + 4C_2^2}}{2}\right)^2,$$

$$C_1 = \sum_i \frac{n_i}{N} f_i^5, C_2 = \sum_j \frac{n_j}{N} f_j^{10} \qquad (4)$$

β is an increasing factor of cross sectional area which is obtained by just dividing the member force P_0 by the allowable fatigue stress at 2×10^6 loading cycle σ_a. Therefore the amendment coefficient for allowable stress is $1/\beta$.

3.3. Effect of double track loading

When a bridge is loaded by trains on its both tracks at the same time, greater stress fluctuation occurs than single track loading. Here the number of double track loading was calculated from its probability and cumulative damage by both single and double track loading was examined. There are various members where the effect of double track loading must be considered. We will deal with the case of the upper cord member of stiffening truss of suspension bridges as shown in Fig. 6 in this report. Member force fluctuation of a respective member can be obtained from the member force fluctuation line which is drawn by the influence line. Let's assume that a member force fluctuation line is obtained as shown in Fig. 7 from the influence line shown in Fig. 6. First we simplify the line to rectangular waves, and then transform the horizontal axis from distance to time by dividing by the speed of the train as shown in Fig. 8. Fig. 9 is the member force fluctuation diagram of both up and down lines obtained in the same way.

1) Double track loading

Probability of double track loading was calculated only for the cases i) and ii). The cases where $\bar{P}_1^u$ and $\bar{P}_2^d$ or $\bar{P}_2^u$ and $\bar{P}_1^d$ overlap were treated as single track loading because their directions of stress are opposite.

i) Double track loading by $\bar{P}_1^u$ and $\bar{P}_1^d$ (Fig. 10)

The number of double track loading within the service life length can be calculated by the equation

$$N_i = (t_1^u + t_1^d) \times n_t^u \times n_t^d \times 365 \times 100/T.$$

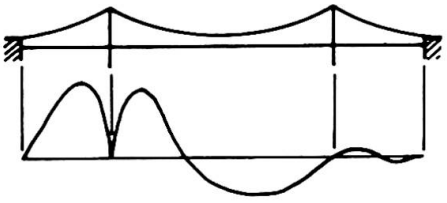

Fig.6 Influence line of upper cord member at the tower link

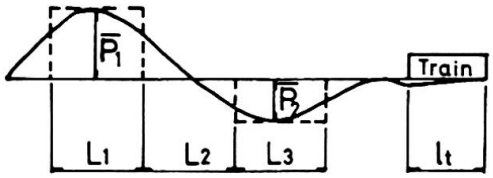

Fig.7 Member force curve

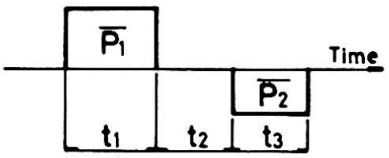

Fig.8 Modeled wave

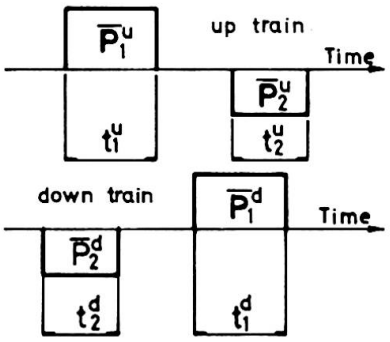

Fig. 9 Single track load

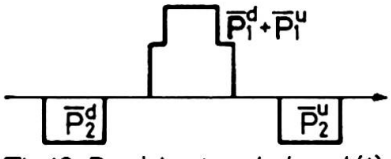

Fig.10 Double track load(i)

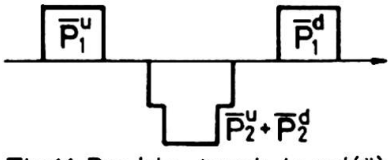

Fig.11 Double track load(ii)

where n_t^u and n_t^d are numbers of trains per day on up and down line respectively and T is service time per day (16 hours). Applying range pair count method to each double track loading, member force fluctuation and number of loading are obtained as follows: (as for the case $\overline{P}_2^d > \overline{P}_2^u$, $\overline{P}_1^d > \overline{P}_1^u$)

a) $P_i^A = \overline{P}_1^d + \overline{P}_1^u + \overline{P}_2^d$, $N_i^A = N_i$, b) $P_i^B = \overline{P}_2^u$, $N_i^B = N_i$.

ii) Double track loading by $\overline{P}_2^u$ and $\overline{P}_2^d$ (Fig. 11)

$$N_{ii} = (t_2^u + t_2^d) \times n_t^u \times n_t^d \times 365 \times 100/T$$

a) $P_{ii}^A = \overline{P}_2^u + \overline{P}_2^d + \overline{P}_1^d$, $N_{ii}^A = N_{ii}$, b) $P_{ii}^B = \overline{P}_1^u$, $N_{ii}^B = N_{ii}$

2) Single track loading

The number of single track loading is obtained by subtracting the number of double track loading from total number of trains.

Up line; $P_s^u = \overline{P}_1^u + \overline{P}_2^u$, $N_s^u = n_t^u \times 365 \times 100 - (N_i + N_{ii})$

Down line; $P_s^d = \overline{P}_1^d + \overline{P}_2^d$, $N_s^d = n_t^d \times 365 \times 100 - (N_i + N_{ii})$

These are calculations for double track lines, however, the same calculation can be applied to four track lines.

3.4. Amendment coefficient for allowable stress

In the checking of fatigue strength, design load for suspended structure is 2.7 t/m per one track and loading length is 370 m in ordinary lines and 400 m in New trunk lines. Service life length is 100 years. The estimated numbers of trains per day on one track in 1990 are as follows,

A route;	New trunk line passenger cars	75 trains
D route;	New trunk line passenger cars	14 trains
	Ordinary line passenger cars	29 trains
	Ordinary line freight cars	86 trains

Based on the above assumptions, the increasing factors of cross section were calculated for suspension bridges in A and D route. We obtained $\beta = 1.23$ for A route and $\beta = 1.30$ for D route. Amendment coefficients were calculated from these values as shown in Table 3. In design of stiffening trusses of suspension bridges, allowable fatigue stress multiplied by amendment coefficients in Table 3 must be used.

Tab.3 Coefficients

Route	Amendment Coefficients
A	0.80
D	0.75

4. CONCLUDING REMARKS

Honshu-Shikoku bridges are expected to be exposed to various conditions which we have never experienced before. And so the fatigue design criteria is rather different from those of usual railway bridges. We doubt that we have obtained enough data to determine the allowable fatigue stress for more than 60 kg/mm^2 class high strength steels and we need more data of various kinds of tests. Now in Fuji city we have a large scale fatigue testing machine which has a capacity of 400 tons dynamic loading. With this machine we are conducting fatigue tests on welded specimens of 80 kg/mm^2 class steels with 75 mm thickness or full size structure models and planning to confirm the allowable fatigue stress and amendment coefficient described in this report.

This report is a summary of studies and discussions by the committee of Honshu-Shikoku bridge super structure of Japan Society of Civil Engineers, sub-committee of fatigue design[10]. The authors wish to express their appreciation to each member of the committee.

REFERENCES

(Note) JSCE; Japan Society of Civil Engineers

1. Standard for Structural Design of Steel Railway Bridges, J.S.C.E., March 1974 (in Japanese)
2. Super structure committee of Honshu-Shikoku bridges, Fatigue testing of high strength welded joint, J.S.C.E, March 1973 (in Japanese)
3. Private Paper, Kobe Steel, Ltd., 1974
4. Tajima, J., et. al., Application of 80 kg/mm^2 class high tensile strength steel to Railway bridges, IIW-XIII-706, 1973

5. Ishiwatari, M., et. al., Fatigue Testing on the HT80 welded joints, Abstract of the 24th annual J.S.C.E., lecture meeting, J.S.C.E., Oct. 1969 (in Japanese)
6. Ito, F., et. al., Fatigue tests on longitudinal butt welded joint by HT80 large size specimens, The News of Railway Technical Research Institute, No.67-88, 1967
7. Tada, Y., et. al., Fatigue tests on steel deck plate, Civil Engineering Journal, No.7-1, 1973 (in Japanese)
8. Effect of weldments on the fatigue strength of steel beams, Frity Engineering Laboratory Report, No.334.2, Lehigh University Institute of Research.
9. Tajima, J., et. al., Fatigue strength of HT80 welded joints, Abstract of the 30th annual J.S.C.E. lecture meeting, J.S.C.E., Oct. 1975 (in Japanese)
10. Super structure committee of Honshu-Shikoku bridges, Fatigue Design on Honshu-Shikoku bridges, J.S.C.E., March 1974 (in Japanese)
11. Ota, S., et. al., Experimental Study on the fatigue strength of welded joints, J.S.S.C., vol. 7, No.72, Dec. 1971 (in Japanese)
12. Ikeda, K., et. al., Improvement of fatigue strength of fillet welded joint in high strength steel, J. of Japan Welding Society, vol. 44, No.2, Feb. 1975
13. Kado, S., et. al., The improvement of fatigue strength in welded high tensile strength steels by additional weld run with coated electrodes, IIW-XIII-772, 1975
14. Ito, F., The estimation of cumulative damage of railway bridge by the train loading, Railway technical research report, No.676, April 1969

SUMMARY

The fatigue design criteria of Honshu-Shikoku bridges is outlined in two aspects. One is the basic fatigue allowable stress for various types of welded joints of 60 to 80 kg/mm2 class high tensile strength steels and the other is the estimation of the effects of stress and loading cycle by the actual train loads.

RESUME

Le critère de la fatigue dans le cas des ponts suspendus entre Honshu et Shikoku est présenté sous deux aspects. L'un est la contrainte admissible de fatigue principale pour les divers types de joints de soudage de 60 à 80 kg/mm2 pour l'acier à haute résistance à la traction, et l'autre est l'estimation de l'effet de contrainte et du cycle de chargement par la charge actuelle des trains.

ZUSAMMENFASSUNG

Die Kriterien für den Dauerfestigkeitsnachweis der Honschu-Schikoku Hängebrücken bestehen aus zwei Hauptteilen. Der eine Teil ist die zulässige Grundspannung für verschiedene Typen von Schweissverbindungen mit hochfestem Stahl (Bruchfestigkeit 60 bzw. 80 kg/mm2). Der andere Teil ist die Abschätzung des Einflusses der Spannungs- und Belastungswechsel unter der wirklichen Zugbelastung.

Vc
Problèmes de fabrication et de montage
Herstellungs- und Montageprobleme
Fabrication and Erection Problems

Leere Seite
Blank page
Page vide

Réalisation du pont à haubans de Saint-Nazaire

Stahlschrägseilbrücke in Saint-Nazaire

Cable-Stayed Steel Box Girder Bridge in Saint-Nazaire

F. CIOLINA — Chef Département Etudes
J.C. FOUCRIAT — Ingénieur
Compagnie Française d'Entreprises Métalliques
Paris, France

Le pont à haubans intégré au viaduc qui franchit l'estuaire de la LOIRE entre SAINT-NAZAIRE et SAINT-BREVIN, est un ouvrage métallique de 720 m de longueur : une travée centrale de 404 m de portée flanquée de 2 travées latérales de 158 m. Il dégage un gabarit de navigation maritime de 61 m de hauteur sur une largeur de 300 m (Figure 1).
Le profil en long de la chaussée est une parabole de paramètre 6 428 m. Il supporte une chaussée de 12 m et deux trottoirs. Le tablier a une largeur hors tout de 15 m.

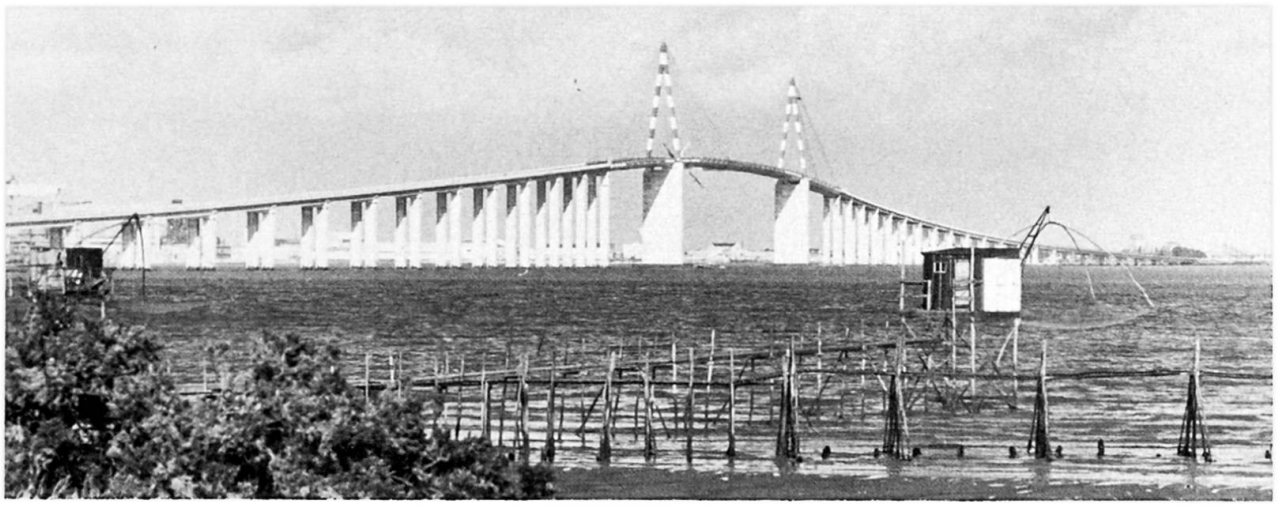

Figure 1 - Pont de SAINT-NAZAIRE

Un pont à haubans a été préféré à un pont suspendu qui aurait nécessité des massifs d'ancrage coûteux en raison de la grande hauteur des piles, environ 50 m et de la profondeur des fondations : 5 m d'eau plus 40 m de vase et sable.

Pour assurer un bon comportement aérodynamique de l'ouvrage, il a été choisi :

- un tablier en forme de caisson assez mince dont la hauteur dans l'axe de la chaussée n'est que de 3,20 m et dont les âmes sont inclinées

- des pylônes triangulaires et un haubanage fixé aux parois latérales des caissons et quasi convergent en tête des pylônes.
  Une telle architecture donne à la structure une grande rigidité de torsion.

Le développement de l'étude aérodynamique a confirmé que le pont ainsi conçu présente une vitesse critique de "flutter" très largement supérieure aux vitesses de vent possible en son site. Par contre, il a fallu le munir de déflecteurs permettant de réduire l'amplitude des oscillations verticales dues aux échappements tourbillonnaires.

La construction de l'ouvrage selon le procédé classique : montage des travées latérales en prenant appui sur des piles intermédiaires provisoires, a été jugé trop coûteux en raison de la hauteur des piles et de la profondeur des fondations. Le processus de construction retenu tire profit du fait que les travées latérales sont en site aquatique et que la C.F.E.M. possède un atelier en bord de la mer Méditerranée à FOS. Quatre tronçons de tablier, longs de 96 m y ont été construits puis acheminés à l'aide de barges marines jusqu'au port de SAINT-NAZAIRE (Figure 2). Là, assemblés deux à deux pour constituer les travées de rive et les amorces de la travée centrale du pont, ils ont été amenés sur le site et placés, en profitant de la marée, sur un système élévateur reposant sur l'embase des piles (Figure 3).

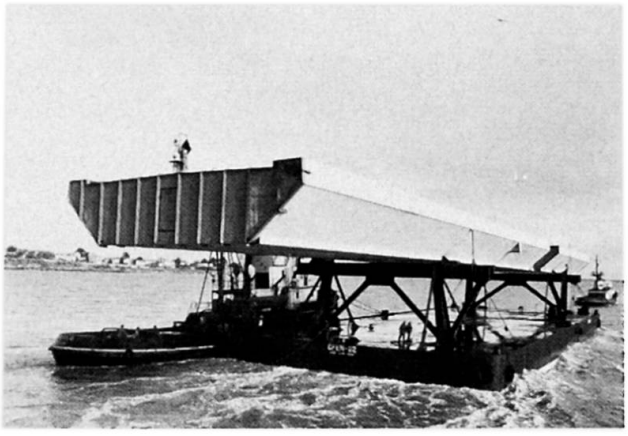

Figure 2 - Transport de tronçon de tablier

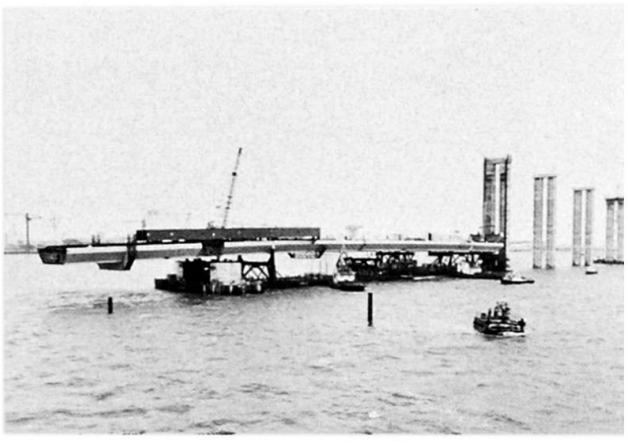

Figure 3 - Mise en place d'une travée latérale

Après construction des fûts des piles principales à l'aide de coffrages glissants, le tablier du pont a été hissé jusqu'à son niveau définitif (Figure 4). Le dispositif de hissage est analogue à celui déjà utilisé par la C.F.E.M. en 1971 lors de la construction du viaduc de MARTIGUES. Le tablier a servi de monte charge et porté le pylône couché, divers engins de levage, une baraque de chantier, etc...
Après que les pylônes aient été redressés, la travée centrale a été montée à l'avancement en porte à faux par tronçons complets de 16 m approvisionnés sous le pont et levés à l'aide d'une chèvre (Figure 5), puis assemblés au tronçon précédent par boulonnage et soudage.

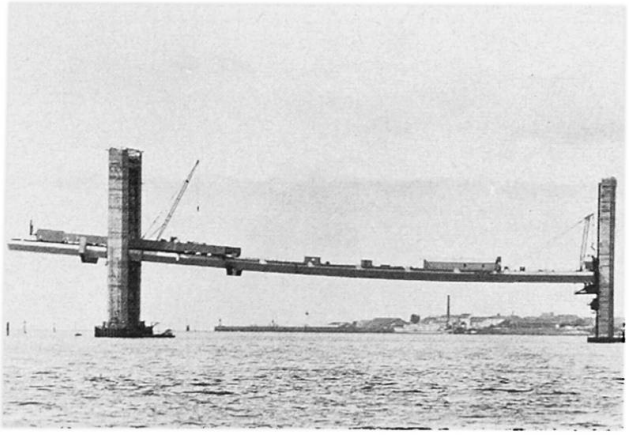

Figure 4 - Travée latérale en cours de hissage

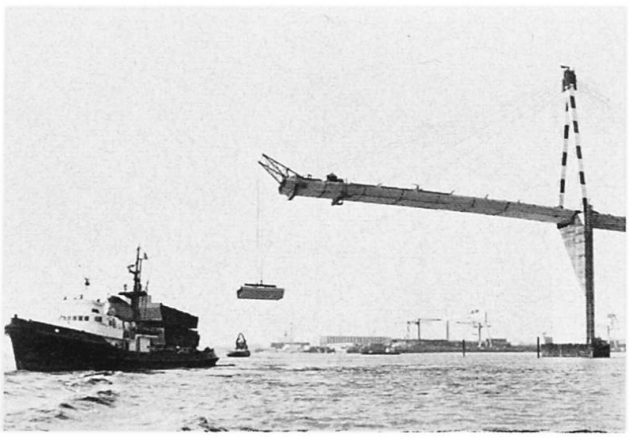

Figure 5 - Levage d'un tronçon de la travée centrale

Des aciers soudables à hautes caractéristiques mécaniques ont été utilisés en certaines parties de l'ouvrage.

Les haubans sont fixés sur les parois latérales de la tête du pylône et sur des appendices des âmes du caisson. La fixation est faite par l'intermédiaire de chapes, d'axes et de rotules sphériques. La résistance effective de l'ouvrage dépend bien sûr, essentiellement de la bonne tenue des parois latérales de la tête du pylône et des appendices du caisson. Ces pièces assemblées à l'ossature par soudage devaient avoir une épaisseur de 80 mm ; Elles sont soumises à des contraintes d'ensemble modérées mais localement des contraintes élevées peuvent apparaître qu'aucun calcul ne peut prévoir avec précision. Il fallait les réaliser en acier très ductile ; Nous avons choisi un acier élaboré au four électrique par la Société MARREL : l'acier AMCO calmé à l'aluminium et dégazé sous vide. Ses caractéristiques sont les suivantes :

- Composition chimique (teneur en %)

0,11	C	0,16
1,45	Mm	1,65
0,10	Si	0,35
0,20	Ni	0,40
	Cv	0,25
	Mo	0,10

- Caractéristiques mécaniques

	E Travers kg/mm2	R Travers kg/mm2	A %	KCV-50° en long kg/cm2
Valeur minimale exigée	30	-	-	3,5
Moyenne des essais	37,1	53,2	31,4	16,9
Moyenne moins 2 fois l'écart type	33,7	49,8	26,7	4,5

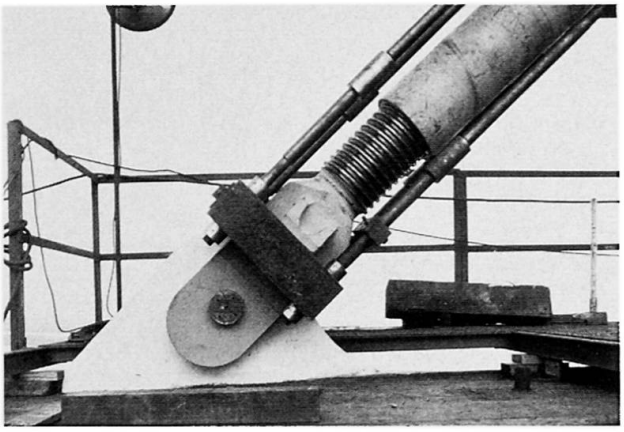

Dispositif d'ancrage des haubans sur les caissons et Dispositif de mise en torsion des haubans

Les chapes ont été pour les mêmes raisons réalisées en acier moulé à haute résistance. En fonction des efforts développés par les haubans, 2 familles de chapes ont été réalisées avec des aciers de caractéristiques différentes :

Nuance d'acier moulé	E kg/mm2	R kg/mm2	A %	KCV-20° en long kg/mm2
30 NCD 8 M				
Valeur minimale exigée	45	80	15	3,5
Moyenne des essais	75,2	87,8	19,9	11,6
Moyenne moins 2 fois l'écart type	69,9	84,1	14,8	9,6
25 MD 25 M				
Valeur minimale exigée	36	65	15	3,5
Moyenne des essais	5I,9	69	22	7,9
Moyenne moins 2 fois l'écart type	47,5	64,7	17,8	4,5

En situation de hissage, les travées de rive ont été considérablement plus sollicitées qu'elles ne peuvent l'être dans l'ouvrage terminé.
Une étude a montré qu'il était plus économique de construire le fond du caisson en acier de limite d'élasticité égale à 42 kg/mm2 que d'adopter une tôle de plus forte épaisseur dont le supplément de poids aurait contribué à augmenter sensiblement les sollicitations.
Il fallait toutefois, que l'acier choisi soit soudable sans qu'il soit nécessaire de prendre de précautions coûteuses.
Une étude confiée à M. SCHNADT nous a permi de sélectionner des aciers présentant avant et après soudage des caractéristiques mécaniques en long et travers satisfaisantes. Le tableau ci-dessous résume les caractéristiques mécaniques exigées et celles obtenues lors des essais de réception des aciers DILLINAL 55/43 utilisés.

	E long kg/mm2	R long kg/mm2	A %	KCV-20° long kg/cm2	KCV-20° Travers kg/cm2
Valeur minimale exigée	43	55	19	7	4
Moyenne des essais	48	59,5	28,1	13,1	5,9
Moyenne moins 2 fois l'écart type	43,1	54,8	23,9	9,3	4,2

Les zones thermo vectomiques d'un échantillon de cet acier prélevé dans une tôle de 14 mm sont :

- en long

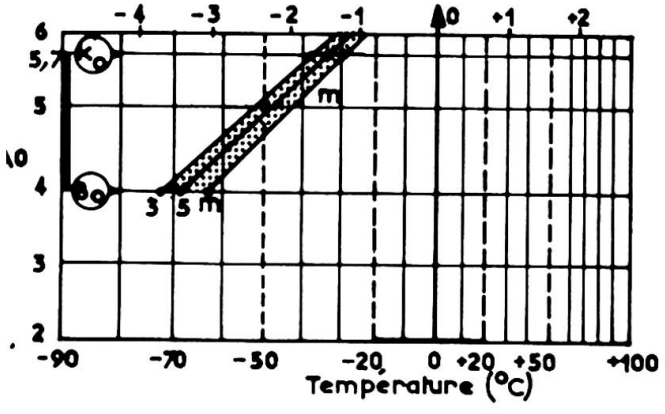

- en travers

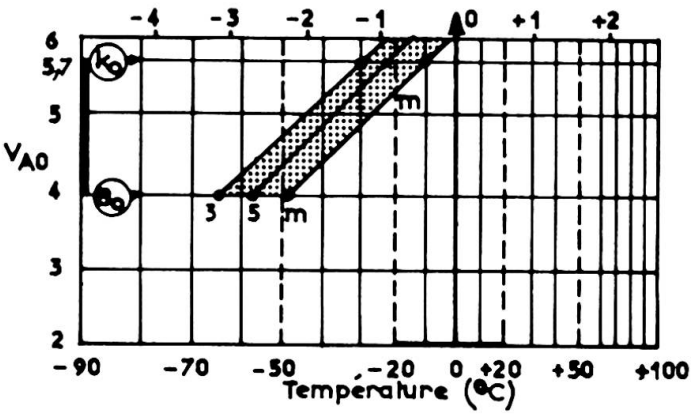

Bien que ce ne soit pas nécessaire pour la résistance de l'ouvrage, il fut décidé de construire les jambes des pylônes en acier Usiten LE 43 Nb Lc. C'est un acier de composition chimique identique à celle de l'acier E 36-4 au niobium calmé à l'aluminium, mais le laminage contrôlé permet d'en relever les caractéristiques mécaniques.

	E Long kg/mm2	R Long kg/mm2	A %	KCV-20° Long kg/cm2	KCV-20° Travers kg/cm2
Valeur minimale exigée	43	55	19	7	3,5
Moyenne des essais	47,1	57,8	26,2	12,4	5,7
Moyenne moins 2 fois l'écart type	43,1	54,9	22,5	7,3	3,75

Une étude faite sur des échantillons de tôles de même composition chimique, a montré que les aciers livrés à l'état de laminage contrôlé n'étaient pas plus sensibles au vieillissement que les aciers à l'état normalisé provenant de la même coulée.

Les épaisseurs des tôles en acier DILLINAL 55/43 et en acier USITEN LE 43 Nb Lc n'excédaient pas 16 mm. Leur soudage a pu être effectué sans préchauffage selon des techniques similaires à celles utilisées pour l'acier E-36.

RESUME

Le viaduc sur la Loire entre Saint-Nazaire et Saint-Brevin comporte un pont métallique haubanné dont la travée principale a une portée de 404 m. Des aciers moulés et des aciers soudables de hautes caractéristiques mécaniques ont été utilisés pour la construction de certaines parties de l'ouvrage.

ZUSAMMENFASSUNG

Die Ueberbrückung der Loire zwischen Saint-Nazaire und Saint-Brevin besteht aus einer Stahlschrägseilbrücke, deren Hauptfeld eine 404 m lange Stützweite hat. Für die Herstellung einiger Bauteile wurden hochwertiger Stahlguss und hochfeste schweissbare Stähle benützt.

SUMMARY

The main span of the cable-stayed steel box girder bridge as a part of the viaduct joining Saint-Nazaire to Saint-Brevin over the Loire is 404 m long. Cast high strength steel and welding high strength steel have been used in building some parts of the bridge.

Application of High Strength Steels to a Long Span Truss Bridge — Osaka Port Bridge

Application des aciers à résistance à un pont à poutres en treillis de longue portée — Pont du port d'Osaka

Anwendung hochfester Stähle für eine weitgespannte Fachwerkbrücke — Osaka Hafenbrücke

ICHIRO KONISHI
Professor Emeritus
Kyoto University
Kyoto, Japan

TOSHIE OKUMURA
Professor
Saitama University
Tokyo, Japan

SHUNJI MINAMI
Adviser
Nissho-Iwai Co., Ltd.
Osaka, Japan

MATSUJI SASADO
Manager
Hanshin Expressway Public Corp.
Osaka, Japan

1. INTRODUCTION

The Osaka Port Bridge is a cantilever truss bridge having a total length of 980m (=235m+510m+235m), including a suspended span of 186m. This bridge has double decks with four lanes each.

The type of the bridge was determined considering location of piers, navigation channel and soil condition.

High-strength steels of 70kg/mm^2 and 80kg/mm^2 classes up to 75mm in thickness which had high weldability were newly produced for the construction of this bridge. Out of the total bridge weight of 40,000 tons, the following amount of the high-strength steels was used.

80kg/mm^2 class high-strength steel (HT80): 4,197tons
70kg/mm^2 class high-strength steel (HT70): 1,075tons

In the application of high-strength steels to a long-span truss bridge, due considerations should be given to design, materials, fabrication and erection.

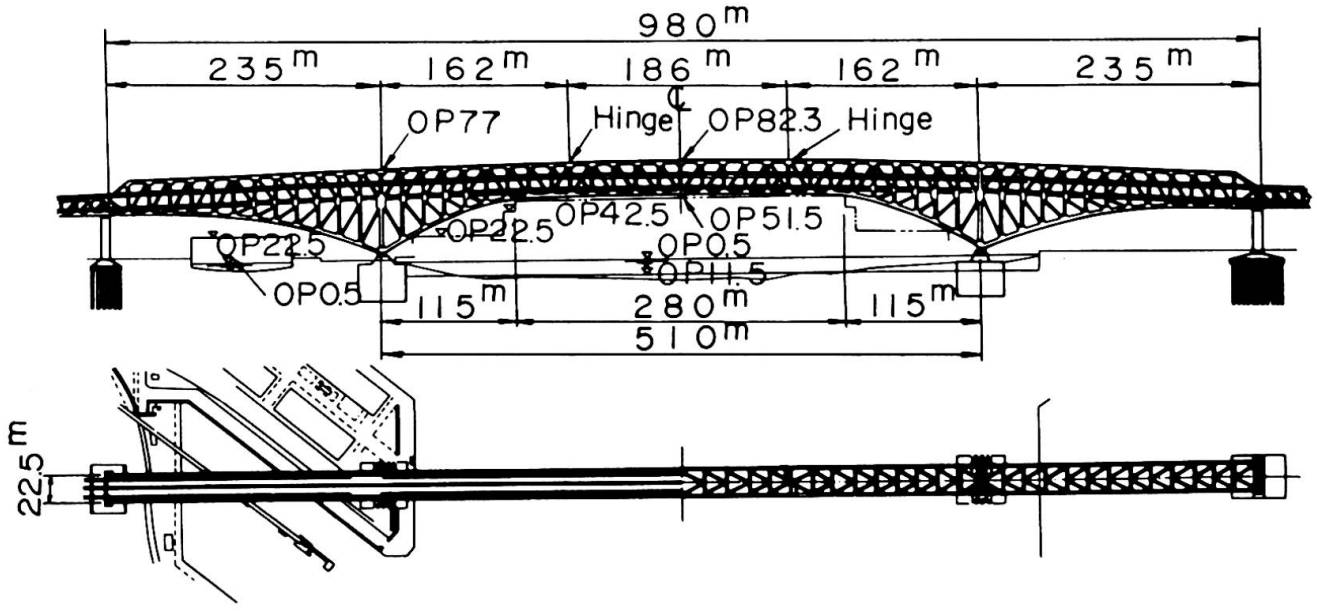

Fig.1 Osaka Port Bridge

2. DESIGN

The conventional truss bridge designs are based on an assumption that the both ends of a truss member are pin-jointed, thus causing axial force alone as section force. In recent years, however, there have been changes in the joint details of the actual truss, from the pin joint to the rivet joint and further to the high-strength bolt joint, which results in the prevention of free rotation of the members at the joints due to the increased rigidity of the connection.

In case of the Osaka Port Bridge, analysis shows that secondary stresses due to the additional bending mements and shear forces caused by connecting members rigidly at panel points are beyond negligible values.

One of the effective ways to minimize the secondary stresses is the use of members with lower flexural rigidity. But, there is a limit to this when a member is subject to higher stresses. In América, "Prebend" method is usually employed to reduce secondary stresses due to the dead load in a long span truss. In this method, however, difficulty lies in the implementation of procedure control and in the method of checking the residual stresses.

It was concluded in the design of this bridge that the secondary stresses due to the bending moments and shear forces caused at the panel points were to be analyzed and evaluated as one of the design stresses, and that thick plates with higher strength were to be used as the material for the chord members for the purpose of obtaining higher member strength without increasing the flexural rigidity of the member sections.

Box sections were employed as the chord members of this bridge. (Fig.2) The depth of each web was limited to one-tenths of the panel length, and the ratio of the sectional area of each flange to that of the entire cross section was made as low as practicable, which led to the use of 75mm thick plate of HT70 and HT80 steels as the web plates.

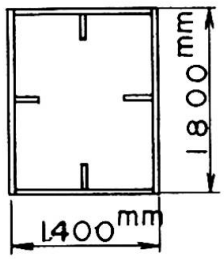

Fig.2 Sectional Form

Longer panel length can present a better proportion between the main truss height and panel length in a long truss bridge, which will result in less slenderness ratio l/r of the members and hence in less effects of the secondary stresses. Therefore, in this bridge the panel length was taken to be 18m to 19m, which is much longer than that of the conventional bridge.

3. MATERIALS

High-strength steels of 70kg/mm^2 and 80kg/mm^2 which were then available in Japan were considered to have too many unresolved problems to be applied for the construction of this bridge. In preparing a new specification it will be an important matter to our technical judgement which limit should be paid attention to - limit of steel manufacture or that of bridge fabrication. In the case of the Osaka Port Bridge, judging the matter in the balance of the above two limits, it was decided, in view of the highly advanced techniques of steel manufacturing in Japan to leave the solution of the problem to steel material wherever possible, and then requirements for the steel manufacture were set forth. In determing the mechanical properties and chemical compositions of the tempered high-strength steels to be employed for this bridge,

Table 1 Specification of HT70 and HT80 steels

	Thickness (mm)	Chemical Composition (%)						Mechanical Property					Toughness
		C	Si	Mn	P	S	Ceq	Y.P. (kg/mm^2)	T.S. (kg/mm^2)	EL. Thickness (mm)	EL. Test Specimen (JIS)	EL. %	
HT70	$6 \leqq t \leqq 50$	$\leqq 0.15$	$\leqq 0.55$	$\leqq 1.50$	$\leqq 0.03$	$\leqq 0.03$	$\leqq 0.49$	$\geqq 63$	70~85	$6 \leqq t \leqq 16$	NO.5	$\geqq 17$	$vE_{-15} \geqq 4.8$ kg·m (V Notch Charpy Value)
										$t > 16$	NO.5	$\geqq 23$	
	$50 < t \leqq 100$	$\leqq 0.17$	$\leqq 0.55$	$\leqq 1.50$	$\leqq 0.03$	$\leqq 0.03$	$\leqq 0.53$	$\geqq 60$	68~73	$t > 20$	NO.4	$\geqq 17$	
HT80	$6 \leqq t \leqq 50$	$\leqq 0.14$	$\leqq 0.55$	$\leqq 1.50$	$\leqq 0.03$	$\leqq 0.03$	$\leqq 0.53$	$\geqq 70$	80~95	$6 \leqq t \leqq 16$	NO.5	$\geqq 16$	$vTrE \leqq -35°C$ (Transition Temperature)
										$t > 16$	NO.5	$\geqq 22$	
	$50 < t \leqq 100$	$\leqq 0.17$	$\leqq 0.55$	$\leqq 1.50$	$\leqq 0.03$	$\leqq 0.03$	$\leqq 0.57$	$\geqq 68$	78~93	$t > 20$	NO.4	$\geqq 16$	

Y.P. : Yield Point T.S. : Tensile Strength EL. : Elongation JIS : Japan Industrial Standards

special considerations were given to the occurrence of cracking, and softening and embrittlement in the bond of weld joints of HT70 and HT80 steels to prevent the possible occurrence of these phenomena in practical use.

The material specification of the steels to be used for the Osaka Port Bridge was set forth in accordance with the following basic conditions; (Table 1.)

(1) The maximum plate thickness of each class of steel shall be as follows.
75mm for $60kg/mm^2$ class steel
100mm for $70kg/mm^2$ and $80kg/mm^2$ class steels

(2) The steels shall have such fracture toughness that they will not be brittle fractured at the service metal temperature of -15°C.

(3) The heat input by welding shall be determined so that the requirements in item (2) above can be met. (50KJoule/cm)

(4) The temperature of preheat is dependent on the grades and thickness of materials. As for the materials to be used for this bridge, it shall be aimed that welding of $80kg/mm^2$ class steel, 100mm in thickness with preheat temperature of 150°C and under, may not result in any weld defects.

(5) The flatness of the steel plate shall not exceed 2mm/m to maintain subsequent fabrication accuracy.

A series of tests were conducted on plate thickness, 25, 50, 75 and 100mm of both HT70 and HT80 in six major mill makers in Japan to confirm the characteristics of materials concerning these phenomena. These tests were intended to investigate chemical compositions, shape and dimension accuracy, mechanical properties, weldability and weld joint performance.

From these tests it was proved that HT70 and HT80 steels can be satisfactorily applied to this bridge. It was also found out that materials produced by the current mass production process to be used for the construction of this bridge had excellent properties.

4. FABRICATION

As a procedure test to determine welding condition, fabrication accuracy, and inspection procedure, the following tests were conducted prior to fabrication;

(1) lamellar tear test,
(2) restrained cracking test,
(3) tests on the performance of corner weld joints,

(4) tests to check residual stresses due to welding, and
(5) tests to investigate the various chracteristics of the actual members using full scale models.

Welding conditions including minimum preheat temperature, maximum preheat temperature, interpass temperature, and preheat temperature for tack welds and baking conditions of welding materials were determined from the results of these tests, under the condition that over 50KJoule/cm of heat input was in no case permitted in the fabrication of this bridge.

Major characteristic procedures employed for the fabrication of this bridge are as mentioned below. Unlike the conventional preheat control method, the following three types of preheating methods were used;

(1) electric preheating type with automatic control,
(2) fixed burner type, and
(3) manual burner type.

The separate preheating method was specified for each type of weld joints. In welding major members, symmetrical preheating and symmetrical welding methods were employed to secure higher fabrication accuracy and minimize residual stresses. To prevent the occurrence of cracking, the welding material having the strength lower than the base metal that is "soft joint" was employed. It was also specified that the fabricators should submit reports of preheat temperature, amount of heat input, amout of angular deformations in butt joints, and dimentional accuracy of members after tack welding and final welding, respectively.

As for the drilling of holes at joints, discussions were made on efficiency and accuracy of drilling, partly because the grip lengths of joints were large due to the use of thick plates and partly because the high-strength steel with high hardness was used. In this bridge, an interchangeable method in which drilling of holes was performed using a template with a bush inserted in each hole was employed, wherever practicable.

5. ERECTION

This bridge has long panel length, which resulted in increase in the weight of single members. Larger members weigh 75 to 110 tons each. This was the biggest factor in determining the erection method. Erection methods are shown in Fig. 3. Erection loads which would be resulted from the below-mentioned erection method were investigated and evaluation of stresses caused by these loads was carried out for each stage of erection.

The two panels at the tower part was fabricated into an assembly of about 540 tons which was then installed by means of 3000 tons floating crane, in order to secure accuracy as well as safety and erection time saving, since these two panels would be the reference points for the erection accuracy.

The anchor and cantilever spans were erected by cantilever method and the maximum weight of a single member at these spans was limited to 80 tons so that it could be erected by a traveller crane.

The suspended span whose length was 186m and whose weight was about 4500 tons was preassembled into one block at the shop and towed to the site by 15,000 tons capacity barge. Finally on February, 26, 1974 suspended truss span was lifted to the height of approximately 60m above sea level using lifting equipment to the final position. For this lifting it took only about 3.5 hours.

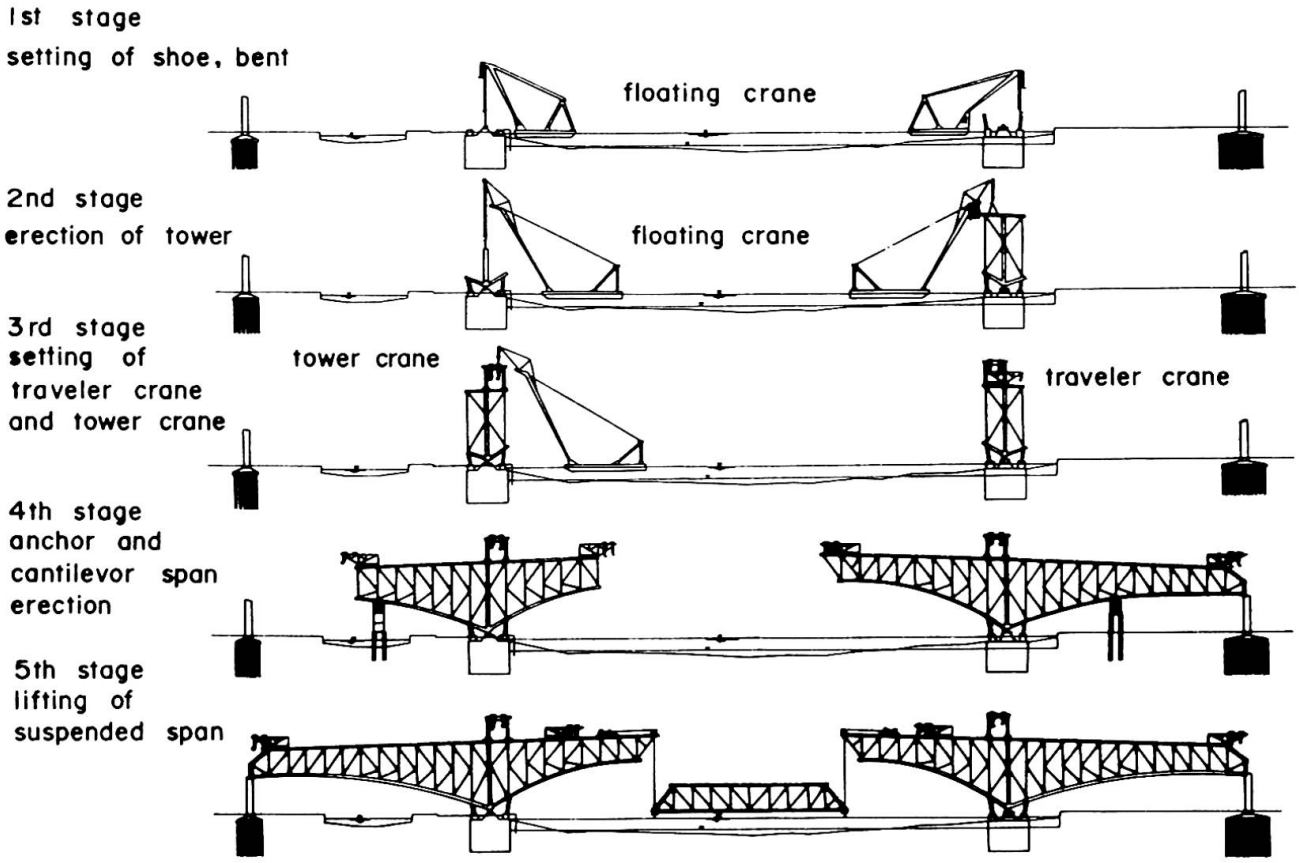

Fig.3 Erection Methods

Photo 1 Lifting of Suspended Span

SUMMARY

High-strength steel was applied in the Osaka Port Bridge after sufficient investigations. The choice of this material lead to compact cross sections and permitted to reduce the secondary stresses at panel points. This choice was confirmed by a serie of tests for different plates of HT70 and HT80 with thickness of 25, 50, 75 and 100 mm. Due attention was paid to the problem of cracking and embrittlement of welded joints during fabrication. This bridge will be ranked as the third longest modern cantilever truss bridge.

RESUME

Les aciers à haute résistance ont été appliqués au pont du port d'Osaka après des recherches approfondies. Ce choix a rendu les sections de membrures compactes et a réduit les contraintes secondaires aux points de jonction. Les matériaux ont été choisis avec soin; ils ont été mis à l'epreuve d'endurance sur des plaques de HT70 et HT80, d'épaisseur 25, 50, 75 et 100 mm. Il a été fait attention que ni fissure ni rupture de fragilité dans les joints soudés ne se produisent en cours de fabrication. Ce pont est le troisième pont moderne cantilever le plus long dans le monde.

ZUSAMMENFASSUNG

Nach verschiedenen ausführlichen Untersuchungen wurden hochfeste Stähle für die Osaka Hafenbrücke verwendet. Damit wurde es möglich, die Querschnitte einzelner Bauteile zu verkleinern, und dadurch die Nebenspannungen an den Knoten zu verringern. Bei der Fertigung wurde besonders die Vermeidung von Rissen und Sprödbruch im Bereich der Schweissstellen berücksichtigt. Für HT70 und HT80 wurde eine Serie von Eignungsprüfungen, jeweils mit Blechstärken von 25, 50, 75 und 100 mm, durchgeführt. Diese Brücke ist nun die drittlängste moderne Fachwerkbrücke mit Kragarmkonstruktion in der Welt.

Choice of Steel Quality of Steel Bridge Girders with Regard to Support Forces during Launching

Choix de l'acier de poutres de ponts métalliques en relation avec les forces d'appui lors du lancement

Wahl der Festigkeitsklasse von Brückenträgern im Zusammenhang mit den Auflagerdrückern beim Einschieben

ALLAN BERGFELT
Professor
Chalmers University of Technology
Göteborg, Sweden

RICKARD WILSON
Consulting Engineer
Göteborg, Sweden

Large steel girder bridges in one or several spans are often erected by launching. The loading cases which occur during the launching procedure are very different from those of the final structures.

The support forces at the launching rolls are concentrated loads acting on the bottom flanges of the main girders of the bridge. During launching these loads move along the whole length of the girder, which means that very large concentrated loads are acting on the flange and an at least partly unstiffened web (as there is of course no economical possibility to arrange stiffeners in extremly small distances). It follows that there may be a risk for local deformation of the flange at the launching support combined with web crippling. This conclusion holds both for deep I-girders and box girders.

The design has to check the safety against both (a) local yielding and (b) buckling, as well as against combined influences.

Web crippling is of course included in various standard specifications and several authors have improved the solution, especially the calculations for combined influence, see e.g. [1]. The limit load is usually considered to be the one for which either the yield stress or the idealized plate buckling load is reached. As in modern steel construction more slender webs are used, the post-buckling range of a plate has to be considered. C A Granholm [2] performed full-scale tests in order to find the web crippling load and suggested that this load (with due safety factor) should be used as limit load. Further improvements [3] have led to the observation that even for girders where buckling is governing the influence of the yield point of the steel σ_y is of great importance (and not only the modulus of elasticity E), which means that the crippling load might be increased by the use of high strength steel.

The various kinds of influences – stresses and buckling – that have to be considered are shown in fig. 1 and are listed below :

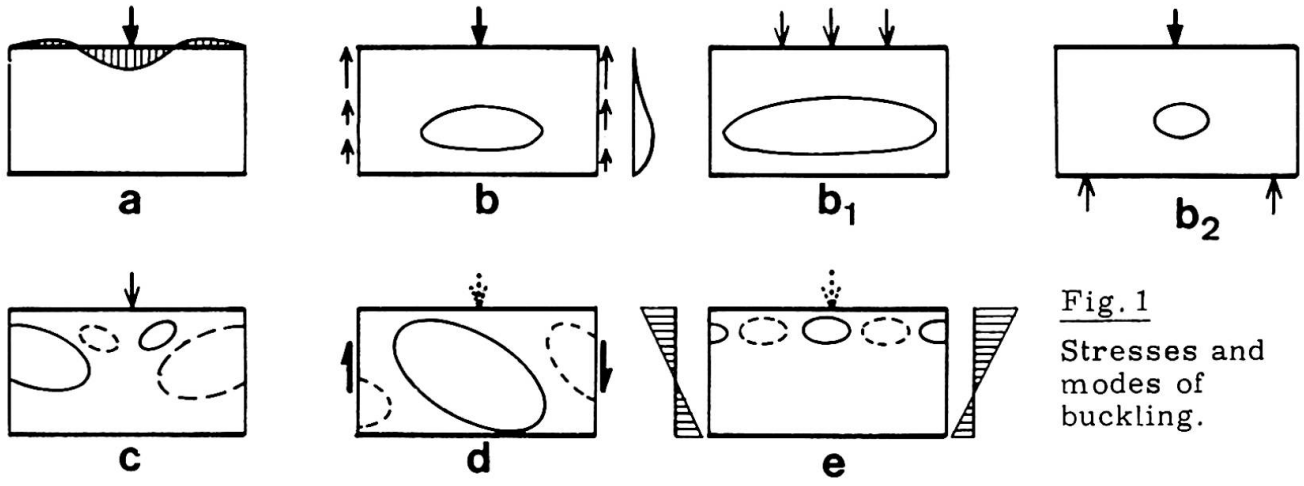

Fig. 1
Stresses and modes of buckling.

a. Local vertical stresses σ_z
b. Plate buckling because of vertical stresses
   b1. Plate buckling of a long part of the web (nearly equal to column buckling) because of distributed load or very stiff flanges
   b2. Plate buckling nearly equal to column buckling because the load is concentrated to a small part of the web due to opposite forces.
c. Shear buckling locally at the load
d. Shear buckling of the girder web
e. Buckling of the girder web due to bending stresses

It is obvious that local effects, such as a) c) and probably e) are interacting mainly with respect to local web crippling. An interaction of the effects b) and d) with respect to buckling occurs in a larger part of the web. The decrease of the bearing capacity due to effect b2) is sometimes greater than the decrease due to the effect e). This explains why it is sometimes found in tests that a large span girder can bear a greater concentrated load than a very short span girder.

Numerous tests have confirmed the obvious result that even if the bearing capacity for a web under a concentrated load mainly depends on the dimensions of the web, also the stiffness of the flange has a definite influence. Preliminary results [4] indicated an increase proportional to the variable (1+0.4 t/d) when $t/d > 2$ approximately, where t/d = flange thickness/web thickness. When $t/d < \sim 2$ the tests indicated even a faster increase. Numerous test [5] in mainly the range $1.5 < t/d < 5$ confirmed the preliminary results and the following formulas are proposed

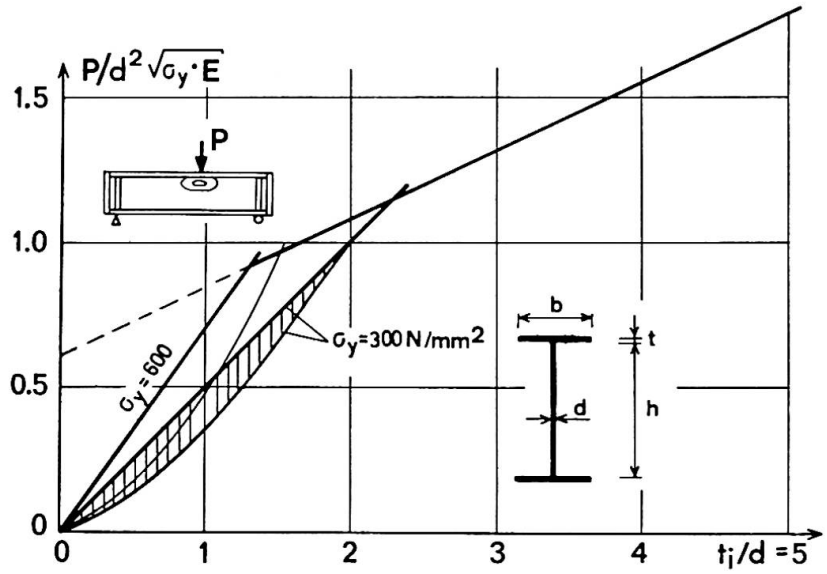

Fig. 2
Yield or crippling load according to Eq. (1).

$$\begin{cases} P^{\text{yield}}_{\text{deform}} \approx 13 \cdot \eta \cdot t \cdot d \cdot \sigma_y \quad ; \quad t/d <\!\sim 2 \quad ; \quad \begin{array}{|c|cccc|} \hline t/d = & 0.5 & 1.0 & 1.5 & 2 \\ \hline \eta = & 0.55 & 0.65 & 0.85 & 1 \\ \hline \end{array} & \ldots (1a) \\ P^{\text{crippl.}}_{\text{failure}} = 0.6 \cdot d^2 \sqrt{\sigma_y \cdot E}\,(1+0.4 \cdot t/d) & & \ldots (1b) \end{cases}$$

Here $P^{\text{yield}}_{\text{deform}}$ indicate a load above which the deformation begins to increase rather rapidly. If the reduction factor η is omitted (that is changed to 1 or in a certain range a little more) the transformed Eq. (1a) gives a theoretical yield failure load. It is seen that not only the yield load but also the crippling load (combined yielding and buckling) depend on the yield point σ_y, but to a different extent.

A theoretical deduction of Eq. (1a) is given in [4], and the corresponding failure load (inserting $\eta \approx 1$ in Eq. (1a)) is deduced in [5]. Both these deductions are based on an approximate model where the flange is regarded as a beam on an elastic spring bed (the bed being the web). More accurate results may be obtained by existing programmes for computations with the finite element method. A closed formula, however, is preferrable for the designer.

The simple formulae (1a) and (1b) hold for a flange width-to-thickness ratio $b/t \approx 25$. If the deviation from the value is great or if the flange is not rectangular, t in Eq. (1a), (1b) should be replaced by t_i from Eq. (2). The web "slenderness ratio" h/d is assumed to be of the order 200 but even great deviations from this value influence the coefficient only very little. If the load is not absolutely concentrated but distributed over the length c the bearing capacity is increased by multiplying with a coefficient f (c) the value of which is in principle given by Eq. (3), up to a maximum of $f(c) \approx 1.3$.

$$t_i = \sqrt[4]{\frac{12}{25} \cdot I_{fl}} \approx t \sqrt[4]{b/25 \cdot t} \quad \ldots (2); \qquad f(c) = \frac{\gamma}{1 - e^{-\gamma} \cdot \cos\gamma}, \quad \text{where } \gamma = c/2L \text{ and } L \approx 6.7 \cdot t \quad \ldots (3)$$

Eq.(1a) corresponds mainly to influence of the kind shown in fig.1a, while Eq.(1b) includes also influences as shown in fig.1c and 1b. To this ought to be added influences as shown by fig.1e, but the tests indicate that this does not give any reduction for bending moments M smaller than 0.6 M_f.

The failure moment M_f is to be calculated with regard to the reduction caused by web buckling. This reduction may be performed e.g. following a simplified method given in [6]. In this method the compressed part of the web is taken into account only by the portion $s = 1.95 \cdot d \cdot \sqrt{E/\sigma}$ and from this portion 2/3 are placed near the neutral axis and 1/3 is placed near the compressed flange.

As an example the bridge in fig.3 will be discussed, which was to some extent damaged during launching. The bridge has a length of about 200 m in 6 spans. A part of the bridge of somewhat more than 3 spans (ca 100 m) was erected by launching in order not to disturb the traffic on a number of under-

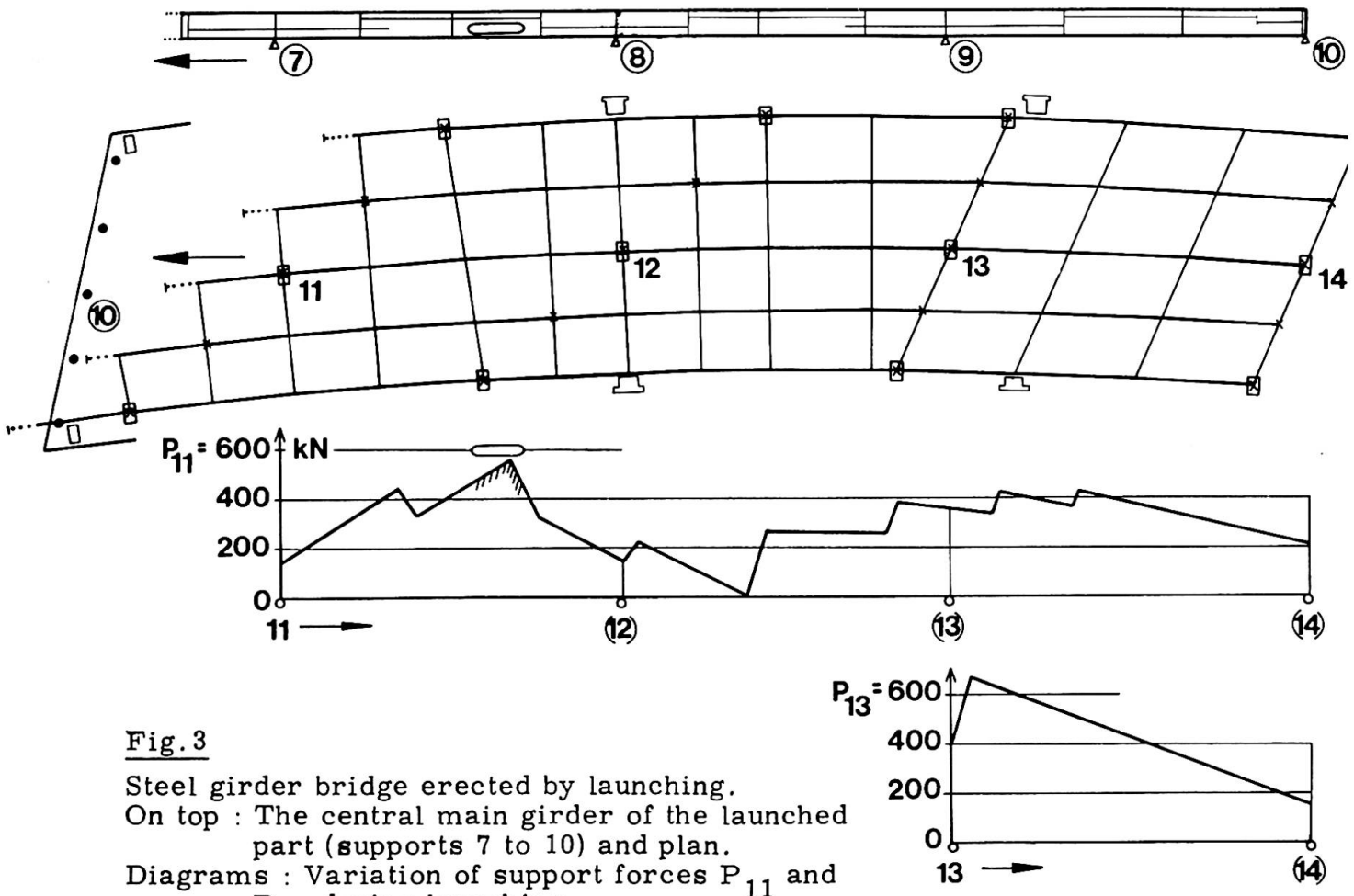

Fig.3

Steel girder bridge erected by launching.
On top : The central main girder of the launched part (supports 7 to 10) and plan.
Diagrams : Variation of support forces P_{11} and P_{13} during launching.

lying railways. The supports had to be placed rather irregularly because of the railway tracks and as the bridge was slightly curved horizontally, it was very laborious to perform a complete analysis of all support forces during the various launching stages. The bridge has 5 main girders and in the final position of the permanent structure all girders are supported at every support line (the launching rolls were 2-roll bogies). In the provisional bridge bed from where the launching started, there were only 3 launching rolls in every support line (using single rolls). The reason for the different roll arrangements was of course the great risks if something unforeseen happened when launching above the railway lines.

Before the launching the supporting forces were only roughly checked mainly using the method of [1]. During launching a buckle was observed in the web in a region of the central main girder web, which is marked with an oval in the girder in fig.3. Because of the buckle a computation of the supporting force was made afterwards for every roll (or bogie) for every stage of the launching. Here only two diagrams are shown of which one gives a reason for the buckle. (The other one gives a greater max. load but there is no risk for the web because of the thick flange).

Fig.3 shows the girder of the bridge laying on the starting bed before the launching. The provisional supporting rolls are marked with squares and the positions of the rolls over the permanent supports are marked with filled circles (only these of the first permanent support line are seen quite to the left). The diagrams of the supporting loads give the load at the start in the utmost left and then the variation as the launching goes on.

The dangerous point, where also the buckle was afterwards observed, is marked with an oval in the force diagram for P_{11} in Fig.3. In this section t/d was 16 mm/12 mm and Eq.(1a) is governing. The steel quality of the bridge girder had $\sigma_y = 260$ N/mm^2. This gives $P^{yield}_{deform} = 13 \cdot 0.8 \cdot 16 \cdot 12 \cdot 260$ N = 520kN = = 52 Mp.

The supporting force was 56 Mp in this point as seen in the diagram in fig.3 and thus larger than the load giving large deformations. The force was, however, less than the failure load (where $\eta \approx 1$) which is $P_{failure} \approx 65$ Mp. At such high loads, the deformations ought to be very large, and the relatively stiff transverse girders would distribute the supporting force to the neighbouring girders. Even with such a load distribution the margin to the failure load was small.

After the launching a part of the flange and the web at the deformed region was cut out and replaced. Inspection showed that the web had small deformations indicating incipient web crippling at some other locations too, and there some small adjustments only were undertaken before the bridge was taken into traffic.

—When the concentrated load is too great there are several possibilities. As already mentioned one can use launching rolls designed with bogies, one can distribute the load by arranging a crane rail below the flange, or one can use a thicker web or use a higher quality for the steel of the web.

For $t/d < 2$, where Eq.(1a) is valid, the advantages of the two latter solutions are immediate apparent. For $t/d > 2$; and Eq.(1b), the best illustration is given by an example. For the bridge just described there were parts having $t/d = 35/12$ and in order to compare the web thickness neeeded for two steels with $\sigma_y = 260$ and 400 N/mm^2 respectively, you use Eq.(1b) :

$$0.6 \cdot 12^2 \sqrt{400\ E}\,(1+0.4 \cdot \frac{35}{12}) = 0.6 \cdot d_1^2 \sqrt{260\ E}\,(1+0.4 \cdot \frac{35}{d_1})$$

From this we find $d_1 = 13.9$ mm, that is 16 % thicker than the 12 mm web. If the difference in steel prize is less than 16 % it is thus cheaper to use the steel of higher quality.

*

References

[1] W Warkenthin : Zur Beurteilung der Beulsicherheit querbelasteter Stegblechfelder. Der Stahlbau 1965, No. 1, p. 28.

[2] C A Granholm : Provning av balkar med extremt tunt liv (Test on girders with extremly thin webs. Report in Swedish) Inst. för Byggnadsteknik, CTH, Rapport 202. Göteborg 1960/61.

[3] A Bergfelt : Incremental Collapse of thin webs subjected to cyclic concentrated loads. Final Report of the IABSE Symposium, Lisboa 1973, p. 39.

[4] A Bergfelt : Studies and tests on slender plate girders without stiffeners. Proceedings of the IABSE Colloquium, London 1971. p. 67.

[5] A Bergfelt - S Lindgren : Local web crippling in thin-walled plate girders under concentrated loads. Summary. (Full original in Swedish, 45 pp plus Appendix 500 pp). Publ S 74:5, Stål- och Träbyggnad, Chalmers University of Technology, Göteborg 1974.

[6] A Bergfelt - B Edlund - H Larsson : Web and flange buckling in light gage steel beams. Int. skr. S 74:8, Stål-och Träbyggnad, Chalmers University of Technology, Göteborg 1975.

SUMMARY

A formula is given for the support forces due to launching that a steel girder can resist. The formula is applied to a bridge with damaged (crippled) web. The use of high strength steel is discussed.

RESUME

Une formule est donnée montrant la force d'appui qu'une poutre peut supporter pendant une construction par lancement. La formule est appliquée à un pont où l'âme est voilée. L'influence de différentes qualités d'acier est discutée.

ZUSAMMENFASSUNG

Es wird eine Formel angegeben für den Auflagerdruck, den ein Stahlträger während des Einschiebens aufzunehmen vermag. Diese Formel wird für eine bestimmte Brücke angewendet, deren Steg beschädigt wurde (Beulen). Die Verwendung von hochwertigem Stahl wird diskutiert.